

STABILITY OF THE KAMLOOPS SILT BLUFFS

by

KEN KING YEE LUM

BASc., University of British Columbia, 1975

A THESIS SUBMITTED IN PARTIAL FULFILLMENT OF
THE REQUIREMENTS FOR THE DEGREE OF
MASTER OF APPLIED SCIENCE

in

THE FACULTY OF GRADUATE STUDIES
Department of Civil Engineering
University of British Columbia

We accept this thesis as conforming
to the required standard

THE UNIVERSITY OF BRITISH COLUMBIA

March, 1979

© Ken King Yee Lum, 1979

In presenting this thesis in partial fulfilment of the requirements for an advanced degree at the University of British Columbia, I agree that the Library shall make it freely available for reference and study.

I further agree that permission for extensive copying of this thesis for scholarly purposes may be granted by the Head of my Department or by his representatives. It is understood that copying or publication of this thesis for financial gain shall not be allowed without my written permission.

Department of CIVIL ENGINEERING

The University of British Columbia
2075 Wesbrook Place
Vancouver, Canada
V6T 1W5

Date

April 26 / 79

ABSTRACT

Stability problems are encountered within the glaciolacustrine silts of the South Thompson Valley near Kamloops, British Columbia. Field investigations have been carried out examining slope failures, piping and collapse features typical of the area. The strength parameters, collapse mechanism and the nature of the cohesion of the silt were examined in the laboratory.

The sensitivity of the soil to slight inputs of water has been examined in detail from the strength and structural stability aspects. A collapse mechanism has been proposed for the lacustrine silt. Although the colluvium derived from the lacustrine silt is known to be highly collapsible, only preliminary laboratory tests have been performed on the colluvial material.

The short and long term stability of the slopes have been studied with consideration given to the effects of urban development. Based on stability considerations, a possible zoning scheme for urban development has been proposed.

TABLE OF CONTENTS

	<u>Page</u>
ABSTRACT	ii
LIST OF FIGURES	vi-viii
LIST OF TABLES	ix
CHAPTER 1. INTRODUCTION	
1.1 Introduction	1
1.2 Geologic History	1-3
1.3 Surficial Geology	3-4
1.4 Climate	4
CHAPTER 2. FIELD RECONNAISSANCE	
2.1 Problems Observed	5
2.1.1 Pipes and Sinkholes	5-7
2.1.2 Slope Stability	8
2.2 Slope Geometry	8-12
2.3 Jointing	12-15
2.4 Soil Sampling	15-17
2.5 Field Seepage Simulation	17-18
CHAPTER 3. BASIC SOIL PROPERTIES	
3.1 Specific Gravity	19
3.2 Grain Size Analysis	19-21
3.3 Mineralogy	21-22
3.4 Atterberg Limits & Field Moisture Contents	23

	<u>Page</u>
CHAPTER 4. LABORATORY TESTS	
4.1 Scanning Electron Microscope Studies	24-28
4.2 Unconfined Compression Tests	29-30
4.3 Triaxial Tests	30-31
4.3.1 Triaxial Test Apparatus	31-32
4.3.2 Saturation Procedure	33-34
4.3.3 Experimental Procedure	34-35
4.4 Triaxial Test Results and Discussion	35
4.4.1 Stress-Strain Relationships	36-39
4.4.2 Volume Changes During Shearing	40
4.4.3 Strength Envelope (P-Q Diagram) ...	36-39
4.5 Unconventional 'Dry' Triaxial Tests	45
4.6 Results and Discussion	45-50
4.7 Consolidation Tests	51-52
4.7.1 Consolidation Apparatus	52-53
4.7.2 Saturation Procedure	53-54
4.7.3 Experimental Procedure	54
4.8 Consolidation Results and Discussion	54-57
4.8.1 Incremental Load Test	57-65
4.8.2 Strain Controlled Test	66-70
4.8.3 Discussion of Combined Results	70-72
CHAPTER 5. STRUCTURAL STABILITY OF KAMLOOPS SILT	
5.1 Literature Review on Collapsible Soils ...	73
5.1.1 Collapsible Soils	73

	<u>Page</u>
5.1.2 Collapse Mechanisms	73-76
5.1.3 Engineering Applications	76-77
5.2 Collapse Phenomenon of Kamloops Silt	78-80
5.3 Collapse Mechanism of Kamloops Silt	80-83
 CHAPTER 6. SLOPE STABILITY	
6.1 Frequency and Extent	84
6.2 Jointing	84
6.3 Modes of Failure	84-90
6.4 Influence of Water	93
6.5 Stability Analysis of Deep Failures	92-93
6.6 Long Term Stability	94-95
6.7 Possible Zoning Scheme	95-97
 CHAPTER 7. SUMMARY AND CONCLUSIONS	
	98-101
 APPENDIX I. SAMPLING SITES & SAMPLE DESCRIPTIONS .	
	103-107
 APPENDIX II. SAMPLE TRIMMING PROCEDURES	
	108-110
 APPENDIX III. APPARATUS COMPRESSIBILITY CORRECTIONS FOR THE CONSOLIDATION TEST	
	111-116
 APPENDIX IV. CONSOLIDATION TESTS ON COLLUVIUM	
	117-119
 REFERENCES	
	120-124

LIST OF FIGURES

FIGURES	<u>Page</u>
1. Topographic Map of the South Thompson Valley	2
2. Horizontal pipe in Colluvium	6
3. Vertical pipe in colluvium	6
4. Sinkholes on the bench surface	7
5. Isolated sinkhole within the colluvium	7
6. Slope failure on the east face of Magazine Gully	9
7. Bench slope facing South Thompson River	9
8. Oblique aerial View of study area	10
9. General slope geometry	11
10. Stereonet plot of joints	13
11. Rose diagram	14
12. Sampling site location	16
13. Grain size distribution curves	20
14. Microphotograph, undisturbed silt, 400X	25
15. Microphotograph, remolded silt, 400X	25
16. Microphotograph, undisturbed silt, 1000X	26
17. Microphotograph, remolded silt, 1000X	26
18. Microphotograph, undisturbed silt, 1000X	27
19. Microphotograph, undisturbed silt, 2000X	27
20. Unconfined compression, stress-strain curves ...	29
21. Schematic diagram of triaxial apparatus	32
22. Stress-strain plot, 'overconsolidated' state ...	37
23. Stress-strain plot, 'normally consolidated'	38

FIGURES	<u>Page</u>
24. % Δ Volume vs. % strain, O.C. stress region	41
25. % Δ Volume vs. % strain, N.C. stress region	42
26. P-Q Diagram for Kamloops Silt	43
27. P-Q Diagram for the O.C. stress region	44
28. Mohr circle of failure at various saturations ..	46
29. Shear strength vs. saturation graph	47
30. Incremental Load Consolidation curve	58
31. Structural collapse rate upon flooding	60
32. ΔH vs Log time plot for incr. load consolidation	62
33. Plot of pore pressure dissipation and amount of consolidation with time	63
34. Strain controlled consolidation curves	67
35. Swell pressure vs time graph	69
36. Composite consolidation curves	71
37. Percent collapse vs P plot	79
38. Slope failures near Pritchard	85
39. Columnar jointing in the lacustrine silt	87
40. Column toppling mode of failure	88
41. Block or slab failure mode	89
42. Rotated intact block failure	90
43. Approximate setback zoning scheme	96
44. Consolidation apparatus compressibility, Curve A	114
45. Consolidation apparatus compressibility, Curve B	115

FIGURES	<u>Page</u>
46. Consolidation apparatus compressibility, Curve C	116
47. Consolidation curves for colluvium	119

LIST OF TABLES

TABLE	<u>Page</u>
I. Hydrometer Analysis Results	20
II. Composition of Kamloops Silt	22
III. Consolidated-drained Triaxial Tests	39
IV. 'Dry' Triaxial Test Results	50
V. 'Consolidation' Tests of Kamloops Silt	55
VI. Results of the Consolidation Tests	56
VII. Observed and Calculated Slope Heights Using Taylor's Charts	92

ACKNOWLEDGEMENTS

I am indebted to my thesis advisor, Dr. R.G. Campanella, Department of Civil Engineering, for his helpful suggestions and guidance. I would also like to thank the British Columbia Department of Highways (Geotechnical and Materials Testing Branch) for their financial assistance and encouragement throughout the course of this thesis.

CHAPTER 1

INTRODUCTION

1.1 Introduction

Geotechnical problems associated with the glaciolacustrine silts of the South Thompson Valley have been examined. The area of study encompasses the silt bluffs on the north side of the South Thompson River just east of Kamloops, British Columbia between Highway number 5 and Harper Road (fig. 1). The problems of slope stability, piping and soil collapse encountered in the semi-arid environment invariably relate to excessive moisture inputs.

This report examines the contrast in behaviour of the silt in its naturally dry state and in its saturated condition. Investigations involve field reconnaissance and extensive laboratory testing of undisturbed silt samples. A possible collapse mechanism is proposed. Basic slope stability calculations are also presented along with a proposed zoning scheme for urbanizational developments.

1.2 Geologic History

The silt of the South Thompson was deposited in a glacial lake referred to as Lake Thompson (Mathews, 1944) during the last deglaciation. Receding ice from the uplands left an ice tongue in the main valley. The tongue separated in the vicinity of Monte Creek (fig. 1), the western lobe retreating toward Kamloops Lake and the eastern one toward Little Shuswap Lake (Fulton, 1965). During the initial receding stage from the

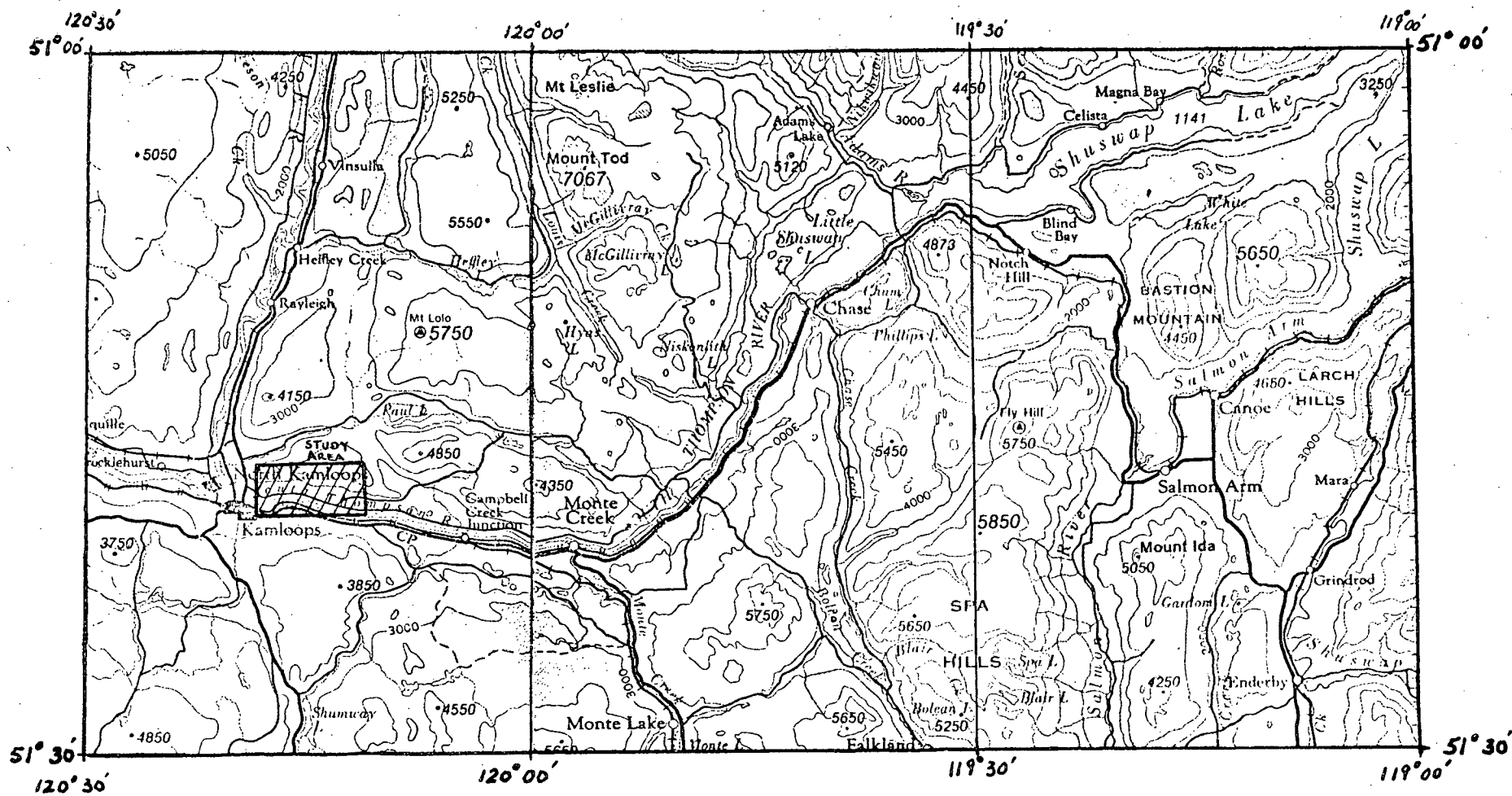


FIG 1. TOPOGRAPHIC MAP OF THE SOUTH THOMPSON VALLEY

adjacent uplands, maximum erosion, transportation, and deposition occurred (up to 20 feet/year) (Fulton, 1965). Much of the silt was derived from the erosion of the till on the uplands adjacent to the valley and entered the Thompson Valley in the vicinity of Kamloops. The coarse portion of the till was left on the upland while the silt was carried into the valley.

With the drying out of Lake Thompson, dessication of the silts resulted, followed by the incision of the South Thompson River which resulted in the formation of a single broad river terrace between 270 and 360 feet below the bench-like remnants of the original lake floor (Ryder, 1971). Gullies formed within the silt bench, draining into the main river channel. Further erosion of the lacustrine silt left the gullies filled with a considerable thickness of colluvium. Today, continuing erosion is resulting in the formation of secondary gullies within the valley fill.

1.3 Surficial Geology

The main deposit within the South Thompson River Valley has been referred to as the South Thompson Silts by Fulton (1965). These glacio-lacustrine silts form well-defined benches on either side of the South Thompson River near Kamloops. The silt is characterized by varving and laminations. Each rhythmite consists of a thick silt layer on top of a thin clay band. The clay bands vary from one inch or less in thickness near the top of the section to half an inch to four inches near the lower section. The silt bands grade from one inch at the top of the section to 250 inches thick at the base (Fulton, 1965). Horizontal laminations parallel to the bedding are evident within the silt bands.

Throughout much of the valley, the silt is covered by a brown loess

capping on the bench surface varying between 6 inches to 10 feet thick. The other soil derived from the lacustrine silt is the colluvial material which covers the slopes below the near vertical bluff face of the benches. Gully floors are also filled by considerable thicknesses of the colluvium. In the field, the colluvial deposits may be identified by its lack of varving (although laminations may be present) and by the presence of two white volcanic ash layers. These tephra layers are thought to be Mazama (6600 yrs.B.P.) and St. Helen's Y (3200 yrs. B.P.) (Fulton, 1975).

1.4 Climate

The semi-arid environment of the Kamloops region has been summarized by Evans and Buchanan (1976):

mean annual precipitation	260.6 mm
mean annual rainfall	186.9 mm
mean annual snowfall	769.6 mm

The hot summers reach a mean temperature of 20.8 °C in July with daily maximums of 29 °C. Most of the rainfall occurs as summer showers during this period. In December, January and February, temperatures drop below freezing. In early March, temperatures rise sufficiently for rapid ice and snowmelt conditions. During this month, the wettest ground conditions exist - especially when combined with the occasional high intensity shower.

The vegetative cover is sparse, consisting mainly of sagebrush and bunchgrass.

CHAPTER 2

FIELD RECONNAISSANCE

A low level flight from Kamloops to Pritchard and down the Okanagan Valley to Penticton was initially carried out. This was followed by a series of ground traverses, joint mapping, a soil sampling program and a field seepage test.

2.1 Problems Observed

2.1.1 Pipes and Sinkholes

Many pipes were found in the colluvial deposits and although less numerous, they exist within the glaciolacustrine silt. Pipes exist as shaft-like voids with their axes near horizontal, near vertical or inclined with the slopes. (fig 2 & 3). Pipe openings as large as 12 feet in diameter have been found. The origin of these pipes has been attributed to (1) the piping process as a result of water erosion in which silt particles are dislodged and carried away by flowing water and/or (2) the collapse of the loose soil structure as a result of wetting.

A related feature is the presence of large ground depressions or "sinkholes" found on the bench surface. They occur either as isolated depressions or in alignment with gullies (fig 4 & 5). These have been attributed to (1) the caving of the ground above a subterranean pipe or (2) to the collapse of soil structure upon wetting, either of the near surface silt or at depth followed by successive caving of the overlying material (Hardy, 1950; Evans & Buchanan, 1976; Nyland & Miller, 1977).



Figure 2. Horizontal pipe in colluvium is approximately 12 feet in diameter. Note the presence of the tephra layer (white, horizontal band).

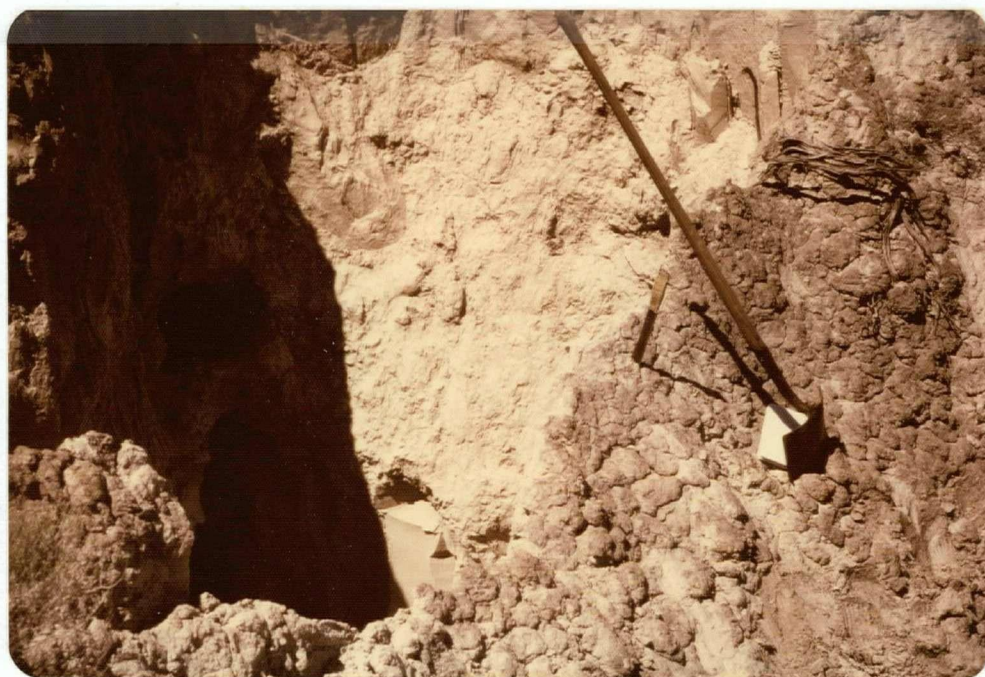


Figure 3. Vertical pipe in colluvium near the base of a steep bluff face within Magazine Gully.



Figure 4. Sinkholes on the bench surface generally appear in alignment with gullies.



Figure 5. A single isolated sinkhole within the colluvium at the bottom of Magazine Gully.

2.1.2 Slope Stability

Although no major slope failures are evident within the study area, instability does exist on a smaller scale. Evidence of shallow slab failures and block failures can be seen on the near vertical slopes facing the South Thompson River and in the steep gully walls within the lacustrine deposit (fig. 6). Colluvial slope failures within the study area are also of small magnitude. However, outside the study area, on the south bluffs of the Thompson Valley, colluvial slope failures are of greater frequency and magnitude due to urbanizational disturbances such as undercutting of the toe of slopes.

2.2 Slope Geometry

Near Kamloops, the silt occurs in benches on both sides of the South Thompson River, sloping gently towards the river at an elevation of 1600 to 1500 feet. The bench terminates at an irregular scarp line running approximately parallel to the river below which a steep irregular bluff wall breaks into colluvial slopes (fig. 7). Many steep sided gullies with depths in the order of 300 feet dissect the benches perpendicular to the river. One of these gullies (Magazine Gully)(fig. 8) was chosen as the detail study area since it contains some of the steepest and highest standing bluff faces, representing the least stable slopes. From eight surveyed sections within Magazine Gully, the slope geometry can be generalized in the form given in figure 9, consisting of approximately 100 feet of lacustrine silt at a 70° slope, breaking into a 35° slope of colluvium that grades into a very slightly concave-up surface which



Figure 6. Evidence of a slope failure on the east face of Magazine Gully.



Figure 7. The bench facing the South Thompson River consists of a steep irregular bluff wall which breaks into colluvial slopes.

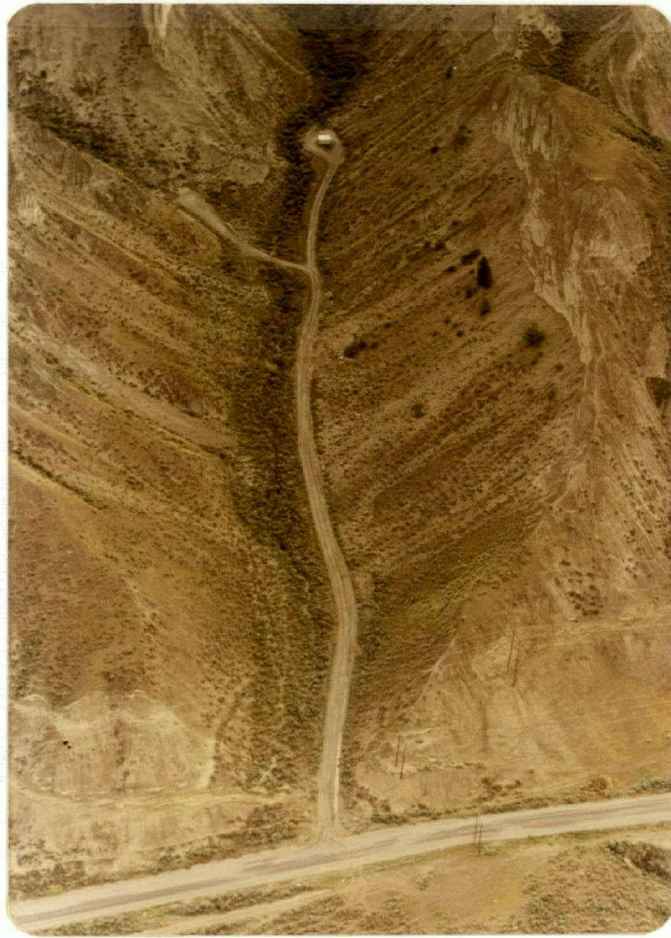


Figure 8. Oblique aerial view of the detail study area (Magazine Gully) looking north.

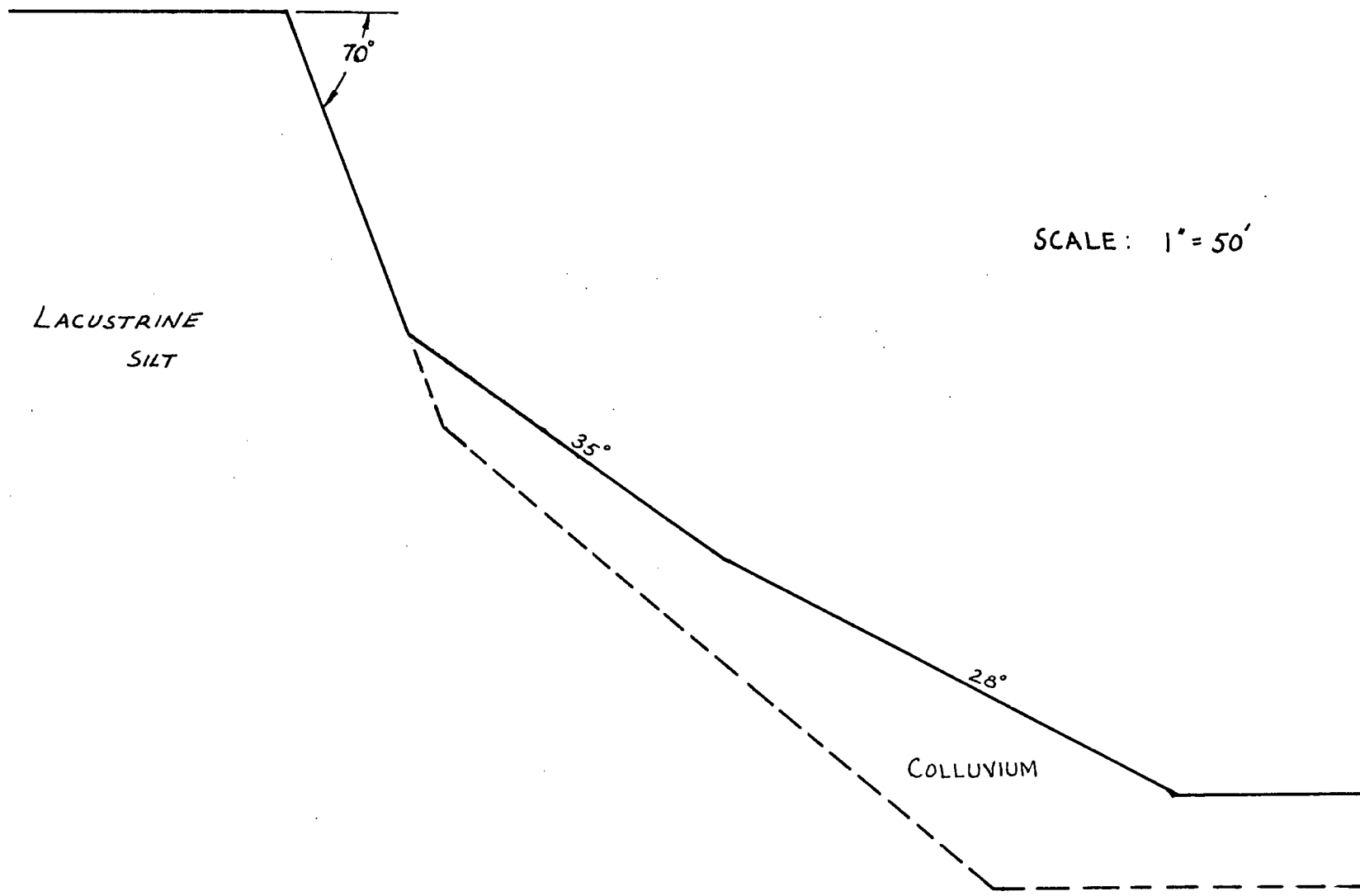


FIG. 9 GENERAL SLOPE GEOMETRY
WITHIN MAGAZINE GULLY

could be approximated by a uniform slope angle of 28° from the horizontal.

Little is known about the depth of colluvium on the slopes, however, a cross-section given by Evans (1976) which was deduced from resistivity and dynamic cone penetrometer data indicates depths of 30 to 60 feet at the gully bottom and 15 to 30 feet midway down the colluvial slopes. The depth of the lacustrine silt deposit is also unknown but it is believed that the silt extends to a minimum depth of 500 feet and possibly greater than 1300 feet in depth (Fulton, 1965).

2.3 Jointing

A small joint survey was carried out by running traverses along the base of the steep bluff face with a Brunton compass. As in all joint surveys, human bias and accessibility problems must be kept in mind. Joint orientations were measured, mainly from the east face of Magazine Gully which trends approximately North-South. The stereonet plot (fig. 10) shows the poles of joints plotted in northern hemisphere projection of a Wulf net (Hoek & Bray, 1974). The joints are mainly steeply dipping towards the western sector. This is expected since joints dipping east would represent unstable conditions on the eastern bluff face. Since the joints are all near vertical, a rose diagram is plotted (fig. 11) with radial lengths representing the number of joints falling within each 10° sector of the stereonet. The rose diagram indicated that four major joint sets exist nearly perpendicular to the almost horizontal bedding. Two major sets exist at strikes of 30° and 120° while two weaker sets occur at approximately 0° and 90° . The combination of these joint sets forms the local columnar jointing seen in the field (fig. 39). This type of

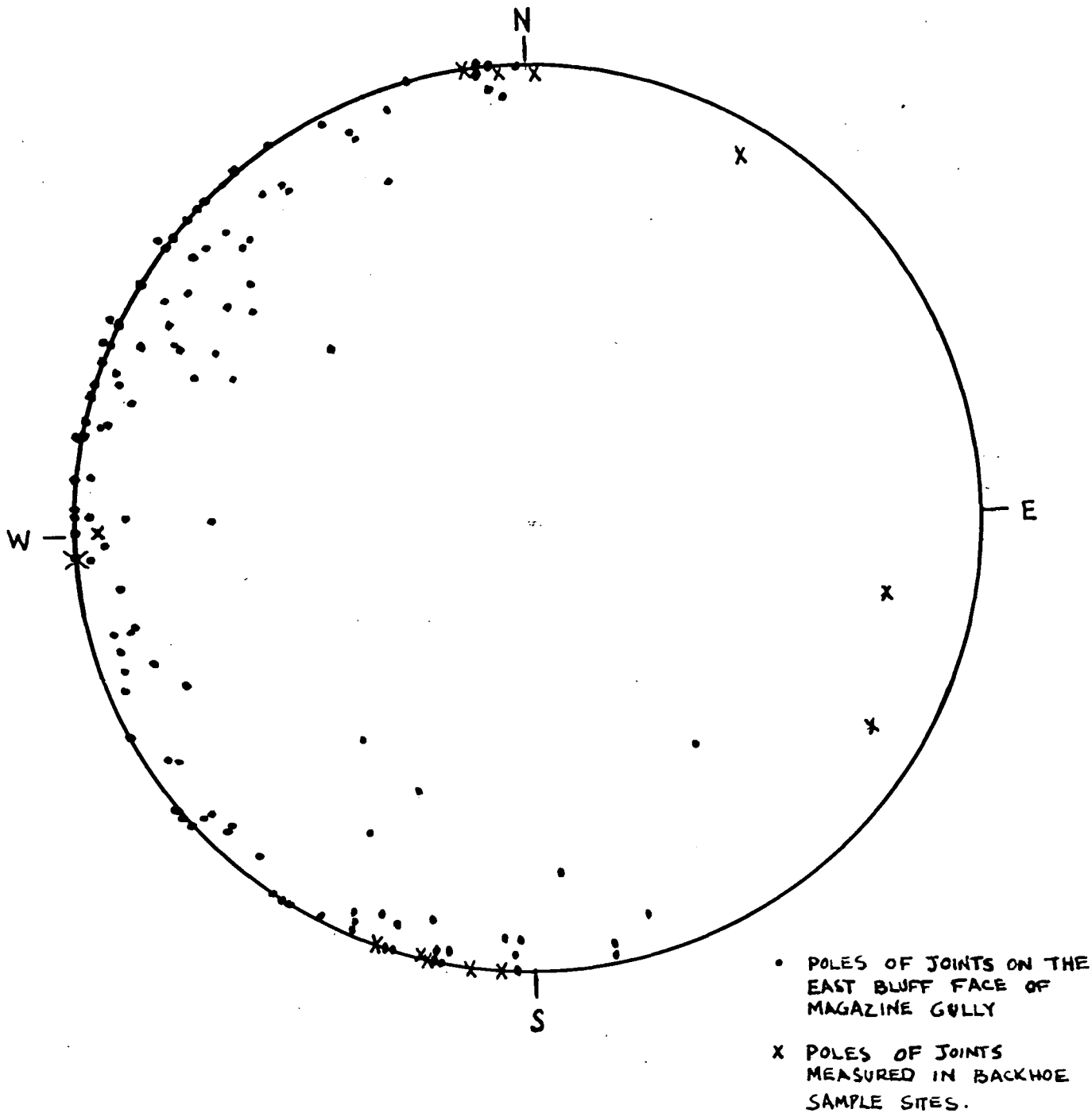


FIG. 10 STERONET PLOT OF JOINTS.

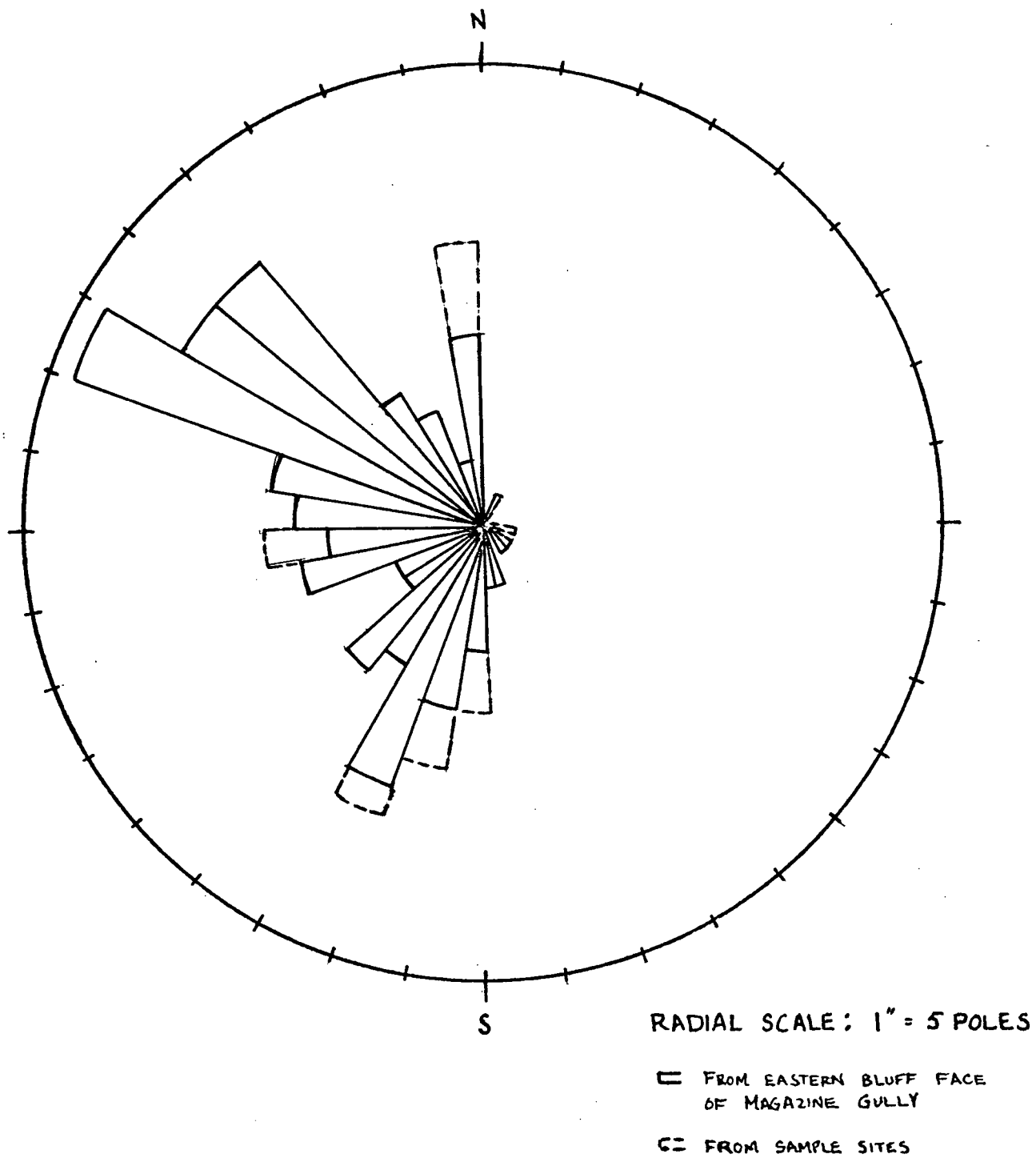


FIG. II. ROSE DIAGRAM

columnar jointing is also typical of the silty loess deposits in the Western United States. It should be realized that this joint survey is limited to a very specific area and may not apply on a regional basis.

Many of the joints are continuous and near planar extending the full height of the bluff exposure with joint spacings of about 4 to 8 feet. Within the top 20 to 30 feet of the section, the joints are more closely spaced, becoming discontinuous fissures. The origin of the jointing is probably due to stress release and shrinkage on dessication.

Most joints show no signs of weathering, but many are coated with a brown weathered film and a few show signs of swelling and slaking along the fracture line.

2.4 Soil Sampling

Difficulties were encountered in attempts by the Department of Highways to retrieve intact undisturbed silt samples by Shelby Tubes. The samples obtained by this method were highly fractured. Therefore, Sampling by backhoe operation was employed.

Block samples were obtained from two backhoe pits on the bench surface adjacent to Magazine gully (fig. 12) at a depth of $4\frac{1}{2}$ to $5\frac{1}{2}$ feet. The blocks were hand carved with a sharp knife, making use of existing in-situ fractures. During sampling, the weather was generally cloudy with brief periods of sunshine. The temperatures reached 31°C with a humidity of 15% (June 29, 1976). To prevent moisture loss, the soil samples were immediately wrapped with "saran wrap" in the field and transported to the Kamloops laboratory for waxing. The samples were then taken by car to the University of British Columbia where they were re-waxed with a low



Figure 12. Aerial photograph of Magazine Gully showing the backhoe sampling site locations (Sites #3 & #4).

permeability, pliable wax and stored in a constant temperature laboratory environment.

Prior to the backhoe operation, surface block samples were obtained from two other locations within the lacustrine deposit for specific gravity determinations and preliminary tests to assess its trimmability and special equipment requirements.

In mid-May of 1977, the study was further extended to include the preliminary consolidation testing of colluvium. Two waxed block samples of colluvium were supplied by the Department of Highways (Geotechnical Branch) in Kamloops. The enclosed descriptions of the location of the blocks are included in Appendix I along with the description of the lacustrine samples and their site locations.

2.5 Field Seepage Simulation

A small trench was excavated 4 feet west of the backhoe sample pit #3 and filled with water to observe the seepage rate and to attempt to cause piping and/or a slope failure to occur on the adjacent pit face.

The small trench was continuously fed from a water truck to maintain approximately 27 inches of water at the midpoint of the trough. The initial seepage under the large capillary head was $1.0 \text{ ft.}^3/\text{min.}$ dropping to about $0.9 \text{ ft.}^3/\text{min.}$ after one hour. The trench was then allowed to drain completely and a small 2 inch diameter indentation (pipe?) was observed at the central base-line of the west side of the trench. The trench was again filled, giving a seepage rate of $0.7 \text{ ft.}^3/\text{min.}$ after another hour. The water left in the trench was then channelled away with the backhoe to determine the position of the wetted front. The front

extended 3 feet to either side of the water trench edges and extended 4 feet and 6 feet below the trench floor on the east and west sides respectively.

The wetted front did not encroach onto the pit face in the time allotted as expected, thus no piping was evidenced on this face. However, on the west side of the trough, the "pipe" formed was large enough to insert an arm into. The "pipe" was a very low strength 'liquefied' channel extending about 8 inches into the face and curving to parallel the trench face, heading south for an unknown distance.

Calculations show that the estimated 160 ft.³ of water pumped into the trench could easily go into the partial filling of the voids in the silt. The total void space within the wetted zone is approximately 250 ft.³, therefore the water input represents only 64% saturation of the soil.

CHAPTER 3

BASIC SOIL PROPERTIES

3.1 Specific Gravity

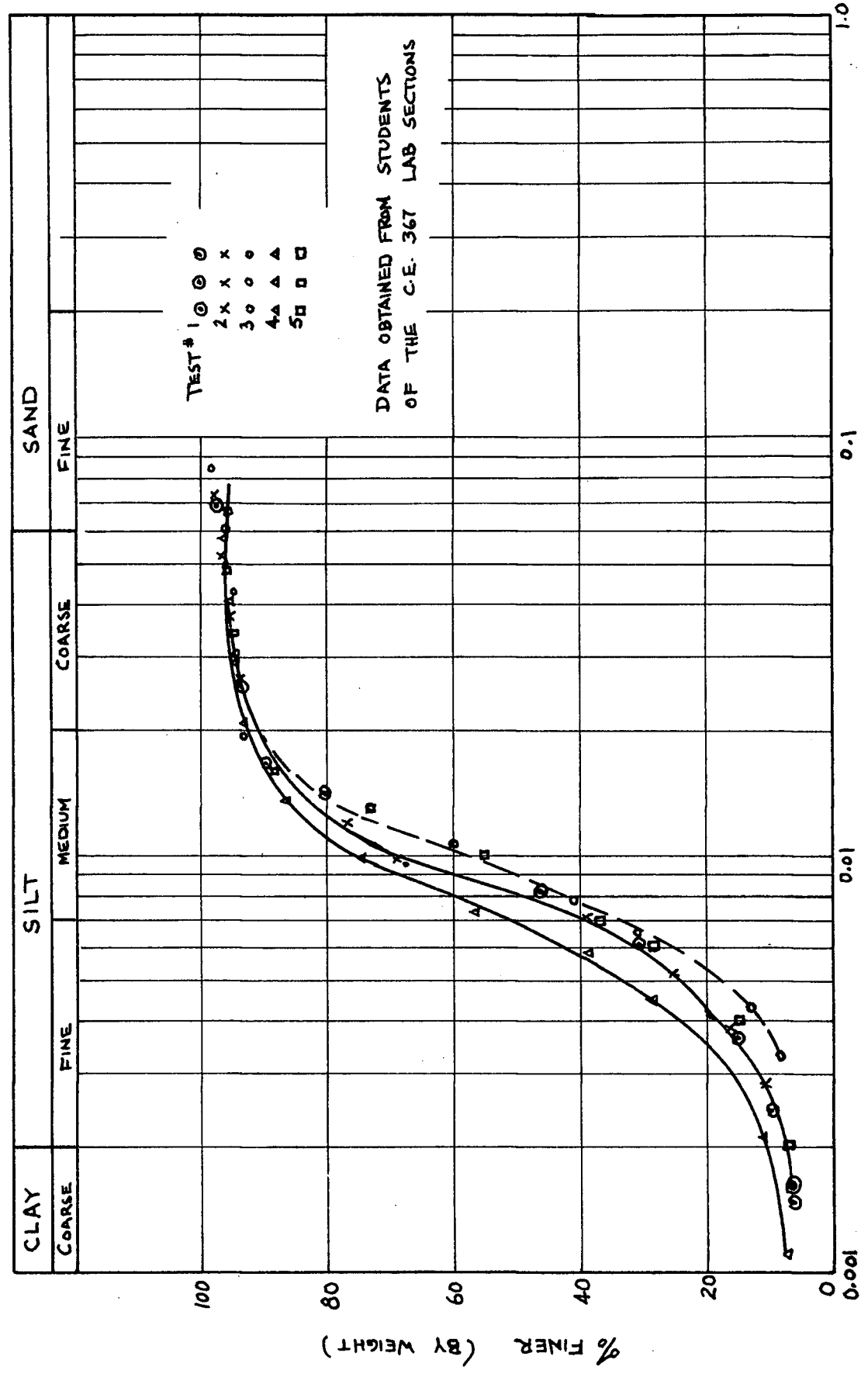
Specific gravity determinations were carried out in the constant temperature laboratory according to the procedure outlined in Lambe (1951). A total of seven tests with samples from four different locations resulted in specific gravities between 2.749 and 2.796 with an average of 2.77 for the lacustrine silt. The high specific gravity is probably attributed to the presence of mica in the silt.

Specific gravities were also determined for two colluvial samples. The sample from the incised creek showed a specific gravity of 2.60 and the sample from the wall of a small pipe had a specific gravity of 2.78. It would seem that the properties of the colluvium is not uniform and will be highly dependent on its location.

3.2 Grain Size Analysis

Hydrometer analysis of the lacustrine silt from site #3 was performed by the undergraduate students at U.B.C. under professor and graduate student supervision. The procedure as described in Lambe (1951) was followed using sodium hexametaphosphate as the defloculating agent. Sample preparation included mixing the sample and defloculating agent in a blender for 10 minutes.

FIG. 13. GRAIN SIZE DISTRIBUTION (MIT CLASSIFICATION) OF KAMLOOPS SILT



PARTICLE SIZE (m.m.)

DATA OBTAINED FROM STUDENTS OF THE C.E. 367 LAB SECTIONS

The data is plotted in figure 13. Table I summarizes the results.

TABLE I. Average results of the hydrometer analysis of the Kamloops silt (lacustrine silt) from site #3.

% sand	4%
% silt	89%
% clay	7%
D ₁₀	0.0027 mm
D ₆₀	0.0092 mm
C _u	3.4

MIT classification: 'fairly' uniform clayey silt.

Data from Evans and Buchanan (1976) agrees with figure 13 even though a defloculating agent was not added in their testing procedure. Their grain size analysis on the colluvium indicates little difference in the particle size distribution as compared to that of the lacustrine silts. This similarity suggests little sorting has resulted and consequently confirms that the silt was transported only a short distance prior to redeposition as colluvium.

3.3 Mineralogy

Mineralogical analysis on the lacustrine silt has been presented by Fulton (1965) and Quigley (1976). Tables IIA and IIB shows a general agreement in the analysis. It should be realized however, that Fulton analysed the silt and sand fractions optically while Quigley used X-ray powder analysis on the whole sample (ie. with the clay fraction included).

TABLE IIA. COMPOSITION OF KAMLOOPS SILT

MINERAL	FULTON (optically)	QUIGLEY (X-ray powder)
quartz	main constituent	abundant
feldspar	major constituent	moderate
mica	major constituent	minor
ferromagnesian minerals	minor constituent	minor

TABLE IIB. X-RAY DIFFRACTION OF CLAY FRACTION ONLY

MINERAL	FULTON	QUIGLEY
montmorillonite	35 - 40 %	abundant
illite/mica	28 - 35 %	moderate
chlorite	27 - 36 %	minor
kaolinite	-	minor

3.4 Atterberg Limits and Field Moisture Content

Data for atterberg limits of the silt has been presented by Evans and Buchanan (1976). Liquid limits given ranged from 27% to 36.8% with an average of 31.1% and the plasticity index ranged from 1.9 to 11.7% with an average of 8.4%. On the plasticity chart, this data would plot close to the A-line within the same region as the silty loess of the western United states studied by Gibbs, Hilf and Holtz (1960).

During the summer, natural water contents measured by Evans & Buchanan (1976) ranged from 0.2% to 2.4% near the surface. Samples from the backhoe operation at a depth of approximately 5 feet had a natural water content of 7-8% in June at the time of sampling. A water gradient is expected to exist with depth but its actual vertical variation is not known and subjected to seasonal and local fluctuations. The regional ground water table exists well below the slopes under consideration within the study area. However, it is highly possible that perched water tables during rapid snowmelt and heavy rainfall above the clay seams within the varved sequence exists.

CHAPTER 4

LABORATORY TESTS

4.1 Scanning Electron Microscope Studies

Three samples were studied under the Etec Autoscan Scanning Electron Microscope on the University of British Columbia campus. The first two undisturbed samples of the lacustrine silt were scanned parallel and perpendicular to the bedding. The third sample was a remolded sample viewed perpendicular to the sedimentation direction. The remolded sample was formed by allowing a well-mixed slurry to slowly air dry under laboratory conditions. The initial water contents associated with the samples were considered low enough that structural alteration was negligible during the drying process (the undisturbed samples had a water content of 7.6% and the remolded sample was at 1.9% water content). "Drying" was achieved by slowly applying a vacuum of 10^{-4} torr to the samples. The samples were then coated with a few hundred Angstroms of carbon (gold-palladium coating was avoided since X-ray micro-probe analysis was desired).

Electron photomicrographs of the soil are presented in figures 14 to 19. Stereopairs (not shown) of the samples showed a strong horizontal preference in orientation of the platy particles in the undisturbed and remolded silt. Structurally, there appears to be little difference between the remolded and undisturbed lacustrine silt other than the void ratio differences (1.14 and 1.28 respectively).

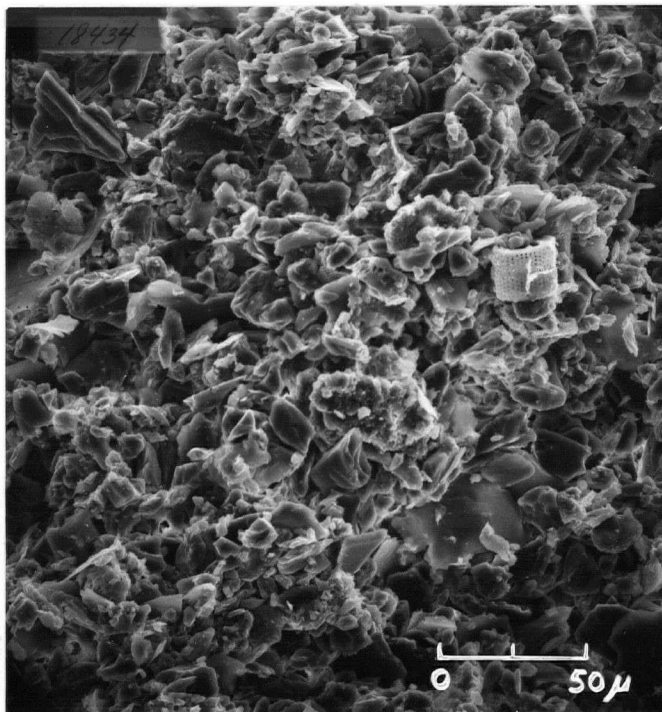


Figure 14. Photomicrograph of the Kamloops silt, undisturbed sample, side view, at 400X magnification.

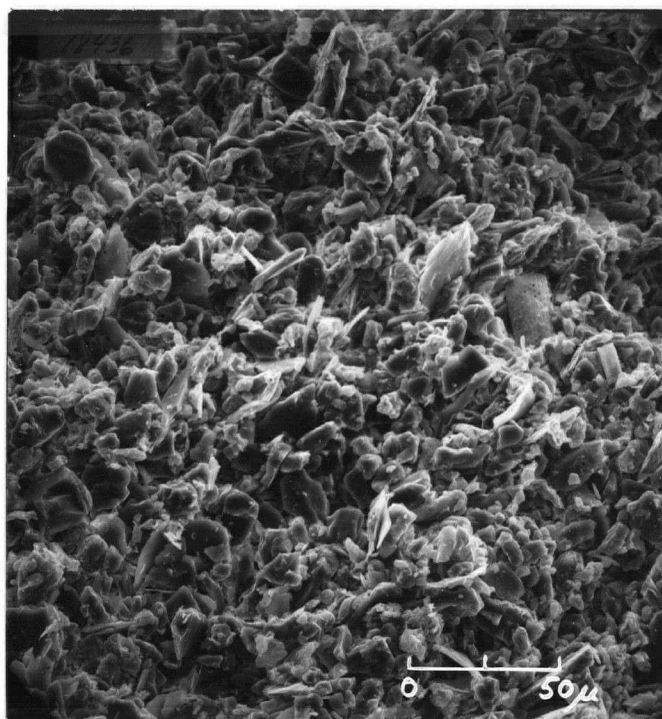


Figure 15. Kamloops silt, remolded sample, side view, 400X magnification.

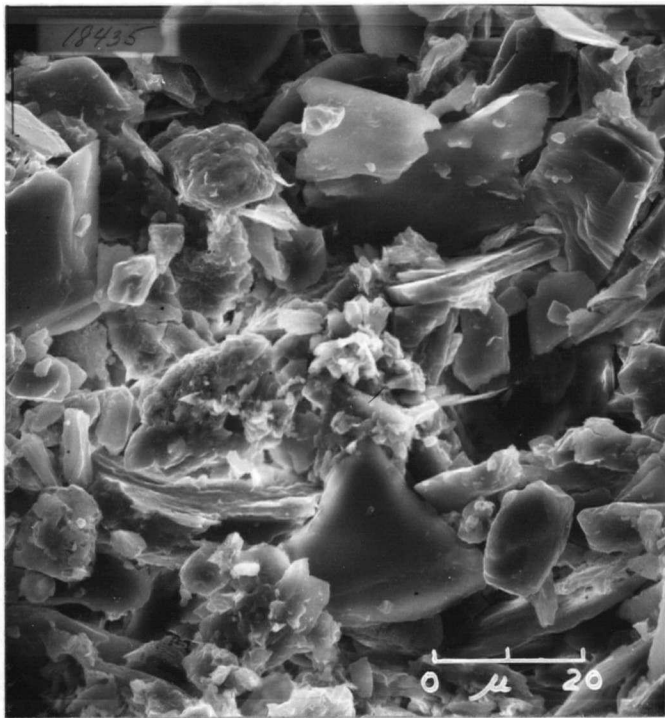


Figure 16. Photomicrograph of undisturbed Kamloops Silt at 1000X magnification, viewed parallel to the bedding.

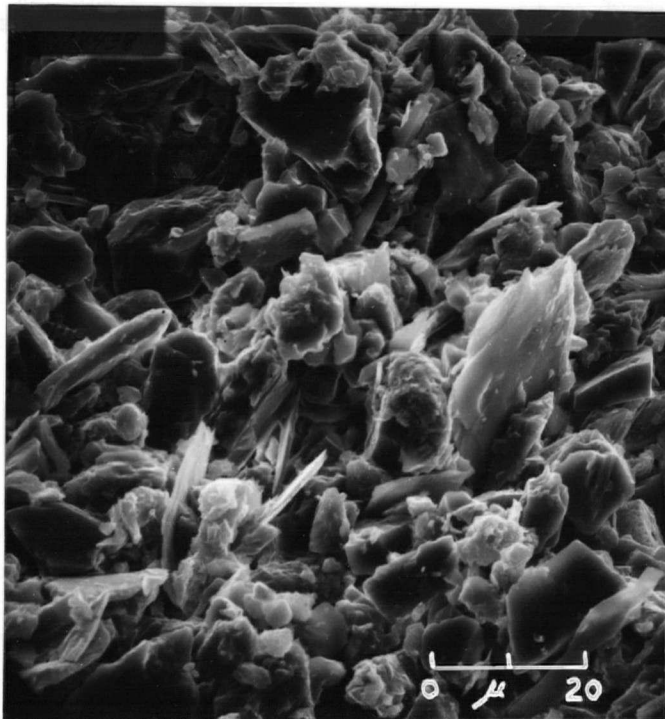


Figure 17. Photomicrograph of remolded silt (Kamloops silt) at 1000X magnification, viewed from the side, ie. perpendicular to the sedimentation direction.

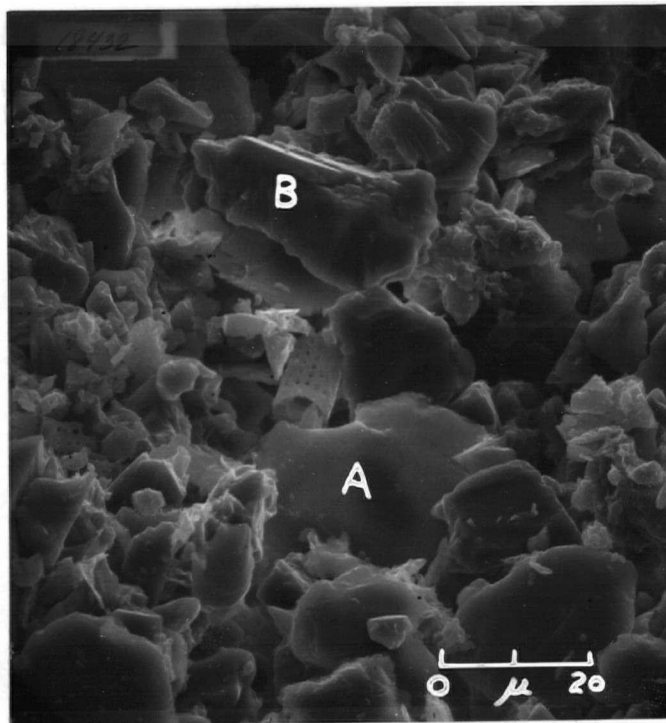


Figure 18. Plane view of the undisturbed Kamloops Silt at 1000X magnification. Particles 18A & 18B were studied under the Electron Microprobe.

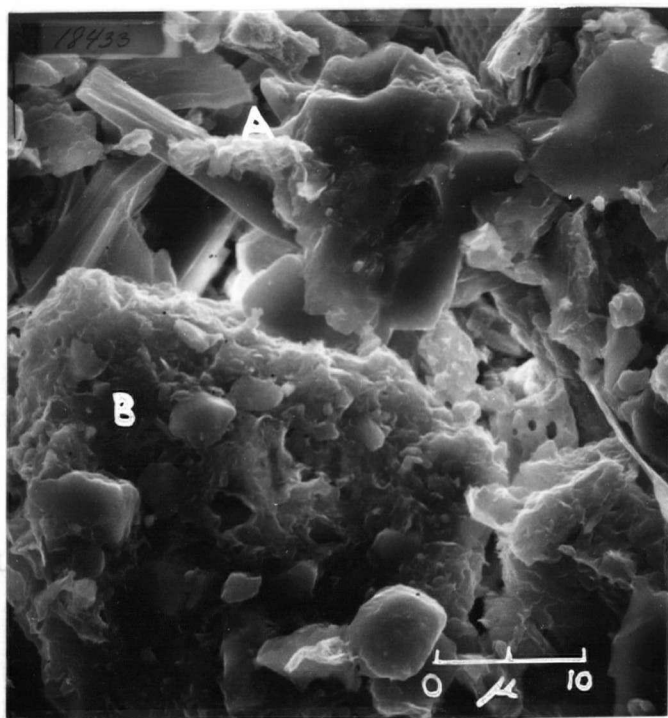


Figure 19. Plane view of the undisturbed silt at 1000X magnification. Peds 19A & 19B were studied under the Electron Microprobe. Note the clay bridging formed by 19A.

A microprobe (Ortec Multichannel Analyser, Model 6200) was used in an attempt to identify the mineralogy of the particles. But interpretation is always difficult when only elemental data can be obtained and the quantitative data being questionable. The particles 18A, 18B, 19A and 19B in figures 18 and 19 yield the following elements, listed in decreasing peak intensity.

Particle 18A: Si, Al, Fe, K, Mg, Na, Ti

Particle 18B: Si, Al, Ca, Fe, K, Mg, Na, Ti

Particle 19A: Si, Al, Mg, Fe, Ca, K, Na, Ti, S

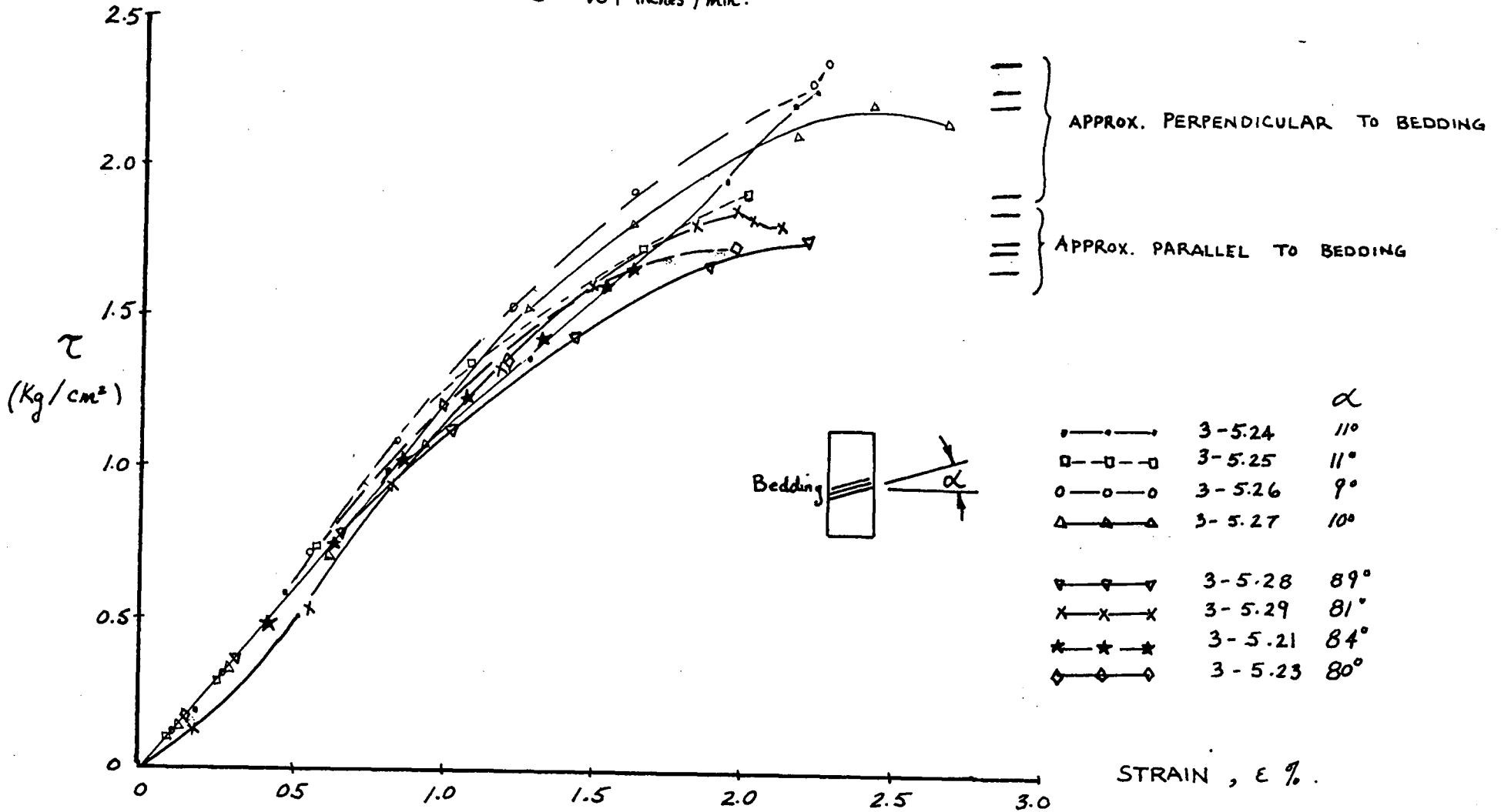
Particle 19B: Si, Al, Fe, Ca, S, Mg, K, Ti

The platy particles in the photomicrographs are probably mica sheets (eg. particle 18A in figure 18). Particle 18B may be feldspar. The clusters of 19A and 19B in figure 19 are possibly montmorillonite. Much of the clay present in the sample exists as clusters or peds, but at the same time, it provides bonding with the silt particles it contacts. The photomicrographs are generally at too small a scale for small bridging clay structures to be clearly visible. Close examination of the larger scaled photographs (eg. figure 19) clearly shows the type of bridging possible between silt grains.

Scattered throughout the sample are siliceous diatoms (melosira granulata). This common species is associated with freshwater lakes and therefore most likely dates back to the last deglaciation.

FIG. 20 UNCONFINED COMPRESSION (ANISOTROPY OF STRENGTH)
 (OF 'KAMLOOPS SILT')

$\dot{\epsilon} = .01$ inches/min.



4.2 Unconfined Compression Test

To determine whether strength anisotropy exists for the lacustrine silt, eight samples were tested in the motor driven unconfined compression apparatus. Four samples were subjected to axial loads perpendicular to the bedding ($\pm 11^\circ$) and four samples parallel to the bedding ($\pm 10^\circ$). All samples were trimmed from the same intact block from site #3. The water content of the silt block was 6.8%. The samples were failed at a constant strain rate of 0.1"/min. or approximately 3% strain per minute. The stress-strain data plotted in figure 20 shows that a slight anisotropy exists with maximum strengths (τ) of 1.93 - 2.36 kg/cm² for samples loaded perpendicular to the bedding. All failed samples exhibited axial splitting which is characteristic of the failure mode of brittle materials in unconfined compression (Townsend, Sangrey & Walker, 1969; Coates, 1970).

4.3 Triaxial Test

To determine the strength envelope of the silt, consolidated-drained triaxial tests were performed on saturated samples. The effective confining pressures used ranged from 0.05 kg/cm² to 3.0 kg/cm². The saturation apparatus and procedure is described in the following sections. Since undrained tests require 100% saturation for accurate pore pressure measurements, drained tests were used. The pore pressure parameter, B, was measured at various stages of saturation until a B-value of 95% or greater was reached. This procedure generally required from 3-7 days of percolation under a small pressure gradient and high backpressures (see section 4.3.2). The sample was then subjected to isotropic consolidation for approximately 24 hours before loading to failure.

All tests were performed with the deviator stress approximately perpendicular to the bedding. The bedding orientation was evidenced by laminations on most of the trimmed samples (the trimming procedures are briefly outlined in Appendix II). With the deviator stress vertical during testing, the laminations were measured to range from 5° to 24° off horizontal with most sample bedding orientations between 5° to 12° .

4.3.1 Triaxial Test Apparatus

The conventional triaxial cell was used in which cylindrical samples 3" high by 1.4" in diameter are sealed from the cell fluid by double rubber membranes. A thin layer of silicone lubricant was applied between the two rubber membranes to minimize frictional resistance. A schematic diagram of the apparatus is shown in figure 21. The top and bottom drainage lines are connected to a "tree" containing a calibrated pipette, a bellofram reservoir and a Tyco Model AB pore pressure transducer. The cell pressure is applied through a clear lucite reservoir attached to the top of the triaxial cell unit. The bottom and top drainage lines are connected to the saturation system.

The vertical deformation rate was pre-set on the 5 Ton Wykeham Ferrance Compression Machine through a set of gears. The deformation rate was checked by a dial gauge during the test. The load was measured by a beryllium copper diaphragm load cell placed above the loading rod. Electrical signals from the load cell and pressure transducer were automatically recorded by the Vidar Autodata Eight unit. Data reduction was carried out by transferring the information onto computing cards and fed to the main U.B.C. computer.

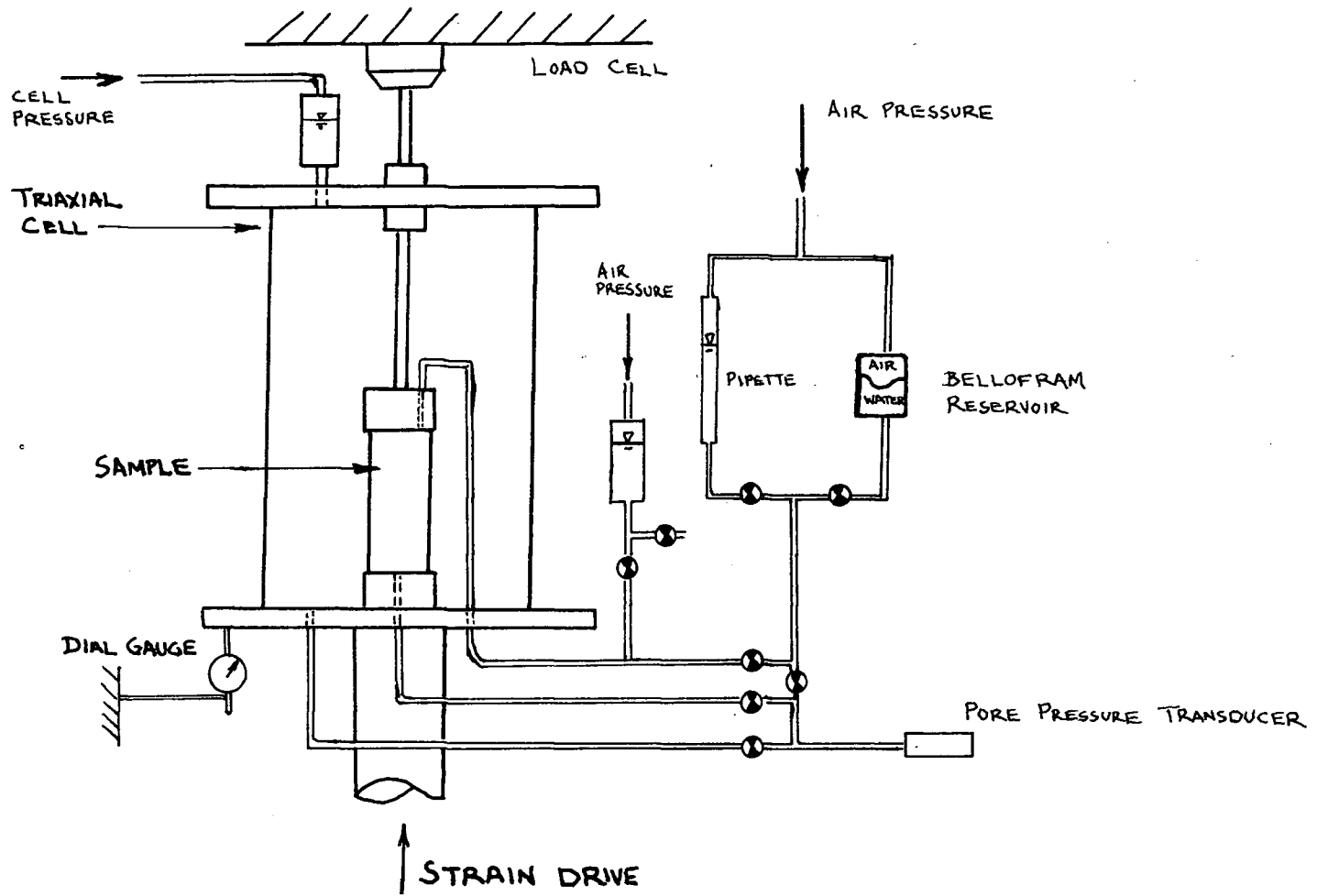


FIG. 21 SCHEMATIC OF TRIAXIAL APPARATUS

4.3.2 Saturation Procedure

In saturating a sample, de-aired water is forced from the bottom drainage line up through the sample and out the top drainage line. The bottom drainage is connected to a lucite reservoir containing a rubber bellofram. The desired air pressure is applied to one side of the bellofram forcing the water out the other side of the reservoir into the sample. The rubber bellofram serves to prevent pressurized air from dissolving into the water in the reservoir and to prevent air from entering the sample when the water in the reservoir is drained. The top drainage line of the sample is connected to a clear lucite reservoir which holds the water which has been flushed through the sample. This reservoir is also pressurized. By controlling the pressures within the bellofram reservoir and the outflow reservoir, a small pressure gradient could be applied to the sample and still maintain a high backpressure.

The actual saturating procedure consists of two stages. Since the sample is essentially dry, the sample is first flushed with water applying a top pressure of 0.1 kg/cm^2 and a base pressure of 0.2 kg/cm^2 (pressure gradient of approximately 13 cm/cm). The cell pressure is maintained at 0.5 kg/cm^2 . This procedure forces air out of the top drainage. The following day, the cell pressure is slowly increased to 4.00 kg/cm^2 in small increments simultaneously with the incremental increase of the top and bottom pressures to 3.60 and 3.80 kg/cm^2 respectively. Each increment is checked such that the effective confining stress at the top of the sample is not greater than 0.5 kg/cm^2 and not less than 0.2 kg/cm^2 . The top and bottom pressures are raised in increments which assures that a pressure gradient of 0.2 kg/cm^2 across the sample is not exceeded.

Flushing is continued at the above pressures until a B-value of 95% or greater is achieved. The water content of all samples were measured after testing and calculations show saturations of essentially 100% (47 - 48% water content) were achieved. Invariably a few samples would show saturations exceeding 100% due to errors in the measurement of sample volume.

4.3.3 Experimental Procedure

After saturation is complete, the top drainage is closed and its pore pressure monitored. The pore pressure is allowed to reach equilibrium and then the sample was consolidated at the desired effective pressure. The test then follows the conventional consolidated-drained procedures outlined by Bishop & Henkel, 1974. The strain rate was selected on the basis of direct pore pressure measurements under single drainage conditions (drainage at the top with pore pressures monitored at the base of the sample). A strain rate of 0.15"/min. (0.5%/min.) produced no significant rise in pore pressure within the sample. However since overconsolidated samples were expected to fail at less than 2% strain, the time to failure would only be 4 minutes. Thus, to allow sufficient time to monitor the behaviour of the silt, a much slower rate of 0.0006"/min. was adopted. This resulted in a testing time of approximately 1 hour. Thus, all overconsolidated samples were tested at 0.0006"/min.

Within the normally consolidated region, sample #3.31 was subjected to the same slow rate. Since failure was not reached until very large strains, subsequent normally consolidated samples (#3.34 and 3.35) were tested at 0.015"/min. to decrease the testing time. It was evident from the Mohr envelope plot that the increase in strain rate did not

affect the soil strength (friction angle).

Various effective confining stresses ranging from 0.05 to 3.0 kg/cm² were used to define the Mohr envelope. The low confining stresses were employed in an attempt to determine the cohesion intercept more accurately. At the lowest effective confining stress of 0.05 kg/cm², slight fluctuations in the height of water in the drainage pipette due to sample volume change during shearing would result in significant changes in the confining effective stress (eg. expulsion of 1 cm³ of water would result in an additional 12 cm. head of water or 0.012 kg/cm² in the backpressure). Therefore, a much larger lucite tube (1.0" I.D.) was employed as the drainage reservoir, sacrificing the volumetric accuracy to attain a steady effective confining stress. The problem of possible swelling of the sample at such low confining pressures during flushing and testing could not be avoided - we can only assume that since the magnitude of swelling is small (as in consolidation sample #3.33) the strength may not be too greatly reduced.

4.4 TRIAxIAL TEST: RESULTS & DISCUSSIONS

The results of the eleven triaxial tests are listed in table III. Water contents were measured on all samples after failure had been attained. Calculations confirm that samples were essentially saturated. Invariably, a few samples showed above 100% saturation which was attributed to errors in measurements of sample dimensions. The void ratios of the triaxial samples ranged from 1.30 to 1.39. As will be seen later, the void ratios obtained from the oedometer mold is somewhat lower and deemed more reliable((section 4.8).

4.4.1 Stress-strain Relationships

A few stress-strain relationships are plotted in figures 22 & 23. Figure 22 presents the stress-strain behaviour of the silt in the over-consolidated stress field. As expected, a peak in strength is realized within this region. Thus the peak stress conditions have been defined as the failure criteria. Being a drained test, the maximum deviator stress corresponds to the maximum principal stress ratio criteria. In all overconsolidated cases, failure had occurred at strains of 1.1% or less (see table III). It should be noted however, that excessive travel of the loading platform of up to 0.7% strain due to improper seating prior to load build-up within the sample was regarded as zero strain. This seating problem results from tilted contact of the sample ends with the loading platforms.

The orientation of the failure planes of the strained samples ranged from 28° to 32° away from the major principal stress direction with one exception: at the lowest confining pressure used (0.05 kg/cm^2), the failure mode resembled that of the unconfined compression test of dry brittle silt - ie. the failure plane was nearly vertical.

Within the normally consolidated stress states, the stress-strain curves exhibited a rapid rise in stress followed by steadily increasing strength with rising strain up to the tested range of 35% strain (fig. 23). At such large strains, the area correction which assumes the sample deforms in a right cylinder is in error and the stresses on the failure plane is ill-defined. Since the stress-strain curves do not level off at reasonable strains, the failure criteria has been defined as the strength of the soil at 20% strain. In the field, strains of this magnitude would most likely continue to failure.

FIG. 22 STRESS-STRAIN PLOT

LEGEND

TRIAXIAL TEST RESULTS, KAMLOOPS SILT
'OVERCONSOLIDATED' STATE

SAMPLE NO.	σ_3' (Kg./cm ²).
▲-▲ 3-1.3	0.493
⊙-⊙ 3-1.4	1.00
×-× 3-1.2	0.20
●-● 4-1.1	0.051

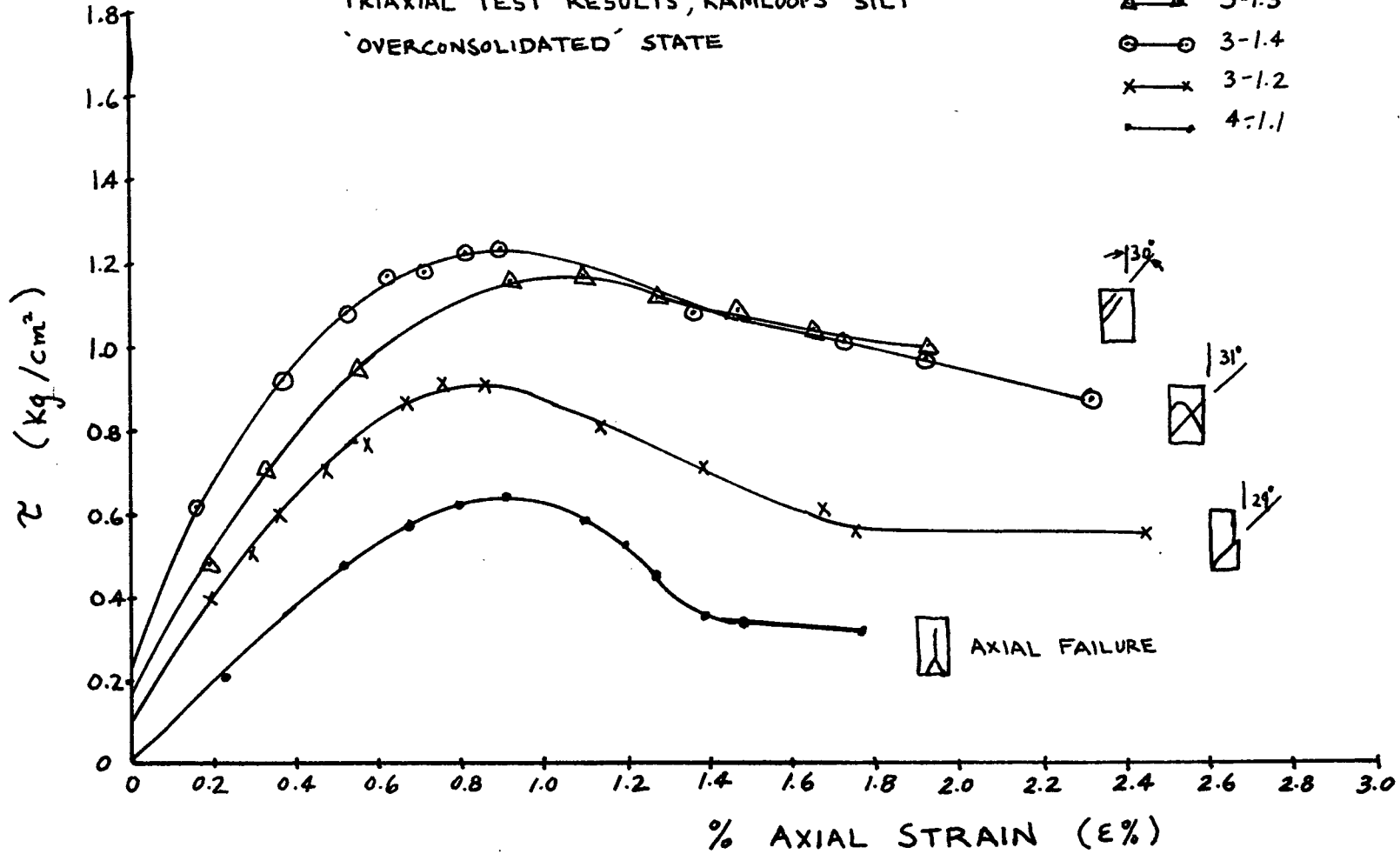


FIG. 23 STRESS - STRAIN PLOT

TRIAxIAL TEST RESULTS FOR KAMLOOPS SILT
'N.C.' STATE

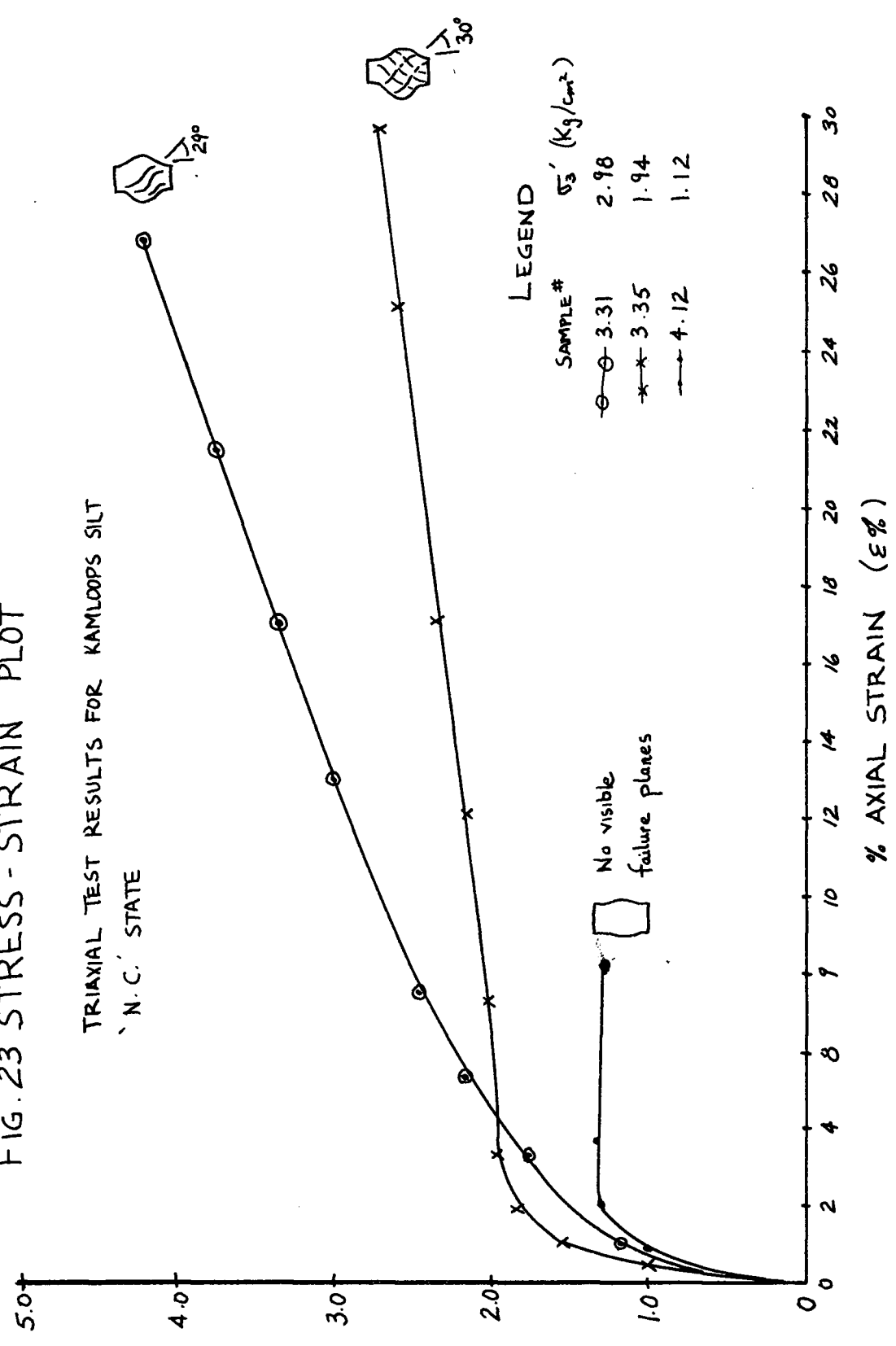


TABLE III. CONSOLIDATED-DRAINED TRIAXIAL TESTS

Test #	Void Ratio	α *	σ'_3	$\frac{\sigma'_1 + \sigma'_3}{2}$	$\frac{\sigma'_1 + \sigma'_3}{2}$	Strain at Failure
3.11	1.38	-	1.100	2.429	1.329	0.97%
3.12	1.41	-	0.200	1.115	0.915	0.75%
3.13	1.33	8°	0.493	1.660	1.167	1.10%
3.14	1.30	11°	1.000	2.223	1.223	0.81%
3.21	1.38	12°	0.157	1.196	0.955	0.98%
3.22	1.30	24°	0.500	1.421	0.921	1.05%
3.31	1.33	15°	2.990	6.635	3.650	20.00% **
3.34	1.34	17°	1.440	3.324	1.880	20.00% **
3.35	1.34	11°	1.90	4.313	2.409	20.00% **
4.11	1.39	5°	0.051	0.700	0.649	0.90%
4.12	1.36	6°	1.12	2.463	1.343	3.17%

natural water contents: 7-8%

final water contents: 47-48%, essentially 100% saturation

* α is the angle between the bedding plane and the σ'_3 axis direction

** samples 3.31, 3.34 and 3.35 are normally consolidated and failure is defined at 20% strain; all other samples are overconsolidated.

4.4.2 Volume Changes During Shearing

Changes in sample volume were measured during shearing by recording the amount of water expelled from the sample into the calibrated pipette. Within the overconsolidated region, a general decrease in sample volume occurred up to the point of failure followed by sample dilatancy (fig. 24). Samples sheared in the normally consolidated region showed a decrease in bulk volume with increasing strain with no dilatant behaviour observed (fig. 25).

4.4.3 Strength Envelope (P-Q Diagram)

The failure stress conditions are plotted in figures 26 & 27 in the form of a $\frac{1}{2}(\sigma'_1 - \sigma'_3)$ versus $\frac{1}{2}(\sigma'_1 + \sigma'_3)$ failure envelope. If α is the slope angle of the best line drawn through such points, it can be shown that $\sin \phi' = \tan \alpha$ where ϕ' is the effective angle of frictional resistance. Similarly, if 'a' is the $\frac{1}{2}(\sigma'_1 - \sigma'_3)$ intercept, then $c' = a / \cos \phi'$ (Lambe & Whitman, 1969). From figure 26, $\alpha = 29^\circ$ and therefore, $\phi' = 33.7^\circ$ within the normally consolidated stress field.

Figure 27 represents the data of the overconsolidated region plotted to a larger scale. Thus $\alpha = 17^\circ$ and $a = 0.58 \text{ kg/cm}^2$. Conversion to Mohr envelope parameters yields $\phi' = 17.8^\circ$ and $c' = 0.609 \text{ kg/cm}^2$.

The existence of the overconsolidated region is noteworthy since the silt is a glaciolacustrine deposit of the last deglaciation, therefore, the maximum overburden stress will not contain a component due to weight of overlying ice. Since sampling depth was between $4\frac{1}{2}$ to $5\frac{1}{2}$ feet and if we assume that only a few feet of silt had been eroded away, there would be insufficient overlying material to produce the overconsolidated

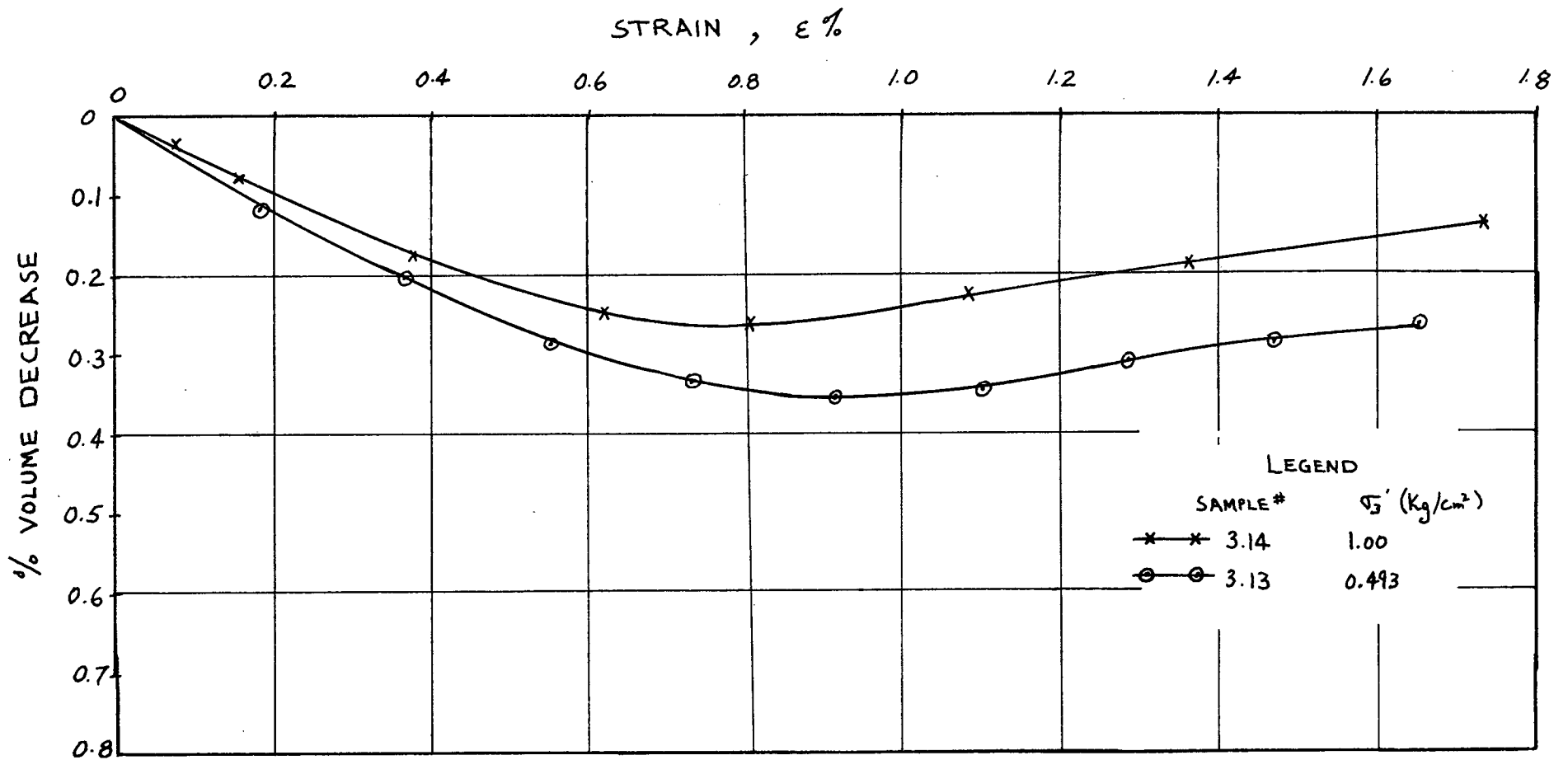


FIG. 24 % Δ VOL. VS $E\%$ FOR O.C. STRESS REGION.

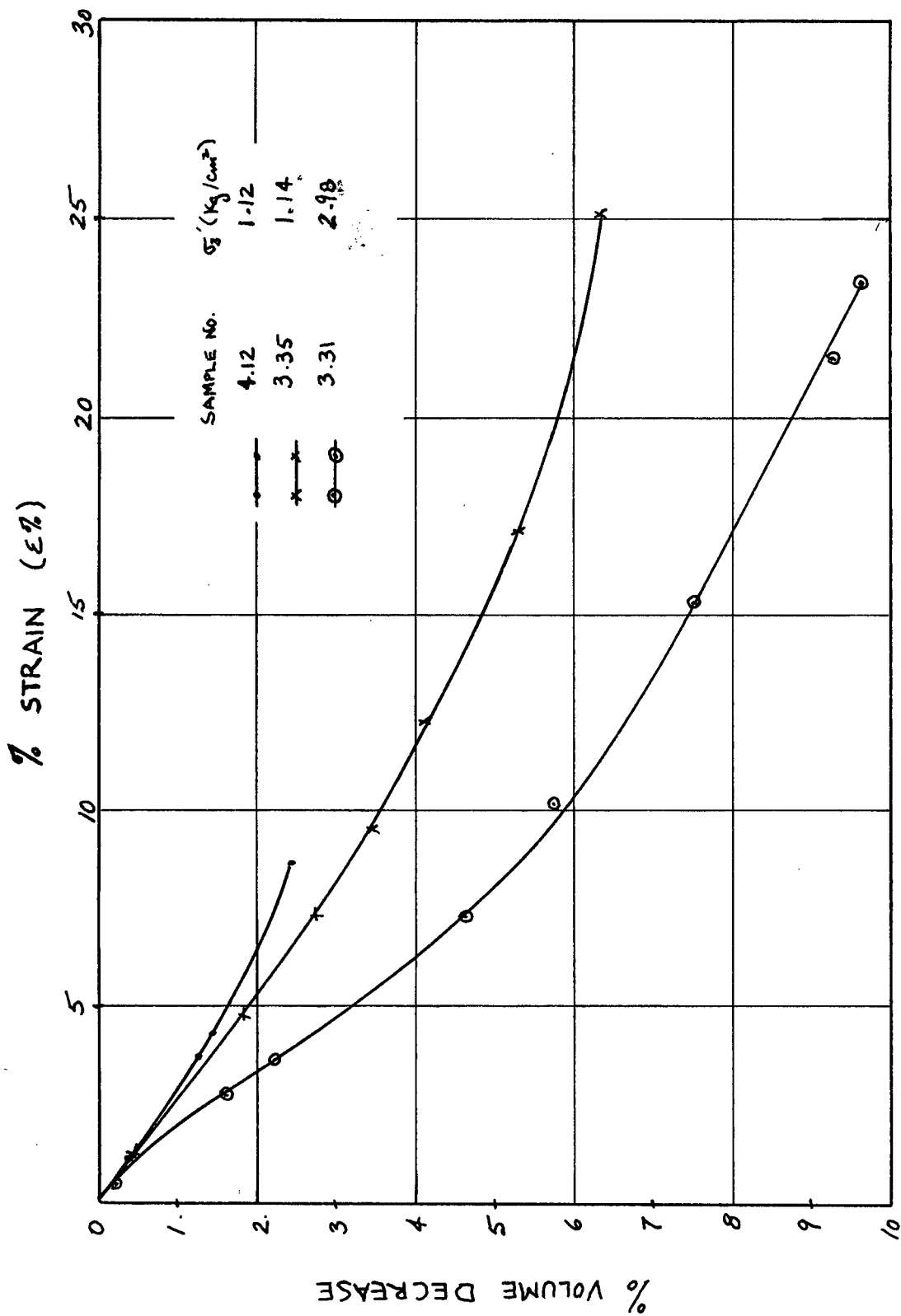


FIG. 25 % Δ VOL. VS. $\epsilon\%$. FOR. N.C. STRESS RANGE

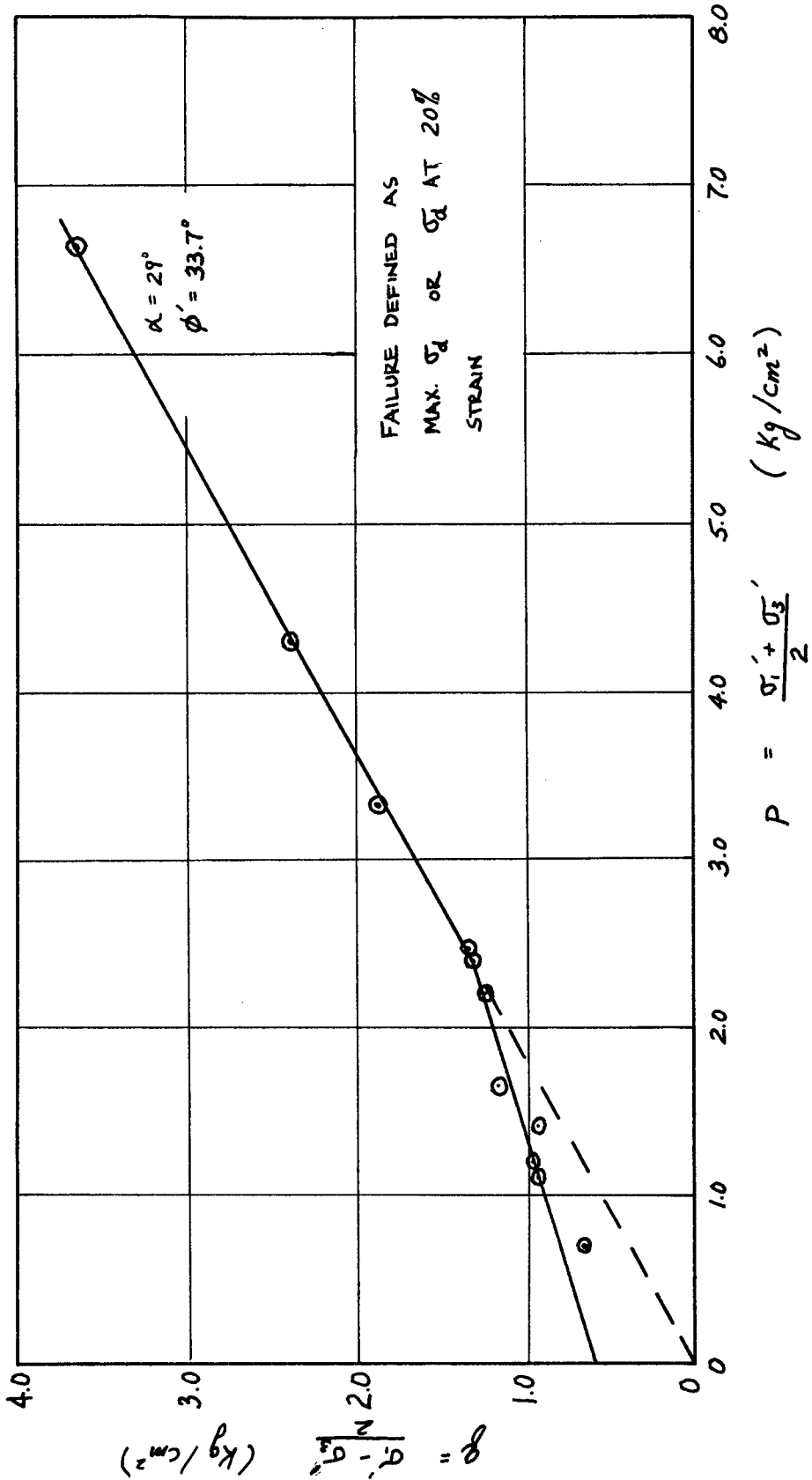


FIG. 26 P-Q DIAGRAM FOR KAMLOOPS SILT
(CD TRIAXIAL TEST DATA)

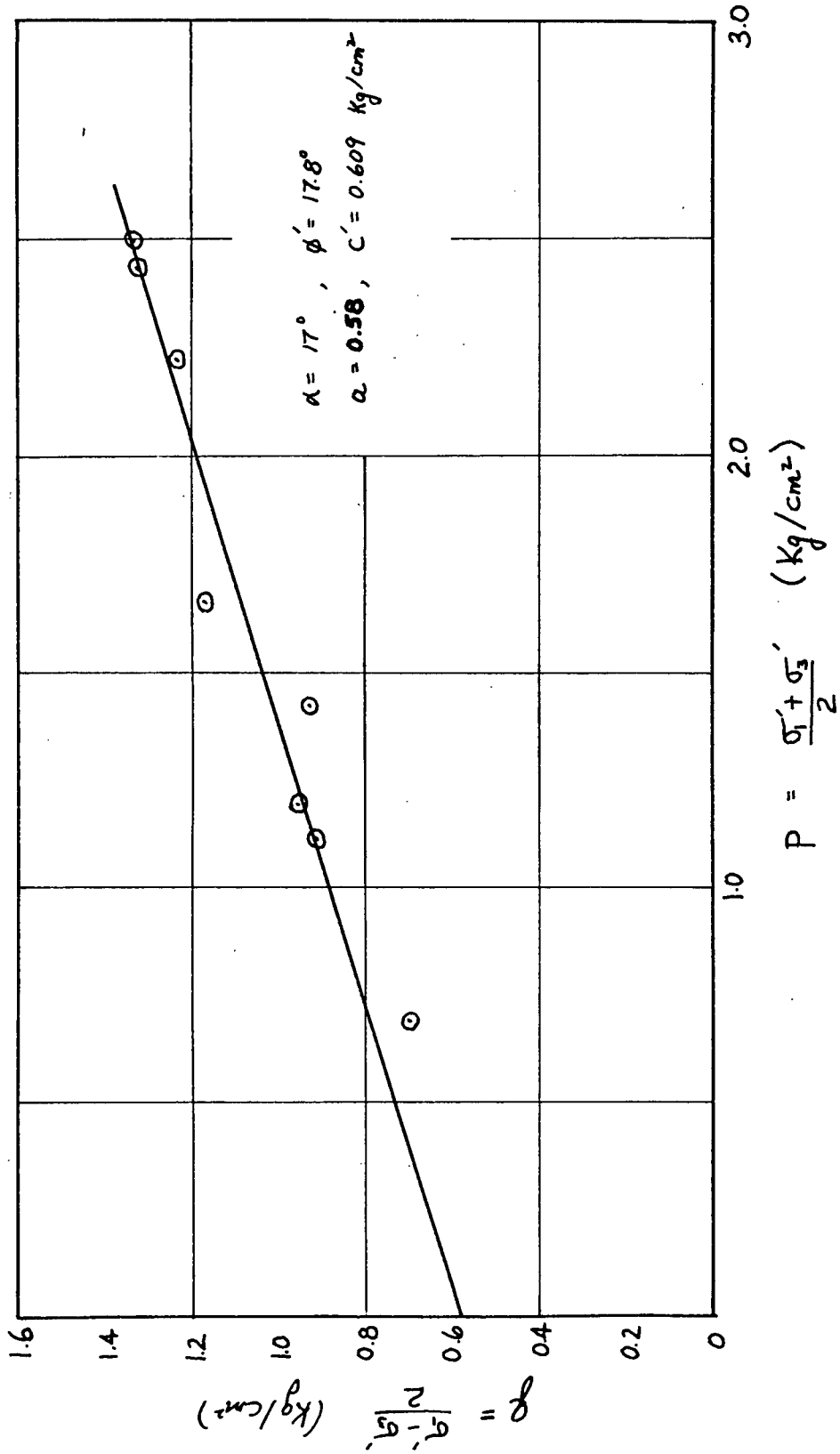


FIG. 27 P-Q DIAGRAM FOR KAMLOOPS SILT (O.C. REGION)

effect exhibited by the silt samples. Therefore, the overconsolidated behaviour of the silt could be due to (1) chemical cementation (2) negative pore water stresses developed during dessication (3) physico-chemical changes and bond formation of the clay due to dessication or (4) a combination of the above. This point will be further discussed after examining the consolidation data in the next chapter.

4.5 Unconventional 'Dry' Triaxial Tests

To determine the effect of water content on the strength of the silt, four triaxial tests were performed at different water contents with a consistent cell pressure of 0.50 kg/cm^2 . The samples were strained at a constant rate of $0.0006 \text{ inches/min}$.

Sample 3.22 was saturated by flushing with water and high backpressures. Sample 3.71 was tested at its natural water content and sample 3.72 was air-dried under constant temperature laboratory conditions for 30 days. Sample 3.73 was oven-dried for 30 days under a constant temperature of 105°C . During testing of the oven-dried sample, precautions were taken to minimize absorption of water from the air. The top drainage of the triaxial apparatus was closed and the bottom drainage was placed in a container of oven-dried dessicant pellets. The sample weight was determined to be the same before and after testing, indicating negligible water was absorbed by the sample during testing.

4.6 Results and Discussions of the 'Dry' Triaxial Tests

The test results are plotted in figure 28 as Mohr circles of failure. From figure 29, it is evident that the strength is sensitive to the

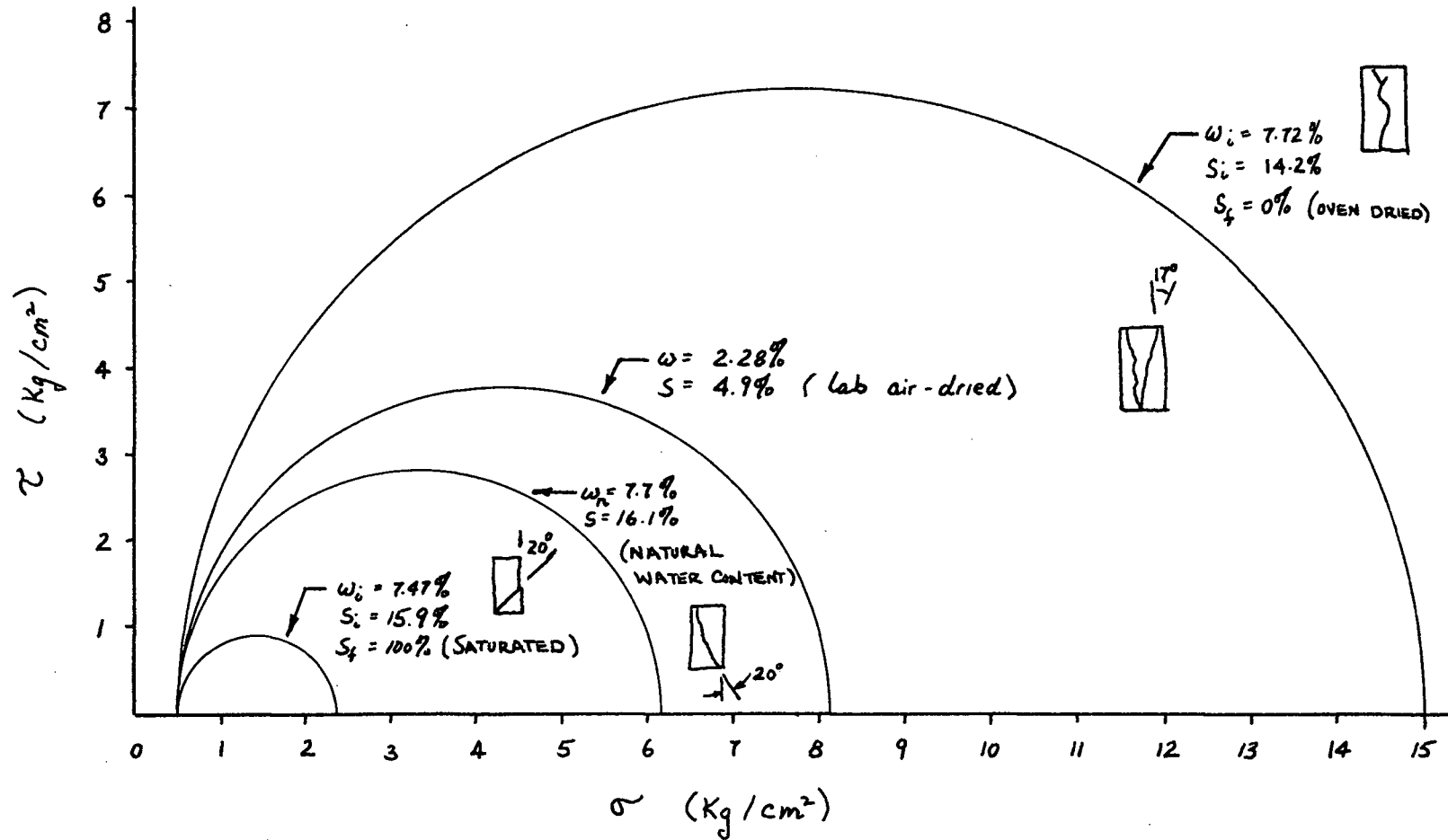


FIG. 28 MOHR CIRCLE OF FAILURE AT VARIOUS SATURATIONS

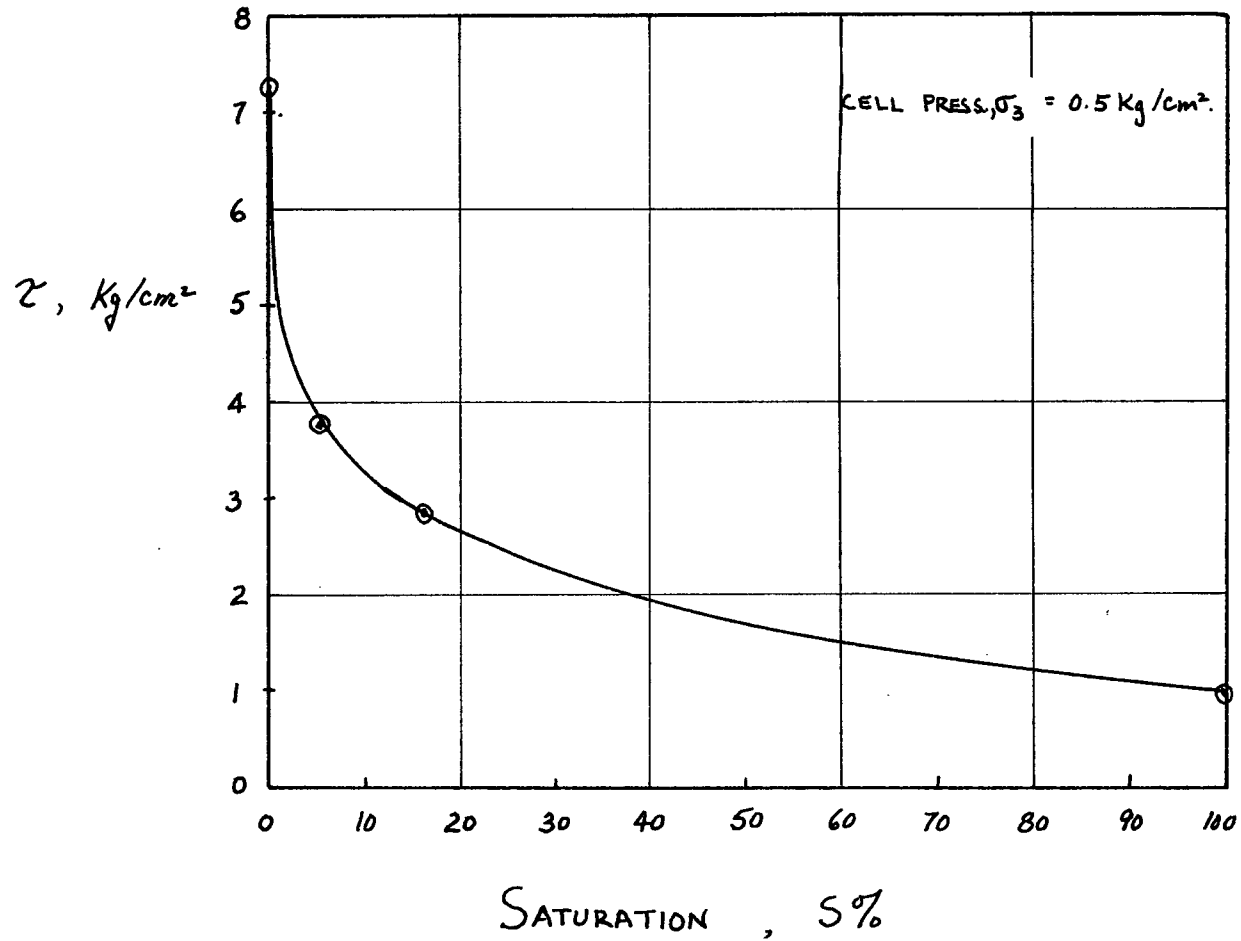


FIG. 29 SHEAR STRENGTH VS. SATURATION
(FOR KAMLOOPS SILT)

degree of saturation, especially towards the drier states. Lutton (1969) found a similar behaviour for Vicksburg loess under unconfined compression. Also, Holtz & Gibbs (1951) reported a different Mohr envelope exists for various saturations of the Kansas and Nebraska loess.

The stress-strain data shows a peak in strength in all four samples tested. Thus under the 0.50 kg/cm^2 confining pressure, the samples were considered to be within the overconsolidated stress range.

The increase in strength exhibited by progressively drier samples may be due to (1) the increase in effective confining stress as a result of pore water meniscii tension, (2) the increase in interparticle bonding of clay particles which may be present between silt grains, or (3) a combination of the above.

For interest, if we assume the total increase in strength to be attributed to water meniscii tension, the magnitude of the negative pore water pressures can be calculated from the Mohr failure criteria. Expressed in terms of principal effective stresses, the criteria is:

$$\frac{\sigma'_1 - \sigma'_3}{2} - \frac{\sigma'_1 - \sigma'_3}{2} \sin \phi' = c' \cos \phi'$$

where σ'_1 and σ'_3 are positive for compression.

In terms of total stresses:

$$\frac{\sigma_1 - \sigma_3}{2} - \frac{(\sigma_1 + \sigma_3 - 2u)}{2} \sin \phi' = c' \cos \phi'$$

where u is the pore pressure, being negative in tension.

Table IV lists the calculated negative pore pressures that would have to develop within the samples to exhibit the strengths measured. The pressure deficiency of 15 kg/cm^2 for the oven-dried sample is only an apparent or "effective" value since there is no free water present within an oven-dried sample. The negative pore pressure of 6.3 kg/cm^2 at 4.9% saturation is in the order of magnitude expected for a silt. Aitchison and Donald (1956) showed that for ideal spherical particles, negative pore pressures in the order of 3.5 kg/cm^2 can be attained for silt-sized particles and pressure deficiencies of 30 kg/cm^2 can be easily realized for clays.

TABLE IV. 'Dry' Triaxial Test Data & Results

Test #	Water content	saturation	σ_3	σ_1	σ_m	α	τ	Calc. U kg/cm ²
3.22	47.8%	100%	0.5	2.341	1.410	24°	0.921	0
3.71	7.71%	16.1%	0.5	6.192	3.346	5°	2.846	-4.067
3.72	2.28%	4.9%	0.5	8.134	4.317	10°	3.817	-6.272
3.73	0.00%	0.0%	0.5	15.048	7.774	3°	7.274	-15.048

All stress values in kg/cm²

4.7 Consolidation Tests

Consolidation testing of silts is not considered standard or conventional. Compared to clays and sands, little information is available concerning the behaviour of silts. Many researchers studying collapsible silts generally perform oedometer tests with the silt at its natural water content (usually low saturation) and with the oedometer mold flooded with water. (Gibbs & Holtz, 1951; Lutton, 1969; Dudley, 1970; Jennings & Knight, 1975).

Although the term 'consolidation' test is adopted in this report, we are not dealing with consolidation in its usual meaning. Conventionally, consolidation is referred to as the expulsion of pore water from the sample leading to compression of the sample. In tests performed on silts, the majority of the 'consolidation' tests are on non-saturated samples and therefore settlements are due to structural changes as the air or air-water mixture is expelled from the soil.

In probing the structure of the Kamloops silt, various consolidation tests were performed. Samples were consolidated at various water contents ranging from saturated to air-dried states. To determine the structural response of the silt to the addition of free ions, samples were flooded with a simulated septic tank effluent and acidic water. Also, samples were remolded into a slurry and allowed to dry out before testing to assess the effect of remolding on structural stability.

Incremental load consolidation was carried out on seven of the 15 consolidation tests of the lacustrine silt. The other eight lacustrine silt samples were tested by the strain controlled method (Byrne & Oaki, 1969). The constant strain rate test was employed since it had the

advantage of producing e -log P data in a much shorter testing time (one hour as compared to the 6 days required for incremental load tests). Also, there is the added advantage of being able to achieve loads much larger than those possible with the incremental load apparatus. Four colluvial samples from the Kamloops area were also tested to determine the degree of structural collapse upon flooding with water (appendix IV).

4.7.1 Consolidation Apparatus

Two setups were used in the incremental load test and two in the strain controlled test. Initially, all consolidation testing was performed with a 3 inch I. D. consolidation ring and a specially designed base fitted into a standard triaxial cell. This allowed the sample to be flushed with water while maintaining a high backpressure to aid in the saturation process. Since the assembly is placed within a triaxial cell, the load was applied through a loading rod, on top of which sits a load cell. For strain controlled tests, the load cell was seated against the rigid frame. For incremental load tests, a rolling belloram air piston was attached to the rigid frame and its loading ram transfers the constant load to the triaxial cell loading rod. At large loads, the compression of the loading rod and load cell become significant. Thus, the compression of the apparatus had to be taken into account when computing the sample deformation. The system compressions (correction curves) are presented in appendix III.

In subsequent tests, since saturation of the sample was not necessary, a simple, more direct loading setup was adopted. For the strain controlled tests, the loading rod and triaxial cell was omitted and the consolidation

ring and porous stones were placed in an open container. With this arrangement, the compression of the loading rod was eliminated, but load cell deflection was still encountered. Appendix III presents the corrections due to system compressibility. For the subsequent incremental load tests, a small simple pneumatic system which was recently designed at UBC was employed. With this system, $2\frac{1}{2}$ " diameter samples were used. System compressibility was essentially negligible and the only extraneous deflections present are due to initial seating deflections which are in the order of 0.003 inches at loads of 450 kg. Thus this simple system eliminates the need for system compressibility corrections due to load cell and loading rod deformations.

4.7.2 Saturation Procedure

Two samples were saturated in the triaxial cell apparatus - one for a strain controlled test and one for an incremental load test. The saturation procedure is similar to that followed in saturating a triaxial sample. Cell pressures were set at 4.00 kg/cm^2 and base drainage pressures were held at 4.10 kg/cm^2 . Thus, the de-aired water was pushed from the belloram reservoir up the sample into the cell reservoir. Since B-values could not be measured in this apparatus, the percolation was continued for an extended period of 30 days in an attempt to insure saturation of the sample.

4.7.3 Experimental Procedure

In the incremental load tests, the applied loads were doubled each 24 hours ($\Delta P/P = 1$) producing 1-day consolidation curves. Increase of the loads were achieved by increasing the air pressure applied to the

loading pistons. Deformation of the sample was measured by a dial gauge attached to the air piston's loading rod as referenced to the fixed frame. Deflections of the dial gauge were corrected for system compressibility when necessary to obtain the true sample settlements.

The strain controlled consolidation tests were performed following the outline by Byrne & Oaki (1969). The sample within the oedometer mold is simply strained at a constant rate while the load is being monitored by a load cell. Thus, high loads can be achieved since we are not limited by the maximum house-line pressures available to the incremental load test apparatus. For saturated samples, the choice of strain rates is generally determined by limiting the pore pressure build-up within the samples to 5-10% of the load. In the case of the highly permeable silt, a strain rate of 0.003 inches/min. produced an insignificant rise in pore pressure within the saturated sample. This strain rate was adopted for most of the strain controlled testing.

4.8 Consolidation Test Results and Discussion

Both incremental load and strain controlled consolidation tests are listed in table V. The colluvial tests which were performed at a later date are listed in appendix IV.

Void ratios of the lacustrine silt ranged from 1.26 to 1.30 with an average of 1.28. All void ratios were calculated before testing by measuring the total sample weight, dimensions within the mold and the water content of the side trimmings of the sample. Recall that the void ratios calculated from triaxial samples were slightly higher due to errors in measuring the sample dimensions. However, with the consolidation ring, the dimensions could be measured accurately by measuring the

TABLE V. 'CONSOLIDATION' TESTS OF KAMLOOPS SILT

Test #	Description	Sample Diam.	Strain Rate	e_o	w%	S%
3.32	saturated	3.0"	0.003"/min.	1.260	43.1%	100.0%
3.33	saturated	3.0"	incr. load	1.279	36.0%	99.7%
3.41	dry, rebounded, flooded	3.0"	dry:0.015 flooded: 0.003"/min.	1.273	40.0%	86.8%
3.42	flooded @ 0.121 kg/cm ²	3.0"	0.003"/min.	1.291	-	-
3.43	flooded @ 0.329 kg/cm ²	3.0"	0.003"/min.	1.283	46.2%	99.8%
3.44	dry	3.0"	0.003"/min.	1.306	2.97%	6.3%
3.45	dry	3.0"	0.00011 in./min.	1.281	2.44%	5.3%
3.51	moist	3.0"	0.003"/min.	1.301	22.8%	48.6%
3.62	dry	2.5"	incr. load	1.277	7.15%	15.3%
3.R1	remolded, dry, flooded @ 6.786 kg/cm ²	2.5"	incr. load	1.141	1.70%	$S_i = 4.1\%$ $S_f = 87.8\%$
3.64	flooded @ 0.890 kg/cm ²	2.5"	incr. load	1.274	36.6%	92.3%
3.66	flooded @ 0.845 kg/cm ²	2.5"	incr. load	1.269	36.1%	93.8%
3.67	dry	2.5"	0.003"/min.	1.263	6.54%	14.3%
3.R2	flooded @ 0.889 kg/cm ²	2.5"	incr. load	1.137	32.9%	94.2%
3.71	flooded with 0.01M HCl	2.5"	incr. load	1.208	-	-

TABLE VI. RESULTS OF THE CONSOLIDATION TESTS

Test #	Description	"max. P" kg/cm ²	Compression Index, C _c	
3.62	undisturbed, dry, S=15.3%	14.5	-	incremental load tests
3.R1	remolded, dry	13	-	
3.64	flooded with water	5.9	0.303	
3.66	flooded with chemical solution	4.5	0.271	
3.33	saturated with water	3.7	0.275	
3.R2	remolded, flooded	2.1	0.151	
3.71	flooded with 0.01M HCl	2.4	0.222	
<hr/>				
3.45	undisturbed, dry, S=5.3%	26	-	strain controlled tests
3.44	undisturbed, dry, S=6.3%	26	-	
3.67	undisturbed, dry, S=14.3%	13	0.240	
3.41	dry, S=14.4%	12	0.240	
3.51	moist, S=48.6%	7.8	0.189	
3.43	flooded, S=99.8%	6.2	0.215	
3.33	saturated, S=100%	6.3	0.252	
3.42	flooded, S=?	5.6	0.225	

inside volume of the mold itself.

The void ratio of the colluvium was 1.07 and 1.35 for the two different sample sites. While the void ratio of the lacustrine silt is fairly uniform, the void ratio of the colluvium appears to vary with location.

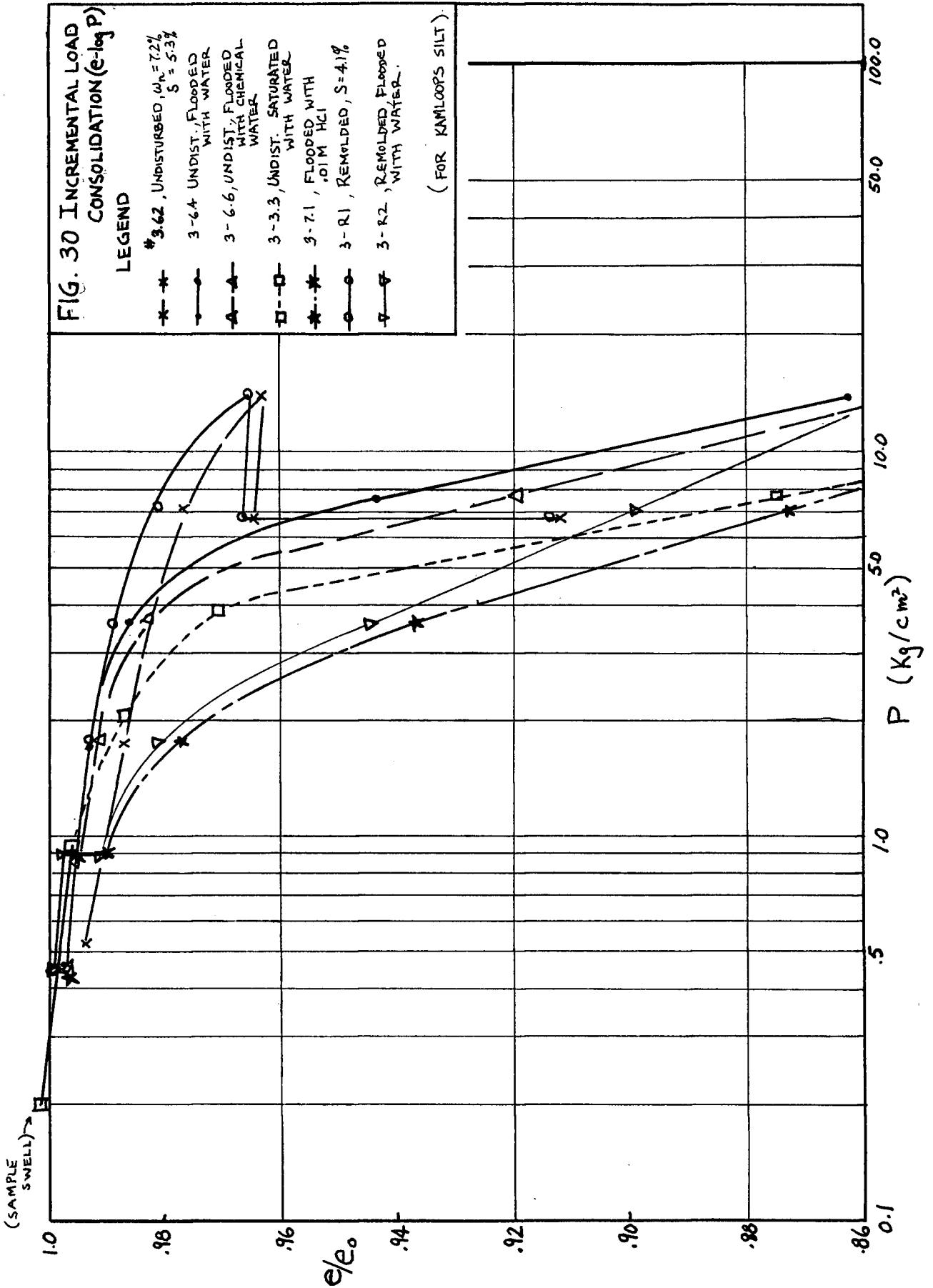
Initially, there was concern that the soil squeezed out due to large initial hydraulic gradients at the top of the incremental load sample would be significant and therefore would alter the shape of the e-log p curve. Since the large gradients are non-existent in strain controlled tests, the comparison of the two sets of data may be affected by the loss of soil in the incremental load test. The amount of soil lost was measured after the completion of 3 of the consolidation tests and it was found that the soil lost was less than 1 gram, representing less than 1% of the soil sample weight and therefore was considered too small for concern.

4.8.1 Incremental Load Results and Discussions

One-day incremental load tests of the lacustrine silt were performed under various conditions:

1. at natural moisture content (#3.62)
2. flooded with de-aired water (#3.64)
3. saturated sample (#3.33)
4. flooded with simulated septic tank effluent (#3.66)
5. flooded with 0.01M HCl (#3.71)
6. air-dried remolded sample (#3.R1)
7. flooded remolded sample (#3.R2)

The e-log p curves of the tests are presented in figure 30. Each curve will be discussed separately.



1. Sample at natural water content (#3.62)

At the water content of 7.2%, the silt behaves as a highly incompressible soil with the 'effective maximum past pressure'¹ of 14 kg/cm^2 . Upon rebound to 6.67 kg/cm^2 , flooding of the sample with drinking water resulted in an additional 3.2% ($\Delta e/e_0$) decrease in bulk volume. The majority of the collapse occurred within the first hour (fig. 31).

2. Flooded sample (#3.64)

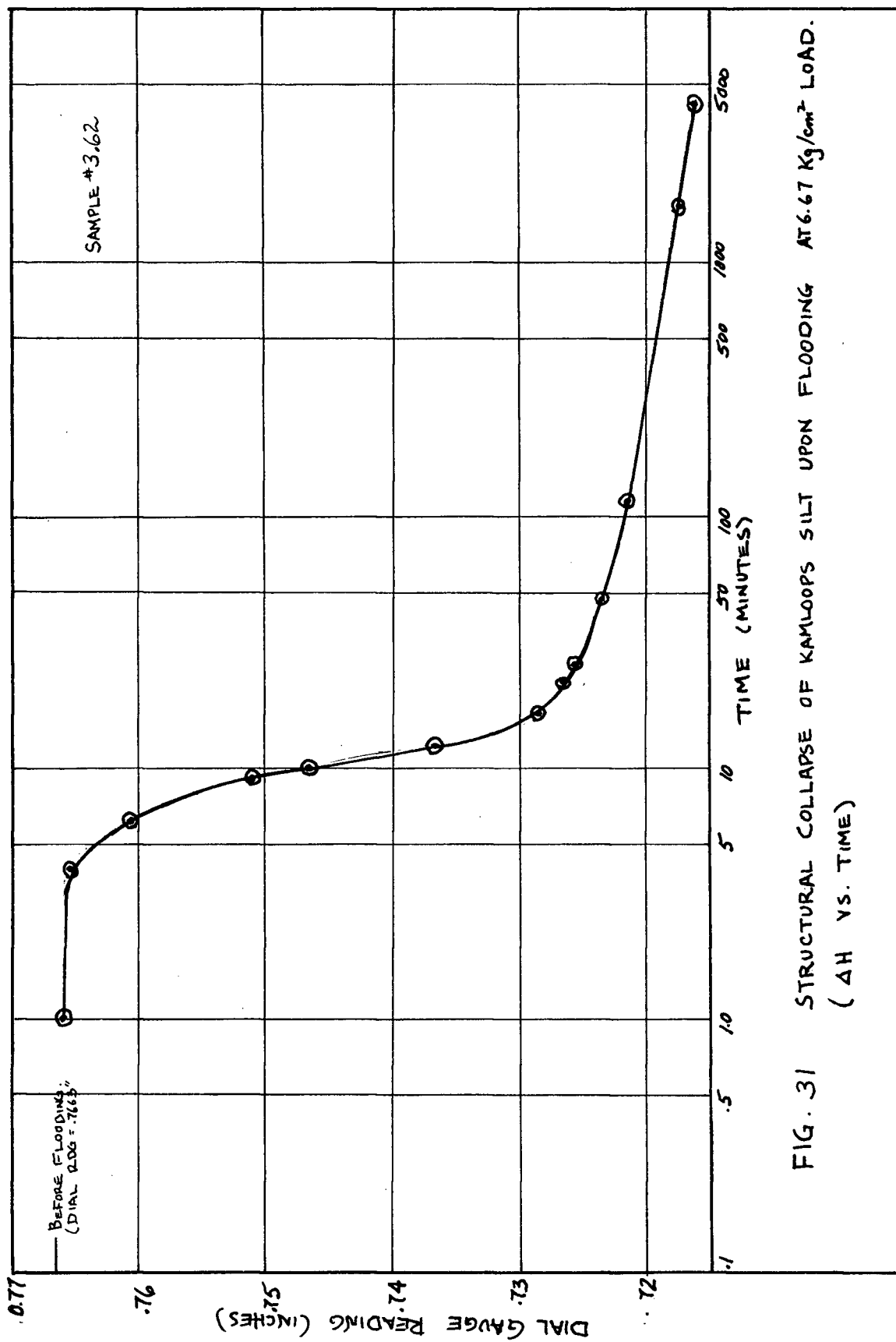
Sample 3.64 was consolidated to 0.89 kg/cm^2 and then flooded with de-aired drinking water. Upon flooding, no additional settlement occurred. Further consolidation in its flooded state resulted in a much lower maximum past pressure than that for the dry sample (4.5 kg/cm^2 as compared to 14 kg/cm^2 for the sample consolidated at natural water content).

3. Saturated Sample (3.33)

The saturation procedure was described in section 4.7.2. The maximum past pressure is 3.7 kg/cm^2 and the virgin slope (C_c) is steeper than that of the flooded sample.

Since the sample was saturated, the pore pressure dissipation could

1. Although the term 'maximum past pressure' or 'maximum preconsolidation pressure' is used in the text, the term is used only to denote the limiting pressure, beyond which deformations increase considerably (ie. the transition to 'virgin' compression). This particular pressure value cannot be considered to be a true preconsolidation pressure because it varies with the degree of saturation and with the type of liquid saturating the soil. Furthermore, the ability of the soil to support loads at stresses below this limiting value may not be due to past stress history, but is most likely due to some type of intergranular bonding such as cementation, clay bridging or capillary tension.



be monitored along with the settlement upon application of each load increment. With each load increment, at least 50% of the settlement occurred within the first 15 seconds. The settlement versus log-time curves (fig. 32) are slightly concave up at the start and are very near to being linear towards the end of each increment. This implies that a large portion of the settlement is due to secondary consolidation. Figure 33 compares the pore pressure at the base of the sample (drainage at the top only) to the measured compression for a given load increment. After 5 minutes, pore pressures have essentially fully dissipated but the settlements continue at almost a constant rate (on a log-time plot). Therefore, at standard load increments ($\Delta P/P=1$), creep behaviour constitutes a substantial role in the consolidation characteristic of the wetted silt.

4. Flooded with simulated septic tank effluent (#3.66)

In some soils, the collapse behaviour is dependent on whether the soil is flooded with drinking water, sewage water or an acidic solution. (Reginatto & Ferrero, 1973). Since leakages from septic tanks could be a concern, the collapse characteristics of the silt is determined by a simulated septic tank effluent. Typical septic tank effluent from Kal Terrace, Vernon, B.C. in 1972 were reproduced in a chemical solution for its exchangeable cation concentrations. Since no septic tank chemical analysis were readily available from the Kamloops area, it was assumed that the concentrations obtained from Kal Terrace were in the order of magnitude expected in the Kamloops region.

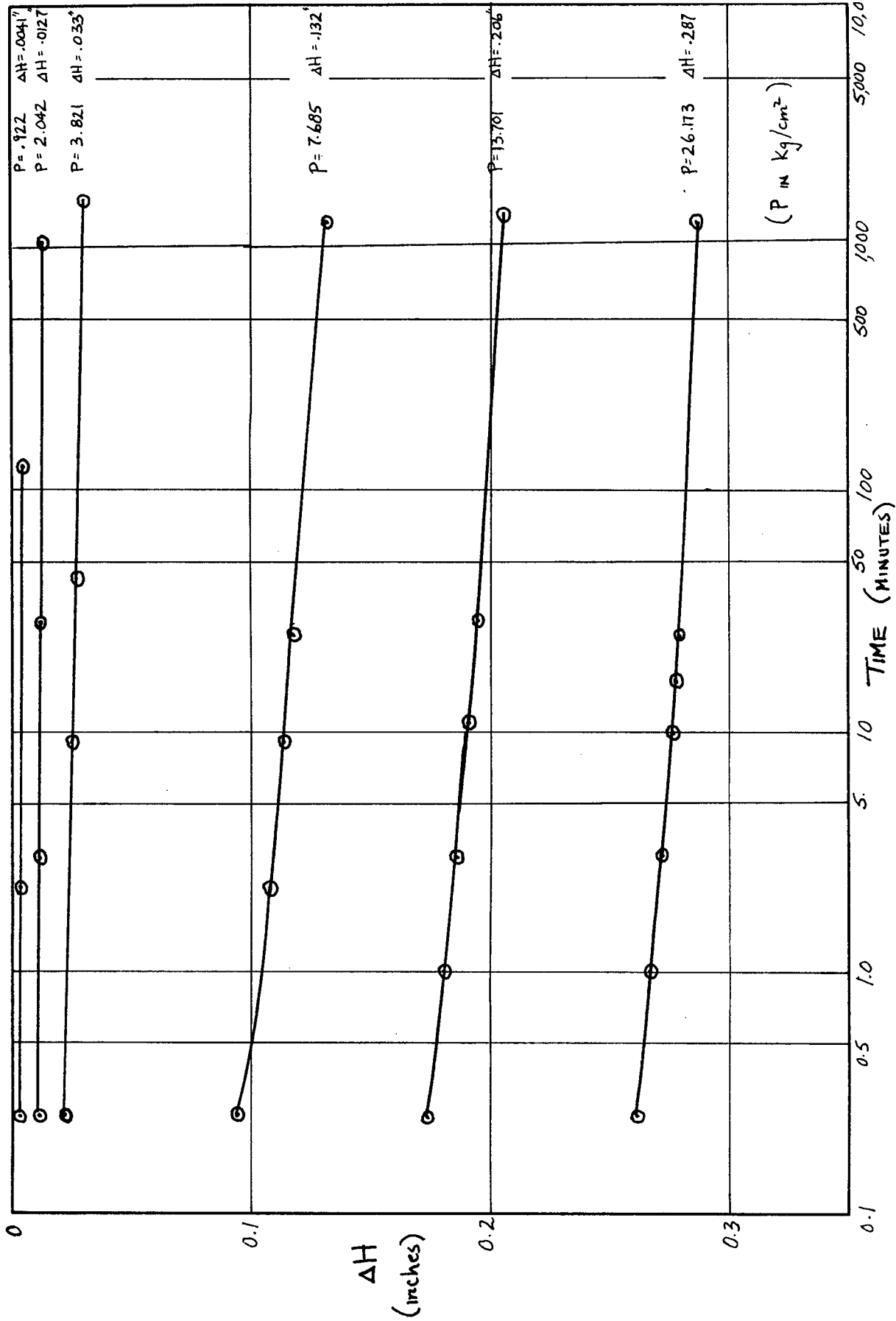
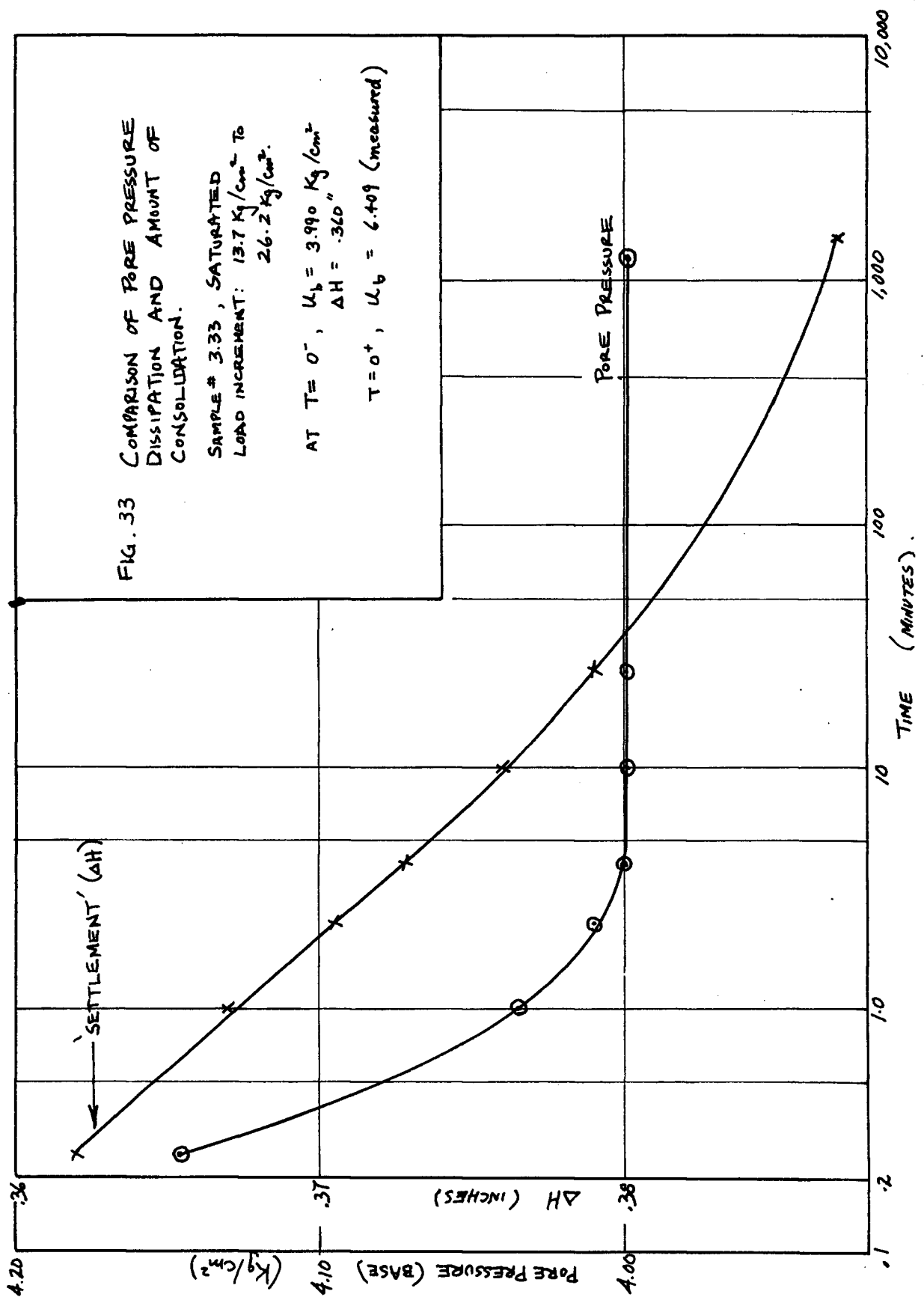


FIG. 32 ΔH VS. LOG(TIME) PLOT FOR INCREMENTAL LOAD CONSOLIDATION OF SATURATED KAMLOOPS SILT (SAMPLE #333, SINGLE DRAINAGE)



The exchangeable cations and their concentrations are:

Ion:	Ca	Mg	K	Na
Concentration (ppm):	71	36	15	68

The pH of the effluent was also duplicated as 7.8.

Figure 34 shows that the consolidation behaviour is not grossly different to that of the samples flooded with just drinking water from Vancouver, although a slight decrease in maximum past pressure is noted. However, the possibility of further settlements on a much longer time scale than that realized in the laboratory must be borne in mind. Also, it should be noted that effects due to chemicals and organic matter not duplicated in the chemical solution are not known.

5. Flooded with 0.01M HCl (#3.71)

It was noted that a drop of 0.5M HCl produced a strong reaction on the silt (appendix I). Thus, a consolidation test was carried out with a strong solution of HCl (0.01M). The resultant consolidation curve exhibited a more compressible behaviour than the samples flooded with drinking water. The maximum past pressure was 2.4 kg/cm^2 as compared to 4.5 kg/cm^2 for the silt flooded with domestic water.

6. Air-dried Remolded sample (#3.R1)

The remolded sample was formed by mixing the silt with distilled water to form a slurry. The slurry was then allowed to dry in the constant temperature laboratory environment for 30 days. The remolded sample was initially conceived as an attempt to re-duplicate the lacustrine silt's

properties. However, from figure 30, we see that the behaviour of the undisturbed lacustrine silt and the remolded sample at the same water content does differ. The remolded sample with its saturation of 4.1% exhibits a maximum past pressure of 13 kg/cm^2 while a lacustrine silt tested at a similar saturation (5.3%) has a much higher maximum past pressure of approximately 26 kg/cm^2 .

Since the void ratio of the undisturbed Kamloops silt is 1.28 while the void ratio of the remolded sample is 1.14, the consolidation curves have all been normalized (e/e_0) in an attempt to account for differences in the shapes of the consolidation curves due to differences in initial void ratios.

7. Flooded Remolded Sample (#3.R2)

In the flooded state, the maximum past pressure of the remolded sample is 2.1 kg/cm^2 with $C_c=0.151$ which is similar to that of the sample flooded with HCl. This similarity suggests that the same type of bonding (eg. calcium carbonate) destroyed by the HCl was also destroyed by remolding the silt and that this bonding was not recovered upon drying.

4.8.2 Strain Controlled Consolidation - Results & Discussions

Eight constant strain rate consolidation tests were performed at various degrees of saturation:

1. laboratory air-dried state (#3.44 & #3.35)
2. at natural water content (#3.41 & #3.67)
3. at moist conditions, $w\% = 23\%$ (#3.51)
4. flooded state (#3.42 & #3.43)
5. saturated state (#3.32)

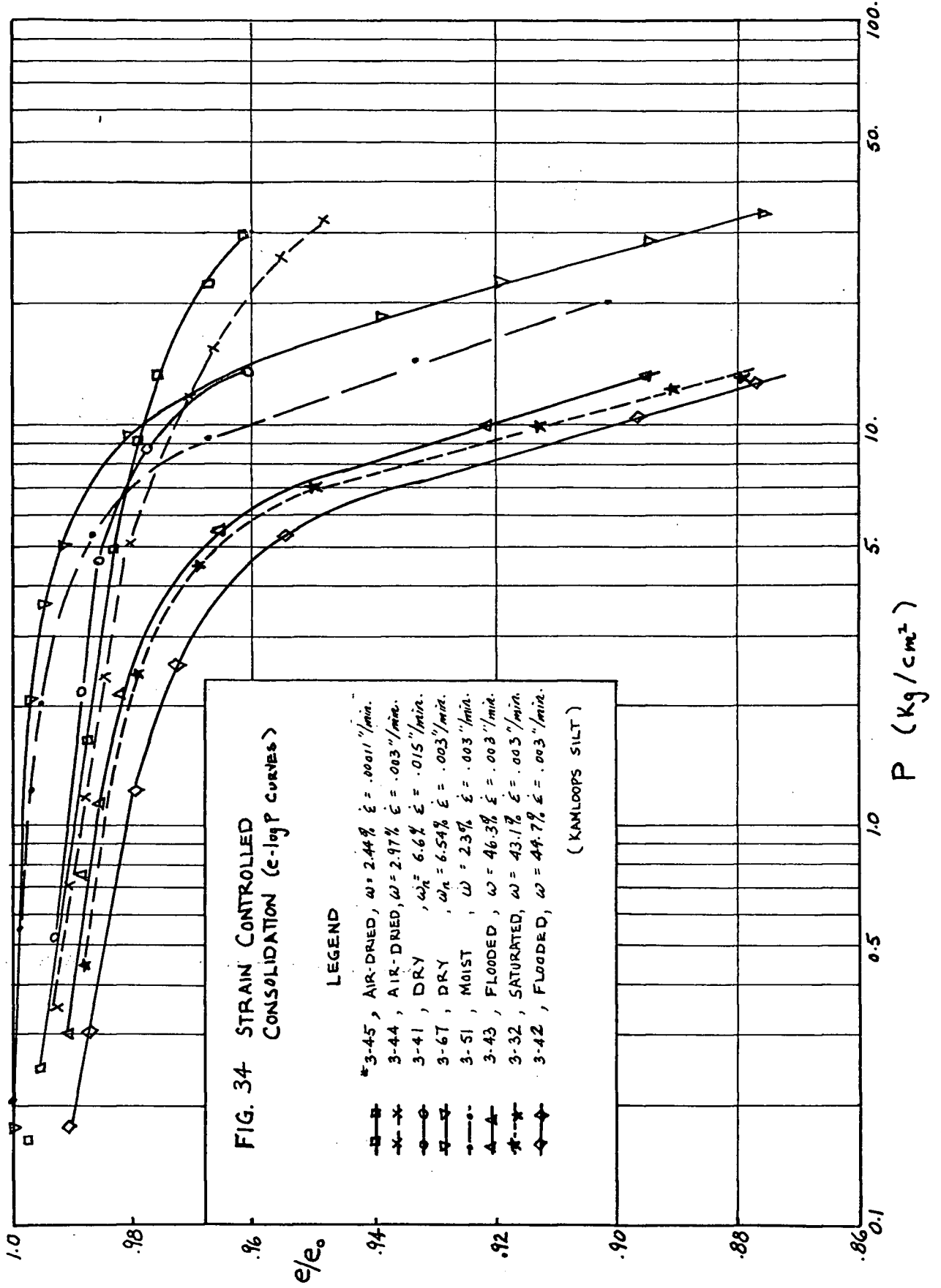
Figure 34 presents the data in an e/e_0 versus $\log p$ plot. Table VI (pg. 56) summarizes the 'maximum past pressures' and ' C_c ' of the consolidation tests.

1. Air-dried state (#3.44, #3.45)

Samples #3.44 and #3.45 were consolidated at different strain rates (0.003"/min. and 0.00011"/min. respectively) in an attempt to determine the effect of strain rate on the shape of the consolidation curves. From figure 34, it is evident that the two consolidation curves diverge at higher stresses, but it is believed that a large part of this difference in consolidation characteristic is due to the slight difference in water content of the samples rather than due to strain rate effects.

2. At natural water content (#3.41, #3.67)

The slight increase in water content from the air-dried state (water content of approximately 3%) to the natural water content (approximately 6.5%) produced a marked decrease in the maximum past



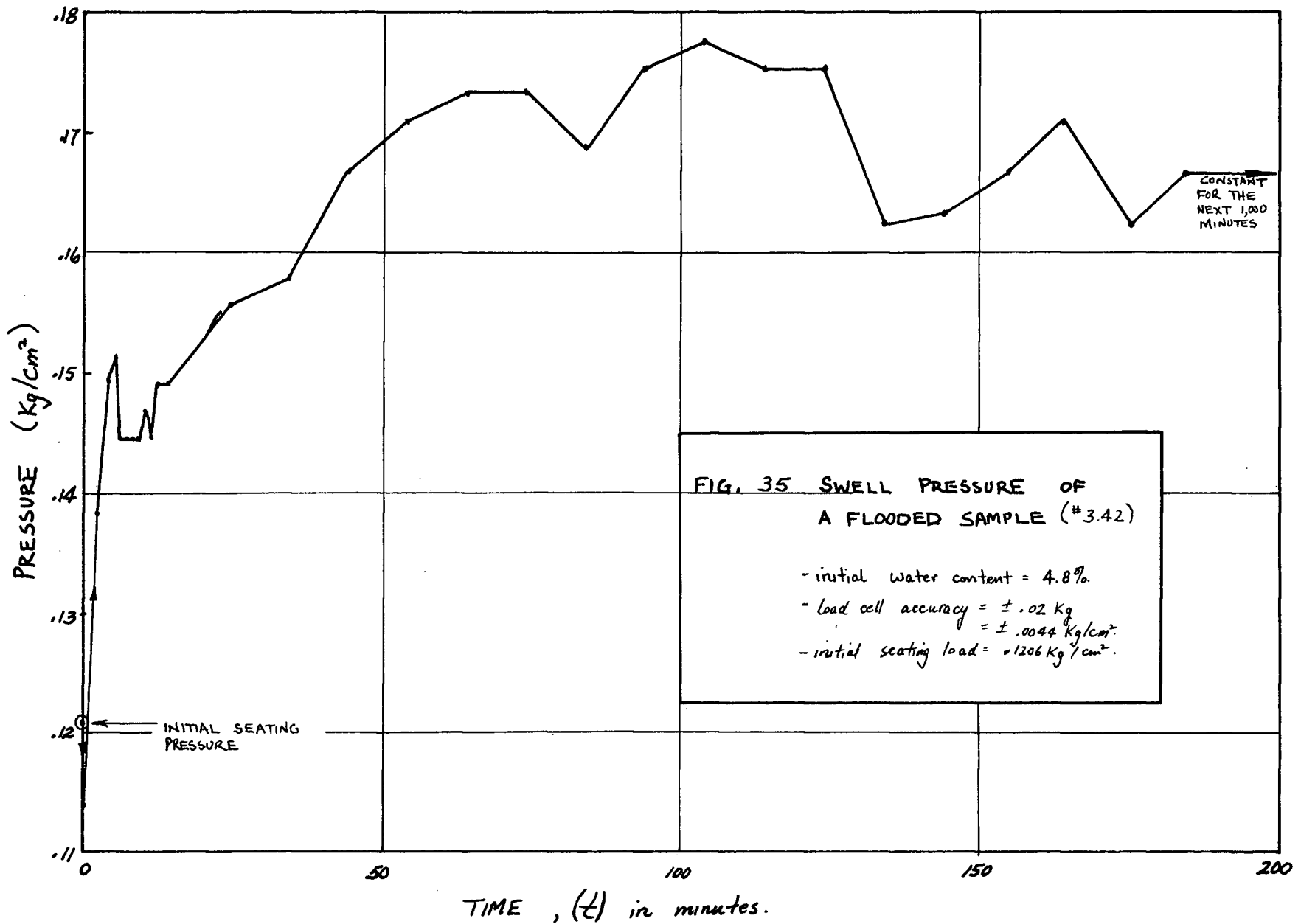
pressure of the silt. The maximum past pressure decreased from 26 kg/cm^2 to 13 kg/cm^2 .

3. Moist state (#3.51)

The water content of 23% of the moist sample was obtained by placing the trimmed sample between two wetted porous stones. The water within the porous stones were absorbed by the silt and distributed uniformly throughout the sample by allowing the silt to stand for two days within the triaxial cell. The test result indicates a further decrease in maximum past pressure as a consequence of increasing the water content of the silt.

4. Flooded states (#3.42, #3.43)

With a constant seating load, the soil response on flooding was noted by the swelling tendencies of the sample at low confining stresses (0.2 kg/cm^2) and slight collapse at higher seating pressures of 0.8 kg/cm^2 . With a strain controlled test, a small seating load is applied to the sample and swelling is prevented by confining the soil between rigid loading platforms. Upon flooding, the response of the sample can be monitored by the heave pressures measured by the load cell. Figure 35 presents the stress response of the soil with time after flooding of the sample. Initially, there is a slight rapid drop in pressure followed by a rapid pressure increase. The initial drop is possible due to the large inward gradient produced upon flooding. The build-up in pressure may be a result of the destruction of capillary tension and the swelling of the montmorillonite within the silt.



The consolidation curves of the flooded samples from the strain controlled test closely approximates the curves obtained from the incremental load tests of flooded samples.

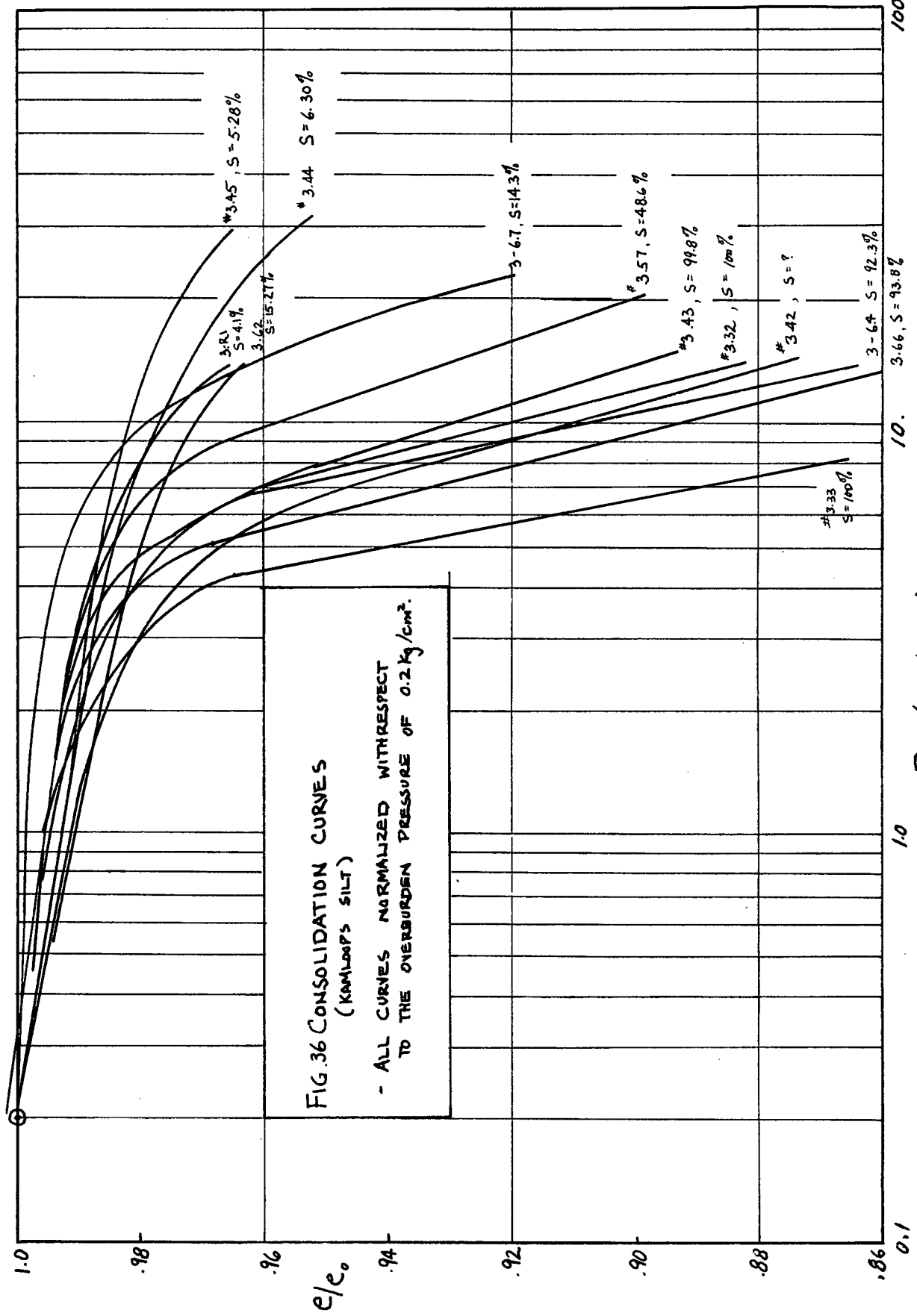
5. Saturated state (#3.32)

The saturation procedure of this sample has been described in section 4.7.2. The resultant data shows little difference in consolidation behaviour between a flooded and saturated sample. Thus it is possible that the slightly higher compressibility of the saturated sample tested in the incremental load procedure is due to a combination of structural disturbance due to initial sample swell and the shock disturbance by sudden pore pressure increases at the beginning of each load increment (Crawford, 1964).

4.8.3 Discussion of Combined Results

Figure 36 plots the incremental load data and strain controlled consolidation data onto one graph. The void ratios have all been normalized to minimize the effects of variances in initial void ratios. Furthermore, all curves are shifted to the same reference point where the normalized void ratio is unity at the field overburden pressure. Since the samples were obtained from a depth of approximately 5 feet, the normalized void ratios of all samples should be unity at 0.2 kg/cm^2 of overburden pressure. This shifting of all the curves accounts for errors in defining the initial seating position of the samples.

Figure 36 clearly reveals the effect of water content on the compression characteristics of the silt. The silt is highly sensitive to changes in



moisture content - especially at low degrees of saturation. In the air-dried state of 5.3% saturation, the maximum past pressure is extremely high (26 kg/cm^2). In the flooded and saturated states, the preconsolidation pressure drops to approximately 6 kg/cm^2 . Samples which are structurally altered by remolding or by ponding with 0.01M HCl exhibits maximum past pressures of 2.1 and 2.4 kg/cm^2 respectively.

Upon wetting by ponding of the relatively dry soil, at high seating loads, a decrease in bulk volume results. The decrease in bulk volume does not follow the classical consolidation theories but instead involves a collapse of intergranular structure which can occur in a brief period of time. The following terms have been applied to this behaviour: collapse, collapsing soil, near surface subsidence, subsidence, hydro-compaction, and hydroconsolidation (Dudley, 1970).

Further discussion of the collapse behaviour of the Kamloops silt is presented in the following chapter along with a brief literature review.

CHAPTER 5

STRUCTURAL INSTABILITY OF THE KAMLOOPS SILT

5.1 LITERATURE REVIEW ON COLLAPSIBLE SOILS

5.1.1 Collapsible Soils

Collapsible soils have been found in various forms throughout the world. In general, they have been located in arid regions and due to the increasing utilization of these areas in recent years there has been a growing awareness of the problem.

The types of soils that display a collapsing behaviour vary tremendously. They can be air deposited, water deposited, residual or man made and generally consist of silt and fine sand forming a loose open structure. In many cases, the soil deposit will collapse under its own weight when saturated. This condition has been termed "truly collapsible" by Reginatto & Ferrero (1973). Other soils will exhibit collapse upon wetting only when sufficiently high stresses are applied to the soil structure. These have been termed "conditionally collapsible" since the externally applied pressure level governs whether collapse will occur or not.

5.1.2 Collapse Mechanisms

The mechanisms involved in the collapse phenomena have been summarized by Dudley (1970). The basic concept is that of open structure of bulky shaped grains held together by some bonding material or force.

This bonding must be susceptible to removal or reduction by the introduction of additional water, allowing the grains to slide into the vacant spaces.

The three commonly proposed mechanisms were summarized by Dudley (1970):

1. Capillary Tension

In many cases, this temporary strength is due to capillary tension within the partially saturated soil. Generally, the soil gains strength until a certain saturation is reached and saturations exceeding this optimal value results in a decrease in soil strength. For silt and fine sand, the peak effective stress value usually exists at moisture contents less than saturation and above 10% moisture (Aitchison & Donald, 1956). When the soil is flooded to near saturation, the capillary tensions are decreased or destroyed, thus reducing the effective stress which reduces the intergranular shear strength, thus allowing the grains to collapse into a more stable arrangement (Moore & Millar, 1971).

2. Clay Coatings and Clay Buttresses

With large particles, the bulk of the intergranular forces may consist of capillary forces. The magnitude of the capillary forces increases with decreasing particle size. However, for clay sized particles, the forces of repulsion, Van der Waals and molecular attraction become much more significant. Thus, with more and more clay particles present in the soil, the effect of capillary forces may become proportionally less as the electro-chemical forces become relatively more prominent.

A number of possible structural arrangements become possible, depending on the geologic origins and history of the soil. When the clay is formed by weathering in place (by authigenesis), a thin clay coating may exist around the individual silt grains. Under dessicated conditions, this structure could have considerable stability; but with the addition of water, the clay plates may tend to swell and separate to some extent, thereby producing a loss of strength.

An alternate structural arrangement could be formed if the clay particles were originally suspended in water. As the deposits dried, the clay plates are drawn into the interparticle contact area of the larger grains. The evaporation process would concentrate the dissolved ions in the fluid causing the clay plates to flocculate into a buttress arrangement. Upon the addition of water, the ion concentration would decrease causing an increase in repulsive force between the clay plates resulting in a decrease of intergranular support.

As the grain sizes decrease into the smaller clay sizes, the capillary forces contribute a lesser portion of the total forces present as the electro-chemical forces increase in magnitude. However, capillarity between clay plates would still be important (Dudley, 1970). Barden, McGown & Collins (1973) also stress the difficulty of distinguishing between the portion of the strength due to capillary forces and that due to clay interparticle bonds:

"There are clearly many possible variations in the structural arrangement of the clay plates between the quartz grains. The nature of the clay bonding is complicated, and it is never clear how much is due to electro-chemical effects and how much to capillary effects. The important point is that in most cases the lower the water content of the clay the greater the bond strength." p. 51.

3. Chemical Cementing Agent

Structural instability may result from the loss in strength of a cementing agent. The rate of structural weakening would depend on the nature and concentration of ions within the incoming water as well as the natural dissolution rate of the chemical cementing agent. In general, the strength breakdown of the chemical cementing agent due to infiltrating water is a slower process than strength loss due to capillary tension dissipation and the collapse of clay buttresses.

In recent years there have been a number of electron microscope studies performed on various collapsible soils. Barden, McGown & Collins (1973) and Collins & McGown (1974) have shown microphotographs supporting the existence of the general collapse structures mentioned above.

For some soils, the collapse phenomena is strongly dependent on the characteristics of the liquid saturating the soil. For example, loessial soils in the Cordoba region of Argentina frequently exhibited more settlement for cases of ruptured sewage pipes than for cases of wetting with plain water (Reginatto & Ferrero, 1973). These soils exhibit even more subsidence when flooded with acidic water.

5.1.3 Engineering Applications

The practical problem facing the engineer involves the difficult task of predicting the presence of these collapsing soils. Many indexes are proposed for predicting the occurrence of collapse based on natural void ratios vs. void ratios at their liquid limit and on dry densities

of the soil (Markin, 1971; Gibbs & Bara, 1967; Denisov, 1961; Dudley, 1970). However, it is commonly agreed that the indices are not completely reliable for differentiating between collapsible and non-collapsible soils (Dudley, 1970; Evans & Buchanan, 1976).

To obtain quantitative information on the amount of collapse, the double oedometer test presented by Jennings & Knight (1957) is commonly used. In this test, two similar samples are tested; one at field moisture content, and one saturated. The total collapse due to saturation under a certain load can be determined simply by considering the change in void ratio between the two curves. However, as the tests do not completely reproduce field conditions, correction factors based on experience in the area must be applied to the test data to predict the collapse that will occur in the field (Dudley, 1970; Jennings & Knight, 1975).

In some cases, the engineer is also concerned with the time required for certain portions of the total collapse to occur. As a rule, however, the durations measured in the laboratory are much shorter than that which is experienced in the field (Rabinovich & Urinov, 1974). Usually settlements due to collapse in incremental load tests stabilize after several hours (fig. 31) whereas the collapse of soils under foundations of buildings sometimes continues for several months. Furthermore, the type of temporary bonding that exists in the soil would be expected to govern the rate of collapse. In the case of capillary suction the drop in strength will be immediate; in the case of the bridging clay, rather slower; and in the case of chemical cementing it might be very slow (Barden McGown & Collins, 1973).

5.2 COLLAPSE PHENOMENON OF THE KAMLOOPS SILTS

The glaciolacustrine silt under study is a conditionally collapsible soil as defined by Reginatto & Ferrero (1973). Whether or not the soil structure will undergo collapse when flooded with water is dependent on its present stress state. At very low confining pressures, the soil exhibits heaving when flooded; and at higher stress levels, collapse occurs. This type of behaviour is also found in some dry clays (Jennings & Knight, 1975). For Kamloops silt, the actual critical confining pressure where no volume change results due to flooding lies between 0.2 kg/cm^2 and 0.8 kg/cm^2 . The heave exhibited at lower stresses is possibly due to the swelling of the montmorillonite (approximately 3-4% of the solids; Quigley, 1976) and/or the dissipation of capillary forces which may be present within the soil.

The 'maximum preconsolidation pressure' is approximately 26 kg/cm^2 for the air-dried state and 6 kg/cm^2 for the flooded state. Therefore, very little subsidence due to wetting would be expected to occur at stresses less than 6 kg/cm^2 (see fig. 37). The collapse is approximately 2% at 6 kg/cm^2 . For the stress levels commonly encountered in footing designs and most engineering problems, the Kamloops silt is not a problem soil from the collapse aspects inspite of its high in-situ void ratio (fig. 37). However, the leaching of the soil by acidic water will cause additional subsidence. The 'maximum past pressure' for the silt flooded with 0.01M HCl is 2.4 kg/cm^2 . At this stress, the laboratory collapse is approximately 2%. At higher stresses, settlement problems may arise especially when differential settlements could easily result due to local flooding by acidic solutions. Although the acidic concentrations

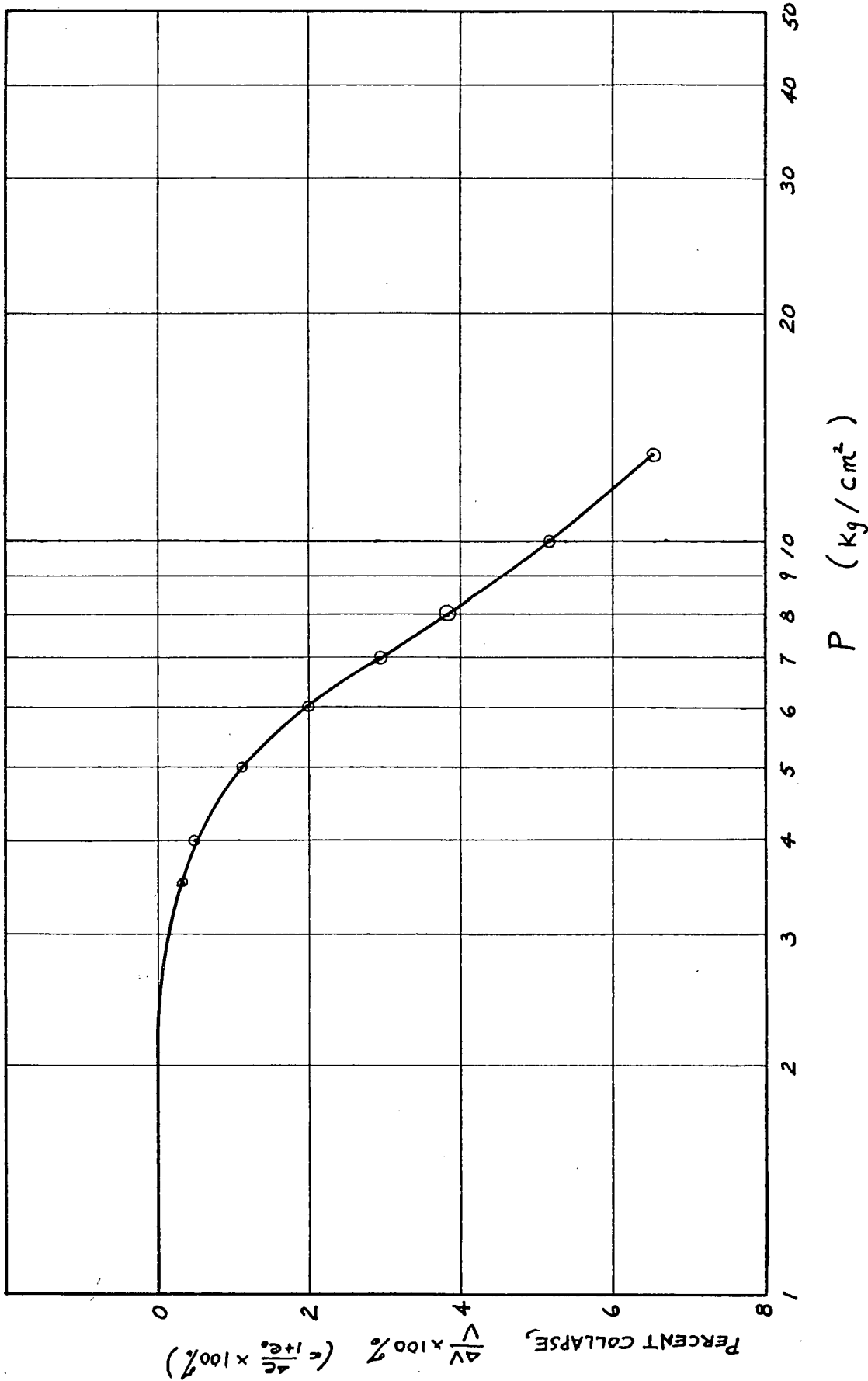


FIG. 37. % COLLAPSE VS P

NOTE: The % Collapse shown are
Approximate values for flooding
 a sample with an initial
 Saturation of 5.3%

encountered in the field due to water percolating through topsoil and decayed vegetation are much smaller than the laboratory concentration, the long term effect of reducing the silt's structural stability is still present.

5.3 COLLAPSE MECHANISM

In order to understand the behaviour of the silt, an attempt must be made to isolate the collapse mechanism involved. Based on the extensive laboratory test results, a hypothesis is proposed.

It appears that the strength exhibited by the silt in its natural dry state is not the result of any one single factor, rather, it is a complex interaction of capillary tension, interparticle clay attraction and chemical cementation. Theoretical computations presented with regard to capillary stresses by Aitchison & Donald (1956) indicates that for unsaturated silts (0.02mm to 0.002mm), the effective stresses may be in the range of 0.35 kg/cm^2 to 3.5 kg/cm^2 . In clays, capillary stresses as much as 100 kg/cm^2 may be realized. For the Kamloops silt, the possible effective stress due to capillary forces as calculated from the strength data (table IV, p.50) is 6.3 kg/cm^2 for a water content of 2.28% and 15.0 kg/cm^2 for an oven dried sample (making the gross assumption that capillary forces may exist in an oven-dried sample (p.49)). The magnitude of these stresses are certainly within reason as compared to the idealized values, especially when consideration is given to the presence of clay within the soil. However, it has been shown that peak effective stress due to capillary tension for silts occur between 10% moisture content and 100% saturation (Dudley, 1970; Aitchison & Donald, 1956).

Capillary tension is considered non-existent in the oven-dried state.

As the water content of the soil increases, capillary tension also increases until at a certain water content, the meniscii forces are at a maximum. Raising the water content further results in a decrease in capillary force and consequently results in a decrease in effective stress within the soil which is reflected by a decrease in soil strength.

Thus, for a soil whose bonding strength is solely due to capillary forces, we would expect an increase in strength with increasing water content until some optimum water content is reached. Beyond this moisture level, the strength would drop again.

A series of triaxial tests were performed (section 4.5, p.45) at the same confining stress but at various water contents to determine if capillary forces were solely responsible for the silt's strength. The resultant strength data (fig. 29, p.47) shows that the soil strength increases with continually decreasing water content; reaching maximum strength in the oven-dried state. In light of the above discussion, this behaviour rules out the possibility that the bonding strength is due solely to capillary forces between silt grains.

The results of increasing strength with continually decreasing water content indicates that interparticle clay is mainly responsible for the silt's bonding strength (Barden, McGown & Collins, 1973). Thus, it is hypothesised that the bulk of the silt's dry strength is largely due to interparticle (clay) forces; that is, the second source of temporary bonding presented by Dudley (1970)(section 5.1.2) is expected to apply to the soil under study. The presence of clay between silt grains produces interparticle attractive forces such as Van der Waals' forces and London forces. Any water present in the soil will migrate to particle contacts

upon being dried and will result in capillary forces to be present also. At lower water contents, the clay plates come closer and closer together, forming stronger interparticle bonds. Upon flooding of a dry sample, the menisci are broken and the ion concentration between clay plates decrease. The reduction of ion concentration within the pores decreases the attractive force between clay plates resulting in separation of clay particles and loss of intergranular strength. The destruction of meniscii forces is also accompanied by a loss of effective stress resulting in a further decrease of intergranular strength. Micro-shearing between grains can occur under sufficient stress levels leading to structural collapse. Thus, it is the clay attractive forces which provides the bulk of the strength with capillary forces contributing to an unknown fraction of the total soil strength.

Searching for more evidence that interparticle clay is the major source of bonding strength, the electron scanning microscope was employed to "visually" study the silt. Although electron microphotographs do not show the presence of clay connectors between most particles, clay bridges frequently occur (fig. 19, p. 27) and may be sufficient to hold the silt particles together in an open loose structure (sec. 4.1).

The electro-chemical effect of increasing water content is reflected not only in the decrease of soil strength but also in the silt's consolidation characteristics (fig. 36). With increasing water content, the soil exhibits lower shear strength and decreasing "maximum pre-consolidation pressure" (sec. 4.8.3).

For some soils, the magnitude of structural collapse is strongly increased by flooding the soil with sewage water (Reginatto & Ferrero,

1973). In the case of Kamloops silt, a sample flooded with simulated sewage water exhibited no appreciable difference in consolidation behaviour as compared to a sample flooded with distilled water (sec. 4.8.1).

However, flooding with a HCl solution produced a marked decrease in soil strength. The resultant additional collapse is probably due to the breakdown of some form of cementing agent -- namely calcium carbonate.

(Quigley, 1976, reports approximately 5% calcium carbonate in the silt; Hardy, 1960, reports 5-6% calcium carbonate). Thus, a small portion of the soil strength is due to chemical cementation.

Further supporting evidence that chemical cementation does exist was obtained by remolding the silt into a slurry and allowing the sample to dry slowly before testing (sec. 4.8.1). If chemical cementation does exist, then remolding a sample into a slurry will destroy the chemical bonding between silt grains. Upon slow drying, the clay interparticle forces should take effect in bonding the silt particles together and give the sample its cohesive strength. This was indeed the case. In the consolidation test, a dried remolded sample behaved in a similar manner to the undisturbed silt in the dry state. However, in its flooded state, the consolidation curve of the remolded sample approximated that of the sample flooded with HCl (fig. 30). This suggests that remolding of the silt has irreversibly destroyed the calcium carbonate bonds.

In summary, all the evidence indicates that the bulk of the silt's cohesive strength is a result of the presence of interstitial clay. Capillary tension and chemical cementation also contribute to a portion of the total bonding strength. Upon flooding with water, it is the decrease in bonding strength which results in structural collapse when the soil is under a sufficiently large load.

CHAPTER 6

SLOPE STABILITY

6.1 Frequency & Extent

Field evidence of past slope failures along the South Thompson Valley are very limited in number and size within the lacustrine deposit. The two adjacent slides near Pritchard represent the only recent, major slope failures (fig. 38). Here, the oversteepening of the slopes by the undercutting action of the South Thompson River is a major factor. Generally, the effect of river erosion is not directly felt at the toe of the silt bluffs.

The bluffs in their natural state appear conditionally stable although on a long term basis, small local silt falls could cause slow recession of the bench edge.

6.2 Jointing

As described in section 2.3, the lacustrine silt is highly jointed with major joint sets at angles of approximately 60 and 30 degrees to the strike of the bluff face within Magazine Gully. A third set strikes parallel to the bluff face and a fourth set exists perpendicular to the bluff face. Locally, these joint sets form the columnar type jointing patterns commonly seen in the field.

6.3 Modes of Failures

In highly jointed slopes, invariably jointing governs the failure modes evidenced in the field. Two major types of silt falls (shallow failures)



Figure 38. Slope failures caused by oversteepening as a result of river erosion of the toe. (Near Pritchard, on the South Thompson River, looking north).

are usually observed:

1. Column Toppling

Local columnar jointing such as those seen in figure 39 provide the setting for column toppling failures. When the overturning moment is increased (eg. by cleft water pressures) or when the stabilizing moment is reduced (eg. by a decrease of soil strength as a result of weathering or wetting), columnar toppling may result. The silt columns commonly break up on impact and "flows" down the colluvial slopes as loose debris (fig. 40).

2. Block Failures

Most of the field instability exists as local block or slab failures. The general geometry consists of a silt block or wedge bounded by joint surfaces failing along a shear surface inclined out of the slope face (fig. 41). The lateral and rear joint surfaces provides little (if any) tensile strength. The bulk of the resistance to failure is due to shear resistance on the inclined potential failure surface. Decrease in this strength due to weathering or introduction of water will result in a sliding failure of the block. The size of this instability is usually limited to only a few hundred cubic yards of soil.

A similar mechanism frequently encountered is failure by rotation of intact blocks. The base of the block rotates out while the upper end of the block moves downwards along the rear joint surface. Rotated intact blocks similar to that in figure 42 are frequently observed in the field.

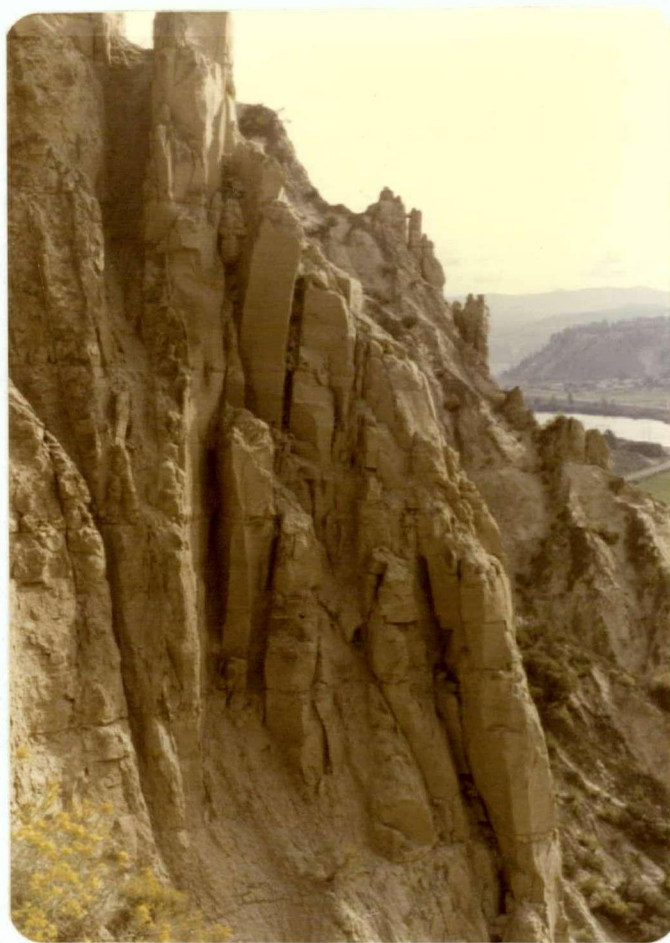


Figure 39. Columnar jointing within the lacustrine silt; slope facing south towards the South Thompson River.

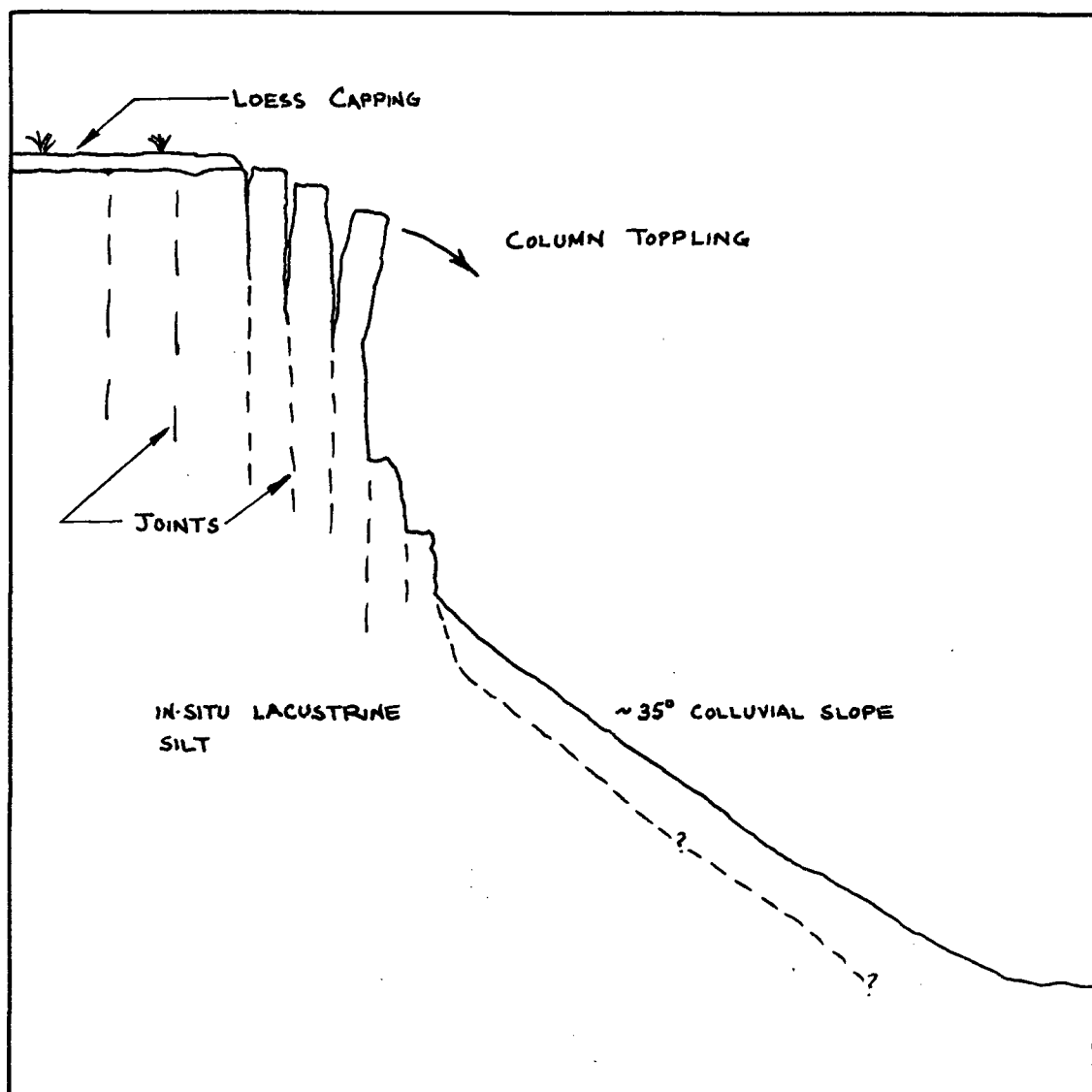


FIG. 40 DIAGRAMATIC REPRESENTATION OF THE COLUMN TOPPLING MODE OF FAILURE

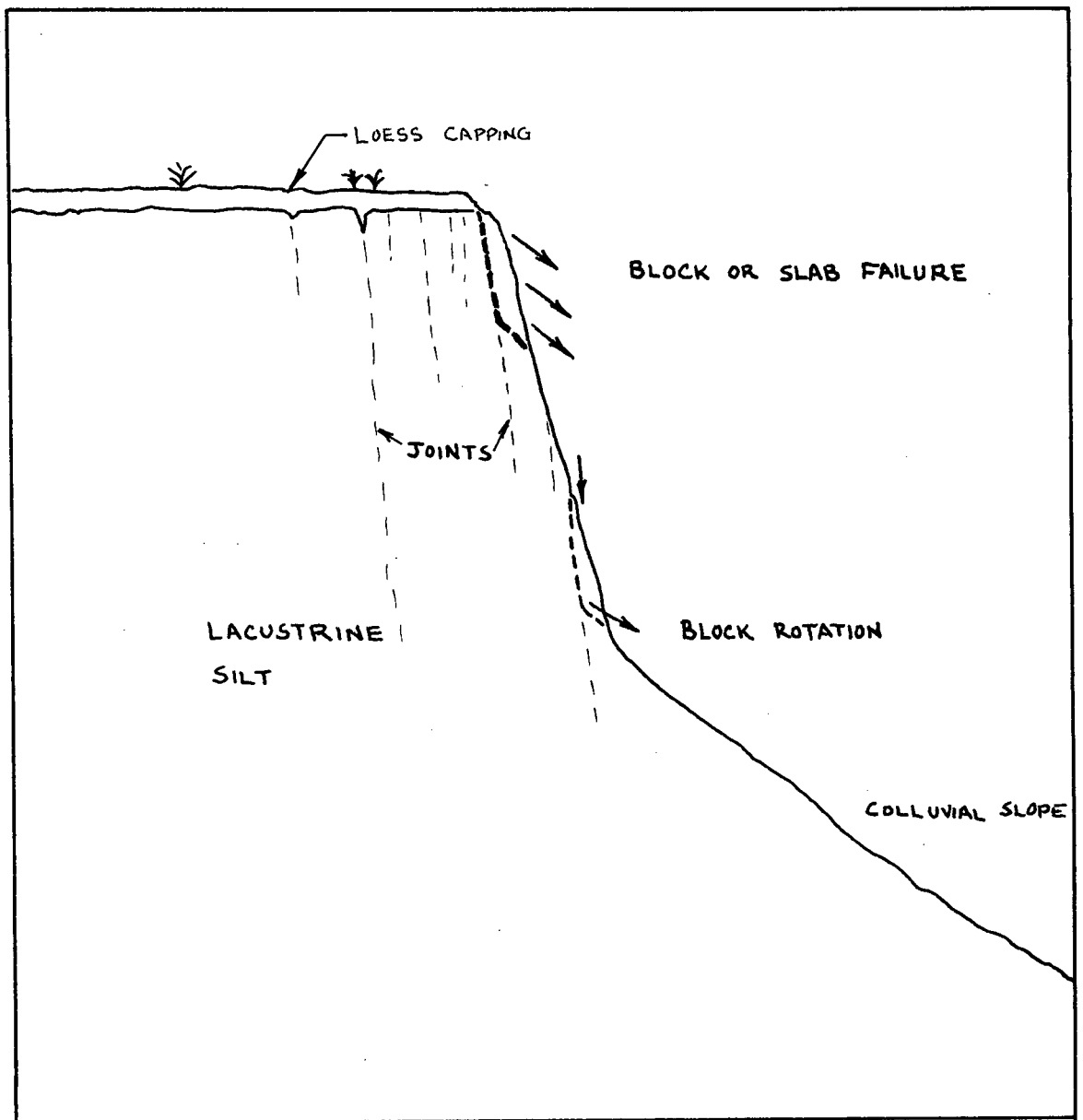


FIG. 41 DIAGRAMATIC REPRESENTATION OF
 (1) BLOCK OR SLAB FAILURE MODE
 AND (2) BLOCK ROTATIONAL FAILURE MODE

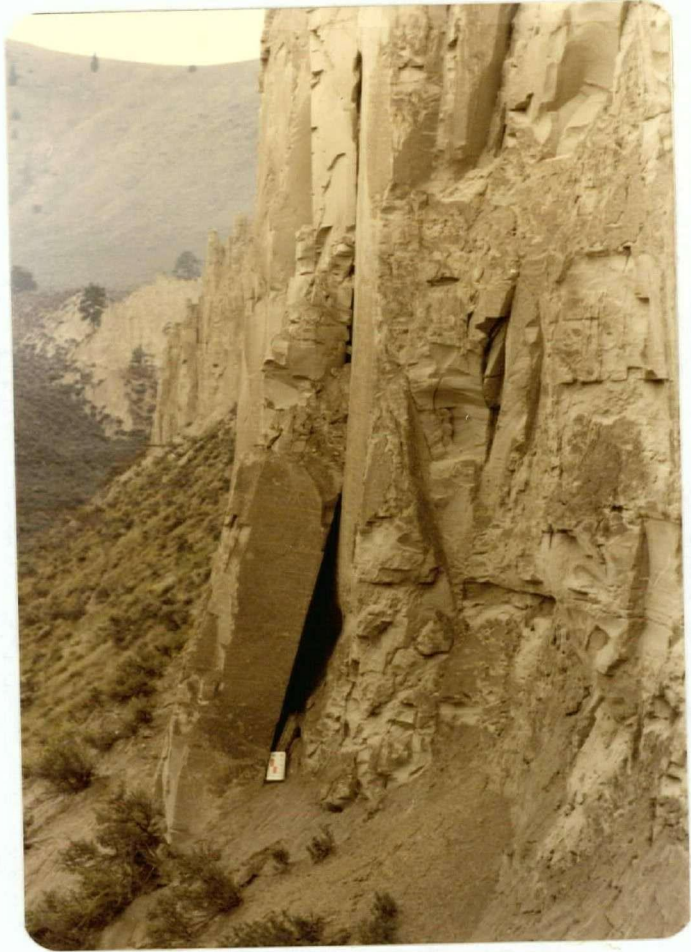


Figure 42. Rotated intact block within Magazine Gully.

6.4 Influence of Water

Stability of the slopes appears to be strongly related to water infiltration as suggested by the correlation of the known past failures during peak rain and snowmelt conditions.

In the long term condition, water causes weathering along joints. Continued percolation by rainwater can conceivably remove the dissolvable chemical cementation such as calcium carbonate. Thus, tensile resistance may be destroyed by the weathering process. Swelling and slaking of the soil near the joints may occur under low confining stresses, resulting in a weak plane which is susceptible to slippage.

The introduction of water into the soil will have an immediate effect on stability by:

1. decreasing the shear strength of the silt (in terms of effective stresses). Gibbs, Hilf & Holtz (1960) also found that a different Mohr envelope (in terms of effective stresses) exists for varying degrees of saturation of the Nebraska-Kansas loess. At low degrees of saturation, a slight increase in water content of a few percent to the Kamloops silt will cause a dramatic loss in soil strength as a result of clay-water interaction within the silt.
2. Increasing the hydrostatic forces on the cracks and joints within the soil.
3. increasing the unit weight of the soil. Although this factor is the least significant, increase in unit weight of the soil can decrease the factor of safety of the slopes when stability depends on cohesion as well as the internal friction angle of the soil.

6.5 Stability Analysis of Deep Failures

Since the strength of the silt is highly dependent on the moisture regime, the field strength parameters may vary as the moisture content increases with depth. Thus, the actual operative strength parameters are not well defined. Analysis must then proceed based on the weakest possible strength of the undisturbed soil - that is, application of the strength data obtained from saturated triaxial samples.

Since the soil strength is not well known, detailed stability analysis is not justified. Hence, the usage of Taylor's stability charts will suffice for the nearly homogeneous soil. Table VII presents the observed bluff heights in the field along with the critical slope heights as calculated from Taylor's charts (Taylor, 1948, p. 459).

TABLE VII COMPARISON OF THE OBSERVED AND CALCULATED SLOPE HEIGHTS USING TAYLOR'S CHARTS.

Measured slope angle (i)	Observed Height	Calculated Height (H_c)
75°	122'	108' ***
66°	45'	126'
71.5°	70'	114'
59.5°	38'	121'
66°	70'	127'
79.3°	93'	99'
70.6°	139'	102' ***

*** factor of safety is less than one.

It can be readily seen from table VII that using in-situ densities coupled with saturated strength data, the factor of safety of the silt bluffs can be less than unity. If jointing is also considered, the slopes would be even more critical. Thus, this simple analysis shows that should the silt bluffs be sufficiently wetted, deep slope failures may result.

6.6 Long-Term Stability

In the long term condition, erosional processes such as block falls will proceed until the angle of repose is achieved. From the triaxial data, this is determined to be approximately 33° (being somewhat dependent on our choice of the failure criteria). In the field, colluvial slopes exist at an average angle of 35° . Without complicating factors such as removal of toe support and added loads, equilibrium will exist at this angle.

In the event of reaching conditions which approximate the parallel flow of water down a saturated slope, the infinite slope analysis could be applied. In the case of the silt bluffs, the stable angle (i) could be found from

$$i = \tan^{-1}((\gamma'/\gamma_s)\tan \phi) = 16^\circ$$

(Lambe & Whitman, 1969, p. 364)

Although the infinite slope analysis is based on assumptions which may never be fully realized in the field situation, nevertheless, it represents the lower bound for instability. In practice, the assumptions of saturated slope and the seepage of water parallel to the slope may never be met exactly but in the event of heavy rain and snowmelt coupled with sewer main ruptures, the above conditions may be locally approximated.

From the preceding rough analysis, the 'safe' slope angle lies between 16° - 33° for the long term condition. In this long term case, only the frictional resistance is considered to be mobilized and cementation and other forms of cohesion are considered to be non-existent. Thus, even

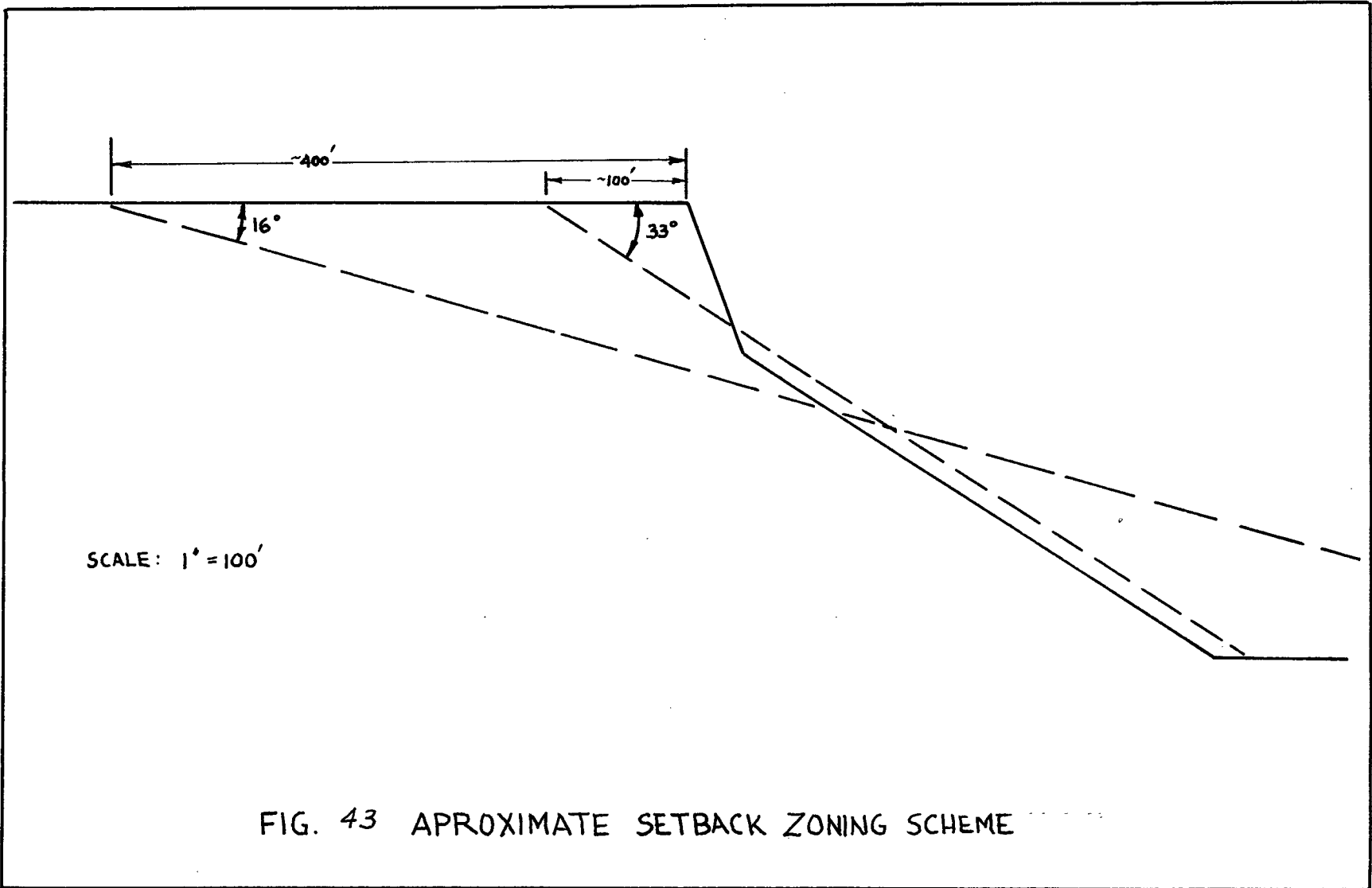
under the conditions of percolation of a weak acidic solution through the soil, the above limits still apply from the sliding failure aspect - although structural collapse may occur under loaded foundations.

6.7 Possible Zoning Scheme

One possible zoning scheme for urban development is based on the angle of repose (33°) and the limiting lower bound slope angle for instability (16°). Considering an idealized section (fig. 43) consisting of 100 vertical feet of bluff face at 70° and 200 feet of colluvial slope at 33° , an approximate safe setback and foreset could be delineated.

Extension of the angle of repose to the top of the section results in a setback of approximately 100'. Within this 100' of the cliff edge, structures of any form should be considered unsafe. Between 100' and 400', a control of the type of structures to be erected should be enforced. Temporary structures such as storage sheds may be allowed. The zone beyond 400' is considered safe for urbanizational developments such as housing projects; although industrial use may have to be further removed from the cliff edge. The setback distances are based on a bluff face of 100' high and slope geometries as given in the idealized section of figure 43. The actual zoning would require the preparation of topographic maps of the area.

The foreset at the base of the slopes may be delineated with a similar approach since soil removed at the top of the bluff must accumulate on the colluvial slopes. Small silt falls which may frequently occur will not be expected to flow past its present toe position since the debris will spread over a large area before impinging on the toe of the slope.



Thus a foreset of 100' may be sufficient under dry conditions. However, when saturated conditions exists, the 400' foreset guideline may be applied if we consider that the soil removed at the top is completely transferred to the lower half of the slope as shown in figure 43. This foreset naturally assumes the advance of the toe in a gradual process and not a result of a high velocity mass failure, in which case, the silt's momentum may result in the debris from spreading further downslope.

CHAPTER 7

SUMMARY AND CONCLUSIONS

In the attempt to understand the behaviour of the glaciolacustrine silt, extensive laboratory testing has been employed. The silt was found to be extremely sensitive to moisture inputs. The lower the water content, the greater the soil strength. Thus, a different Mohr envelope of failure (in terms of effective stresses) exists for each degree of saturation. In the silt's fully saturated state, consolidated drained triaxial tests yield a cohesion intercept of 0.609 kg/cm^2 and a friction angle (ϕ') of 17.8° for the overconsolidated stress range. Within the normally consolidated stress field, the internal friction angle is 33° . The above strength parameters were obtained by axial loading (deviator stress direction) perpendicular to the bedding plane. Although the soil strength is anisotropic, the variation has been shown to be small.

The sensitivity of the silt to moisture content is also reflected in the soil's structural stability, and hence, in its behaviour in the consolidation apparatus. In the silt's naturally dry state, ponding by water results in soil heave at low confining pressures while structural collapse occurs under higher stress levels. The slight heave is probably due to swelling of the 3-4% montmorillonite within the soil while the collapse mechanism revolves around the physico-chemical behaviour of the clay-water system within the soil.

Intergranular bonding by Van der Waals' forces, London forces and other attractive forces of the clay plates constitutes the bulk of the

bonding strength exhibited by the silt in its naturally dry state. The clay may exist as bridges and connectors or as thin coatings at silt grain contacts. Upon flooding the soil with water, the ion concentration of the bounded water layer decreases and the clay plates tend to separate slightly, resulting in a decrease of intergranular bonding strength. Under sufficiently high stress levels (above 6 kg/cm^2), microshearing between grains occur, leading to structural collapse of the loose open network ($e_o = 1.28$). Capillary forces must necessarily exist in a moist soil and meniscii forces between clay-clay and clay-silt contacts may be substantial although the actual portion of the bonding strength due to capillary forces is not known. Since structural collapse is insignificant below stress levels of 6 kg/cm^2 , collapse as a result of flooding is not a problem under stresses commonly encountered in engineering practice. However, additional collapse will result as stresses as low as 2.4 kg/cm^2 when the soil is flooded with acidic water. The dissolution of calcium carbonate (5-6% by weight) by the acidic solution leads to the further loss of intergranular bonding strength.

Under the present natural conditions of the silt bluffs, limited slope failures are evident in the field. Where they do occur, they exist as small shallow block failures. These failures have been observed to correspond to peak rainfall and snowmelt conditions. Thus under usual conditions, large mass failures are not expected to occur. However, introduction of excessive water into the slopes as a result of urbanizational disturbances, or abnormally wet climatic conditions, can possibly lead to large scale slope failures. The failure mechanism and its corresponding factor of safety are dependent on the jointing system.

Four, near vertical joint sets within the detail study area forms a local columnar-type jointing pattern. Slope failures may be bonded laterally by combinations of the joint sets (trending approximately 0° , 30° , 90° , and 120°).

A simple analysis has indicated that large scale failures can occur under saturated states. However, since the soil strength (at 40-50% saturation) drops to nearly the strength level of the saturated soil, field saturations during unusually wet conditions may reduce the soil strength sufficiently to induce failure.

A long term zoning proposal for urbanizational developments may be based on the angle of repose (33°) and on the safe slope angle calculated from an infinite slope analysis (16°). The area between the present cliff edge and the 33° projection of the colluvial slopes should be considered unsafe for structures of any form. This zone includes the probable failure plane assumed in Taylor's analysis. In the long term situation, material removed from the upper section must collect at the lower part of the slopes. Assuming the mid-height of the slope profile remains fixed, the soil is eroded from the upper section and deposited in the lower section, a marginally safe zone could be delineated between the 16° slope projection and the 33° projection. Construction within this region should be restricted to temporary structures such as small storage sheds. The area beyond the 16° projection may be considered safe for housing developments. However, caution must be exercised in the surrounding areas exhibiting evidence of sinkholes and pipes. Naturally, certain controls must be enforced within all urbanized areas. Control of runoff and drainages must be observed to prevent the decrease of soil strength

with wetting, as well as to prevent the formation of "liquified pipes" such as the one formed in the field seepage test. Undercutting of the slopes by roads and extending property limits by removal of soil from the base of the slopes must be prohibited or strictly controlled.

APPENDICES

- APPENDIX 1 : SAMPLING SITES AND SAMPLE DESCRIPTIONS
- APPENDIX 2 : SAMPLE TRIMMING PROCEDURES
- APPENDIX 3 : COMPRESSIBILITY CORRECTIONS OF THE CONSOLIDATION APPARATUS
- APPENDIX 4 : CONSOLIDATION TESTING OF COLLUVIUM

APPENDIX 1

SAMPLING SITES AND SAMPLE DESCRIPTIONS

APPENDIX 1SAMPLING SITES AND SAMPLE DESCRIPTIONS

A. Glacio-lacustrine Samples

Site #1:

One block sample was obtained from the base of the bluff face running parallel to the South Thompson River near the Eastern Indian Reserve boundary. This near surface sample was transported unwaxed and was consequently used for specific gravity measurements only. The silt had laminations of coarse and medium silt sized particles with shiny flakes (possibly mica) lying approximately parallel to the laminations. The sample showed signs of weathering, reflected by the presence of small (0.1mm - 1mm) dark patches throughout the sample.

When the silt was placed in water, rapid slaking occurred parallel to the laminations, followed by the breakdown of the sample to a cohesionless mass.

Site #2:

A small block sample was obtained from the Western bluff of Magazine Gully beside a recent silt fall. The unwaxed sample was used for specific gravity determinations and preliminary consolidation testing to assess the apparatus requirements such as load cell capacity.

The sample is a medium fine silt exhibiting the same weathering

patterns as sample block #1, but lacking visible laminations. When submerged in water, slaking resulted.

SITE #3 & #4:

Sites 3 & 4 are backhoe sample sites on the bench surface beside Magazine Gully (fig. 12). At both sites, the brown loess cover was 1 - 1½ feet thick and samples were obtained from a depth of 4½ to 5½ feet. Samples were hand carved with a sharp knife, following existing joints where possible. Jointing generally consisted of discontinuous fractures. Many of these planes showed a rusty-brown weathering surface. Joint orientations were noted and plotted in the stereonet of figure 10. At site #4, many unweathered fracture surfaces existed and these are likely due to disturbances by the scrapping action of the backhoe. This made large intact samples difficult to obtain. At site #3, the silt remained intact and free of disturbance by the backhoe. As a consequence, much of the samples were obtained from site #3.

The block samples obtained are undisturbed glaciolacustrine silt. At site #3, this was confirmed by the presence of a ¾" thick dessicated dark grey clay seam at a depth of 4 feet. This nearly horizontal continuous layer represents part of the varved sequence which is characteristic of the lacustrine deposits. At site #4, a clay seam of 1" thickness also existed above the sampled horizon.

All samples were marked in the field as to the site number and orientation (top and bottom). The orientation was further confirmed in the laboratory by the distinct presence of thin laminations in the trimmed samples.

The light buff colored samples exhibited similar weathering patches as the silt block from site #1. Rapid slaking was also observed when the silt was submerged in water. When the silt was wetted with a drop of 0.5M HCl, the sample effervesced and left a craterlike pitted surface. However, a drop of 0.01M HCl produced no observable reaction.

B. Colluvial Samples (sites #5 & #6)

Two colluvial block samples were supplied by the Geotechnical and Materials Branch of the Department of Highways in Kamloops to extend the study to the preliminary laboratory investigation of the consolidation characteristics of the colluvium. Both samples arrived at U.B.C. as waxed blocks. Descriptions of the sample locations were included.

SITE #5:

Site #5 was described as "the side of an incised creek at the bottom of Magazine Gully, 5 feet south of profile line B".

The colluvial sample was a medium brownish-grey silt with abundant roots and root holes throughout the sample. Irregular fragments of intact lacustrine silt (light buff color) are scattered within the block. The pieces of lacustrine silt ranged from 1mm to 2 cm across and formed sharp contacts with the matrix material.

The sample was definitely weaker in strength than the lacustrine silt samples of sites 3 & 4. No laminations were visible in the sample. When placed in water, the sample slowly lost its cohesive strength, although the roots held the main mass together. When wetted with a drop of 0.5M HCl, the sample exhibited the same effervescent

characteristics as the lacustrine silt with perhaps slightly more vigor.

SITE #6:

This colluvial sample was described as being taken from the wall of a 1 ft. diameter pipe near an ash layer by the fork in the road within Magazine Gully.

The medium-fine silt had a medium brownish-grey color and contained flecks of white powder (ash?). The strength is also much weaker than the lacustrine silt and contained less roots and root holes than the previous colluvial sample. No fragments of lacustrine silt was present within the sample. When submerged in water or wetted with 0.5M HCl, the reactions were similar to that of the sample from site #5.

APPENDIX 2

SAMPLE TRIMMING PROCEDURE

APPENDIX 2SAMPLE TRIMMING PROCEDURE

A. Triaxial Sample Trimming

The final cylindrical triaxial samples are approximately 3' high by 1.4' in diameter. Due to the brittle nature of the silt, careful, time-consuming trimming of the sample is mandatory to prevent chipping. To obtain a triaxial sample, the waxed silt block is unwrapped and cut into smaller rectangular sections. These smaller blocks are usually cut at least 2" larger than the final sample dimensions in order to ensure minimal disturbance of the final sample. The main block is cut with a flexible, wide set 30" swedish saw blade (10 teeth to the inch). The frame is removed since its added weight and rigidity tends to cause occasional fracturing of the sample. The small block is then further trimmed with a sharp knife to the required sample diameter in the trimming box. The laminations of the silt becomes distinctly visible under this procedure. To obtain the correct sample height is slightly more difficult since fine trimming of the ends by a knife tends to cause chipping at the edges. Slow scrapping motions of a thin wire saw does eliminate this problem and square edges can be obtained.

B. Sample Trimming Procedure of Consolidation Samples

The silt block is trimmed with a sharp knife in the trimming apparatus to within $1/16$ to $1/8$ inches of the inside diameter of the consolidation ring. The sharp edged ring is then placed on top of the sample. The silt outside the contact area is further shaven to nearly the exact ring dimension, taking care not to overtrim. The consolidation ring is then pushed $1/8$ " at a time while the area immediately beneath the ring's cutting edge is trimmed to almost the exact ring size. The sample size had to be very near that of the consolidation ring's inside diameter before advancing the consolidation ring into the sample to prevent chipping of the brittle silt which would result in voids between the ring and the sample itself. Even when much care is taken to ensure minimal chipping, when trial samples were immediately extruded from the ring after trimming for inspection, the rare void may exist between the ring and the sample itself due to brittle fracturing. The lost in soil was however very minimal and the volume of the sample lost represented less than 1% of the total sample volume.

APPENDIX 3APPARATUS COMPRESSIBILITY CORRECTIONS FOR CONSOLIDATION TESTS

APPENDIX 3APPARATUS COMPRESSIBILITY CORRECTIONS FOR CONSOLIDATION TESTS

The compression of the consolidation apparatus contributed a significant percentage of the measured compression of the sample. Where applicable, the apparatus compression is the result of deformation of the loading rod, loading cell or seating problems associated with slight warps in the porous stones etc.

A. Correction Curve A (fig. 44)

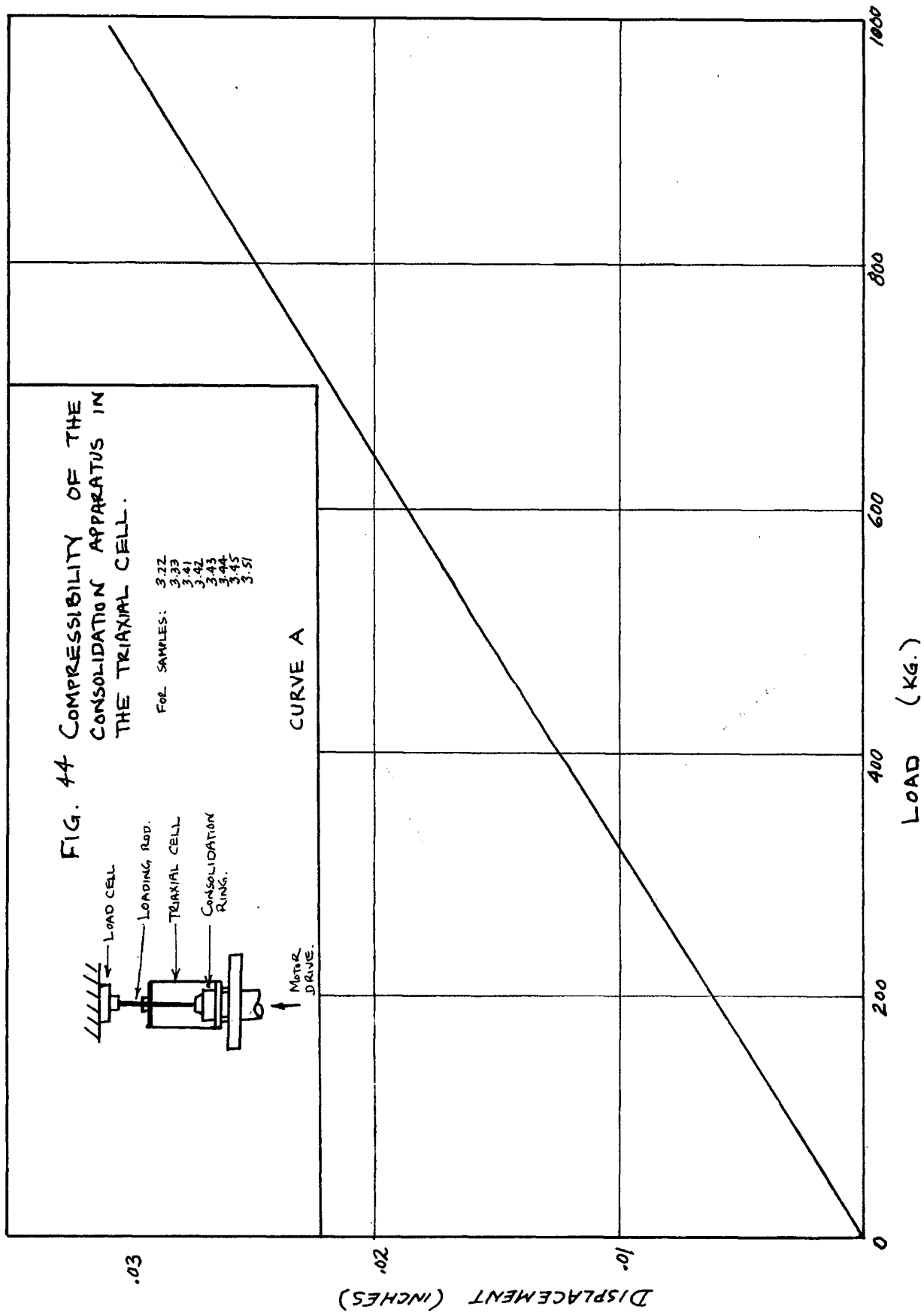
This curve applies to the system compressibility of the apparatus setup with the consolidation ring mounted inside the triaxial cell. The majority of the compression correction is due to the combination of the deformation of the 1/8" diameter by 8" long, stainless steel loading rod and the deformation of the beryllium copper diaphragm load cell. Little strain is attributed to improper seating since the correction curve is linear through the origin. This correction curve applies to consolidation tests 3.22, 3.33, 3.41, 3.42, 3.43, 3.44, 3.45 and 3.51.

B. Correction Curve B (fig. 45)

The correction curve of figure 48 applies to test 3.67 only since a more direct loading setup was used which excluded the loading rod and triaxial cell. The large strains required for load buildup indicates seating problems. When the porous stones were examined closely, a slight warp was noticed in the top porous stone.

C. Correction Curve C (fig. 46)

The extension of this study to include colluvium required a third layout which is similar to that of the apparatus used in developing the correction curve B except that a different load cell was used. With this set of equipment, a slight hysteresis was measured when loading and unloading. When applying the corrections, only the loading curve was applied. The data of samples 5.10 and 5.11 were adjusted by this correction curve.



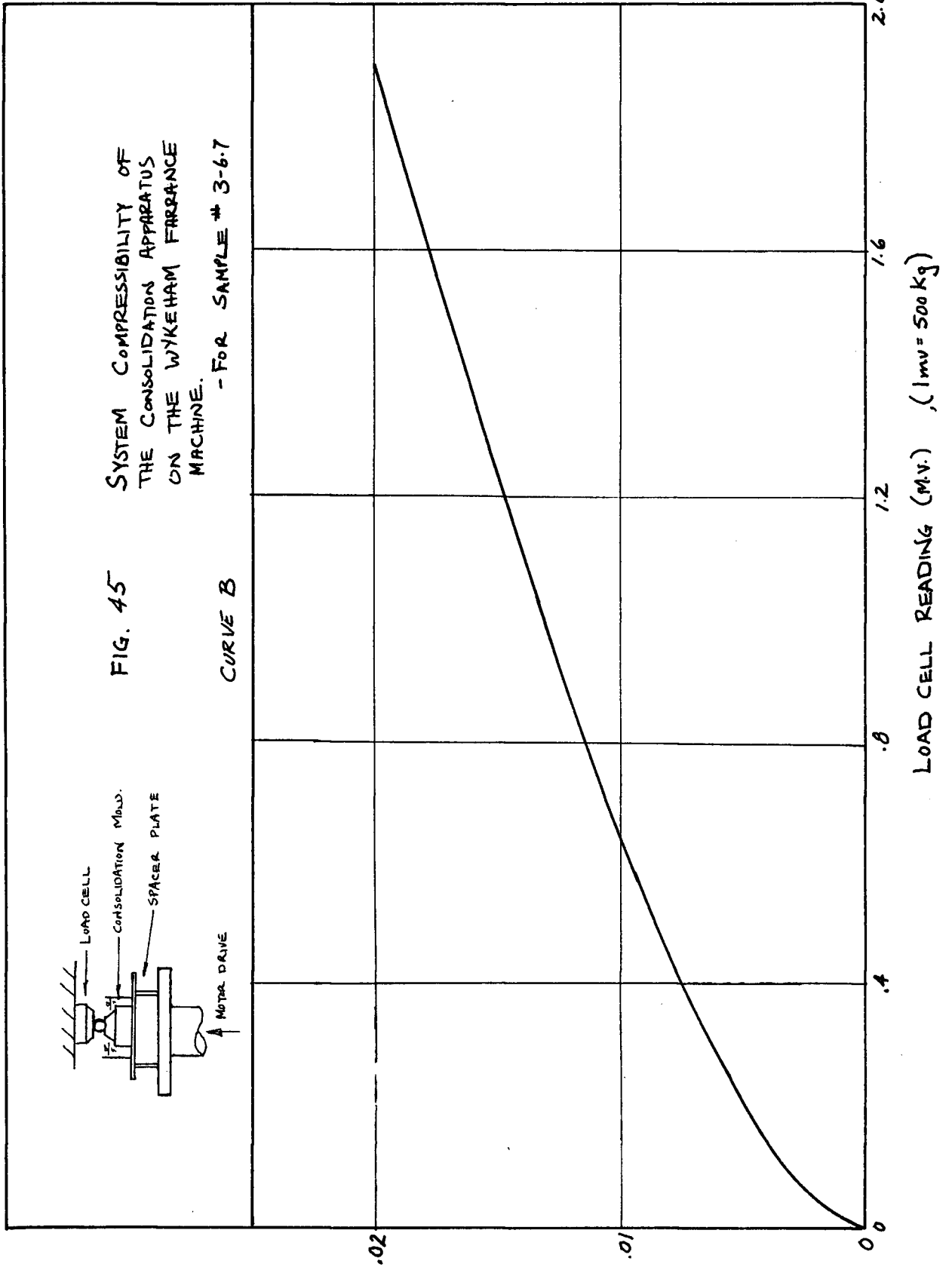
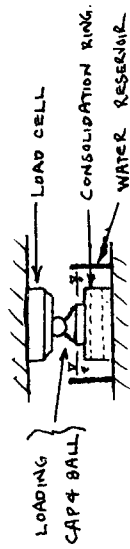
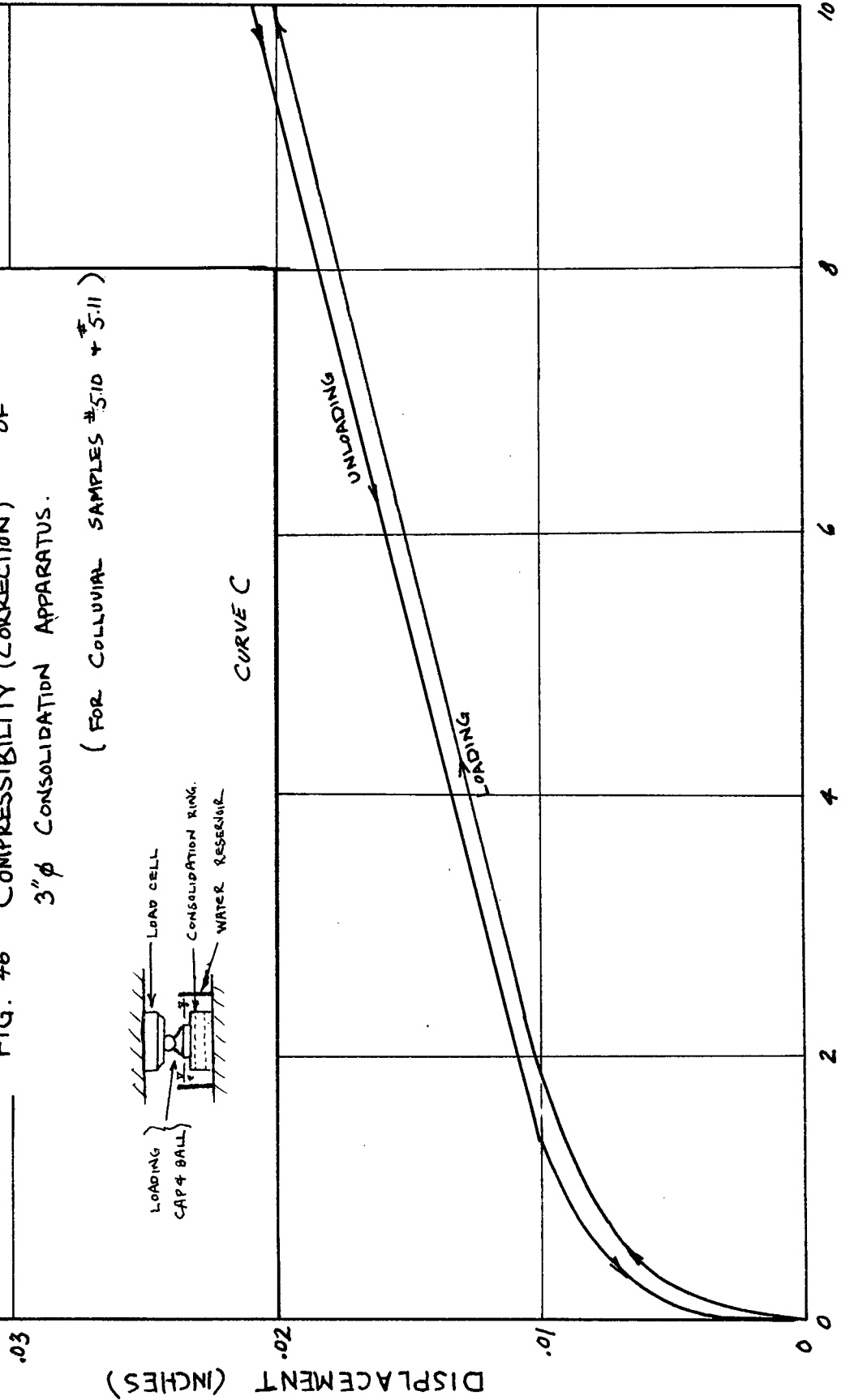


FIG. 46 COMPRESSIBILITY (CORRECTION) OF
 3" ϕ CONSOLIDATION APPARATUS.
 (FOR COLLUVIAL SAMPLES #510 + 5.11)



CURVE C



LOAD CELL READING (millivolts) , CALIBRATION: 1mv. = 134 Kg.

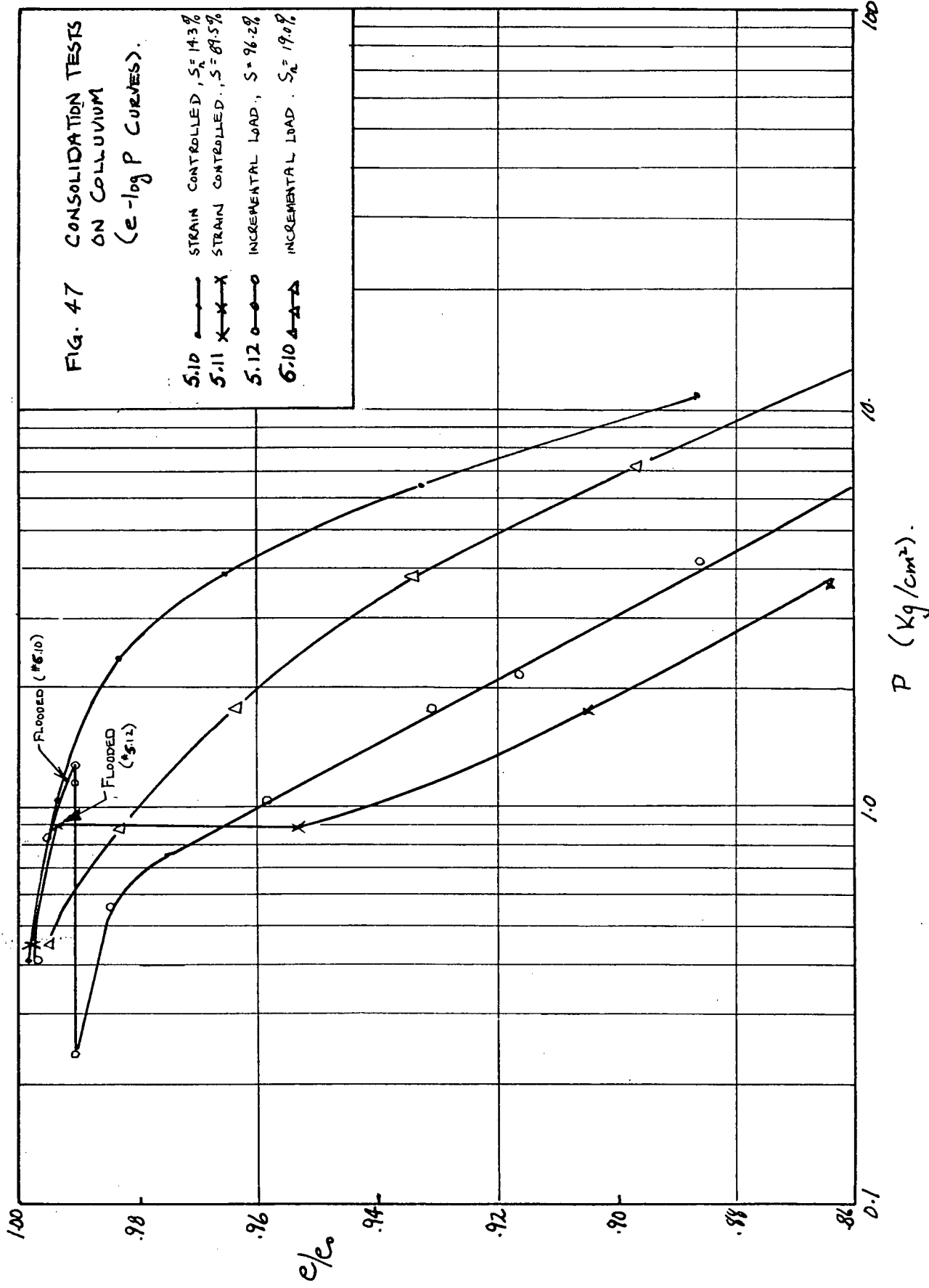
APPENDIX 4CONSOLIDATION TESTS ON COLLUVIUM

APPENDIX 4CONSOLIDATION TESTS ON COLLUVIUM

From the hand specimens, it is readily evident that the colluvium is not uniform from one location to the next (see appendix 1). Laboratory tests of the two colluvial samples also results in significant differences of properties:

	Site #5	Site #6
specific gravity (G_s)	2.60	2.78
water content ($w\%$)	6.9%	9.2%
void ratio (e_o)	1.07	1.35

The consolidation curves for the colluvium are presented in figure 47. It is apparent that the "maximum past pressures" for colluvium are much lower than that for the intact lacustrine silt. Flooding by water causes large settlements even at low loads. Since the testing program was limited, it was not confirmed whether the soil was truly collapsible or not. However, under even small pressures, collapse on wetting does occur and will present engineering difficulties.



REFERENCES

1. Abelev, Y.M., 1975. Compacting Loess Soils in the USSR. Geotechnique, V. 25, No. 1, pp. 79-82.
2. Aitchison, G.D., 1956. Some Preliminary Studies of Unsaturated Soils: The circumstances of Unsaturation in Soils With Particular References to the Australian Environment. Proceedings of the 2nd Austr-New Zealand Conf. on Soil Mech. & Found. Eng.
3. Aitchison & Donald, 1956. Effective Stresses in Unsaturated Soils. Proceedings of the 2nd Austr-New Zealand Conf. on Soil Mech. & Foundation Engineering, pp. 192-199.
4. Badger, W.W. & Lohnes, R.A., 1973. Pore Structure of Friable Loess. Highways Research Record #429, pp. 14-25.
5. Barden, L; McGown, A.; & Collins, K., 1973. The Collapse Mechanism in Partly Saturated Soils. Eng. Geol. V. 7, pp. 49-60.
6. Black, David, & Lee, 1973. Saturating Laboratory Samples by Backpressure. Journal of Soil Mech. & Found. Eng. Proceedings of the ASCE., V. 99, No. SM1, pp. 75-93.
7. Bishop, A.W. & Blight, G.E., 1963. Some Aspects of Effective Stress in Saturated and Partly Saturated Soils. Geotechnique, V. 13, pp. 177-197.
8. Bishop, A.W. & Henkel, D.J., 1974. The Measurement of Soil Properties in the Triaxial Test. Edward Arnold Ltd., London.
9. Byrne, P.M. & Oaki, Y., 1969. The Strain Controlled Consolidation Test. Soil Mechanics Series No. 9, Univ. of British Columbia.
10. Coates, D.F., 1970. Rock Mechanics Principles. Canadian Mines Branch, Dept. of Energy, Mines & Resources. Mines Branch Monograph 874, Ottawa, Canada.
11. Cockfield, W.E. & Buckham, A.F., 1946. Sink-hole Erosion in the White Silts of Kamloops. Trans Roy. Soc. Can., 3rd ser., V. 40, sec. IV, pp. 1-10
12. Collins, K., & McGown, A., 1974. The Form and Structure of Microfabric Features in a Variety of Natural Soils. Geotechnique, V. 24, No. 2, pp. 223-254.

13. Crawford, C.B., 1964. Interpretation of the Consolidation Test. Journal of Soil Mechanics and Foundation Div., ASCE, SM5.
14. Daly, R.A., 1915. A Geological Reconnaissance Between Golden & Kamloops, B.C. Along the Pacific Railway. Canadian Geol. Survey, Mem. 68, 260p.
15. Denisov, N.Y., 1961. Pore Pressure and Strength of Underconsolidated Clay Soils. Proceedings of the 6th Int. Conf. On Soil Mech. & Found. Eng. V. 1, pp. 208-212.
16. Dudley, J.H., 1970. Review of Collapsing Soils. Journal of the Soil Mech & Found. Div., Proc. of ASCE, SM 3, pp. 925-947.
17. Evans, S.G. & Buchanan, R.G., 1976. Some Aspects of Natural Slope Stability in the Silt Deposits Near Kamloops, B.C. 29th Canadian Geot. Conf. Vancouver, B.C., Oct. 13-15, 1976.
18. Fookes, P.G. & Denness, B., 1969. Observational Studies On Fissure Patterns in Cretaceous Sediments of S.E. England. Geot. V. 19, pp. 453-477.
19. Fulton, R.J., 1965. Silt Deposition in Late-Glacial Lakes of Southern B.C. American Journal of Science, V. 263, pp. 553-570.
20. Fulton, R.J., 1967. Deglaciation in the Kamloops Region, B.C. GSC Bull. 154.
21. Fulton, R.J., 1975. Quaternary Geology and Geomorphology of the Nicola-Vernon Area, B.C. GSC Mem. 380.
22. Gibbs, H.J. & Bara, J.P., 1967. Stability Problems of Collapsing Soils. Journal of the Soil Mech. & Found. Div., ASCE, V. 93, No. SM4, pp. 577-594.
23. Gibbs, H.J.; Hilf, J.W.; Holtz W.G. & Walker, F.C., 1960. Shear Strength of Cohesive Soils. ASCE Research Conf. on the Shear Strength of Cohesive Soils. Univ. of Colorado, June, 1960.
24. Hardy, R.M., 1950. Construction Problem in Silty Soils. Engineering Journal, V. 33, pp. 775-779.
25. Henkel, D.J. 1972. The Relevance of Laboratory-measured Parameters in Field Studies. Stress-Strain Behaviour of Soils, Proceedings of the Roscoe Memorial Symposium, Cambridge University, R. Parry (ed.), G.T. Foulis and Co. Ltd., Oxfordshire, pp 669-675.
26. Hoek, Evert; & Gray, J., 1974. Rock Slope Engineering. London, Unwin Brothers Ltd. 309 pp.

27. Holtz, W.G. & Gibbs H.J., 1951. Consolidation and Related Properties of Loessial Soils. Symposium on Consolidation Testing of Soils, 44th Annual Meeting of ASTM, Atlantic City, N.J., June 18, 1951.
28. Horta Da Silva, J.A. 1971. Relationships Between the Collapsing Soils of the Luanda & Luso Regions. SMFE, Proceedings of the 5th Regional Conf. for Africa, V. 1, 1971.
29. Hutchinson, J.N., 1972. Field and Laboratory Studies of a Fall in Upper Chalk Cliffs at Joss Bay, Isle of Thanet. Stress-Strain Behaviour of Soils, Proceedings of the Roscoe Memorial Symposium, Cambridge University, R. Parry (ed.), G.T. Foulis & Co. Ltd., Oxfordshire.
30. Jennings, J.E. & Knight, K., 1975. A Guide to Construction On or With Materials Exhibiting Additional Settlement Due to "Collapse" of Grain Structure. Sixth Regional Conf. for Africa on Soil Mech. & Found. Eng., Durban, South Africa, Sept., 1975, pp. 99-105.
31. Lambe, T.W., 1951. Soil Testing For Engineers. New York, John Wiley & Sons, 165 p.
32. Lambe, T.W. & Whitman R.V., 1969. Soil Mechanics. New York, John Wiley & Sons, 553 p.
33. Lo, K.Y., 1965. Stability of Slopes in Anisotropic Soils. ASCE Journal of Soil Mech. & Found. Eng. V. 91, SM4.
34. Lo, K.Y., 1970. The Operational Strength of Fissured Clays. Geot. V. 20, No. 1, p. 57-74.
35. Lohnes, R.A., & Handy, R.L., 1968. Slope Angles in Friable Loess. Journal of Geology, V. 76, No. 3, pp. 247-258.
36. Lowe, J.; Zaccheo, P. & Feldman, H., 1964. Consolidation Testing With Back Pressure. Journal of the Soil Mech. & Found. Eng. ASCE. V. 90, No. SM5, Part 1, p. 69-86.
37. Lutton, R.J., 1971. A Mechanism for Progressive Rock Mass Failure As Revealed by Loess Slumps. Int. Journal of Rock Mech. Min. Sci, V. 8, No. 2, pp. 143-151.
38. Lutton, R.J., 1969. Fractures and Failure Mechanics in Loess & Applications to Rock Mechanics. Research Report S-69-1, Aug. 1969, U.S. Army Engineer Waterways Experiment Station, Vicksburg, Mississippi.

39. Markin, B.P., 1971. Effect of Initial Density on the Compaction of Loess Soils by Heavy Compaction. Soil Mechanics and Foundation Engineering, Translated from the Russian by the Consultants Bureau, pp. 361 - 362.
40. Mathews, W.H., 1944. Glacial Lakes and Ice Retreat of South-Central B.C. Roy. Soc. Canada Trans. 3rd Ser. V. 38, sec 4, p. 39-57.
41. McGowan, A.; Saldivar-Sali, A. ; & Radwan, A.M., 1974. Fissure Patterns and Slope Failures in Till At Hurlford, Ayrshire. Quarterly Journal of Engineering Geology, V. 7, No. 1, pp 1-26.
42. Milovic, D.M., 1971. Effect of Sampling on Some Loess Characteristics. Proceedings of the Specialty Session on "Quality in Soil Sampling". 4th Asian Conf., Int. Soc. for Soil Mech. & Found. Eng., Bangkok.
43. Moore, P.J. & Millar, D.V., 1971. The Collapse of Sands Upon Saturation. Proceedings of the 1st Austr-New Zealand Conf. on Geomechanics, Melbourne, pp. 54-60.
44. Mustafaev, A.A.; Chigniev, G.D. and Nazirova, G.R., 1974. Rheological Nature of the Deformations caused by Swelling In Clays and by Collapse in Loess Soils. Soil Mech. & Found. Eng., V. 11, No. 5, pp. 325-330.
45. Nyland, D. & Miller, G.E., 1977. Geological Hazards and Urban Development of Silt Deposits in the Pentiction Area. B.C. Ministry of Highways & Public Works, Geotechnical and Materials Branch.
46. Quigley, R.M., 1976. Mineralogy, Chemistry and Structure of the Pentiction & South Thompson Silt Deposits. Research Report to B.C. Dept. of Highways, Faculty of Eng. Science, University of W. Ontario, London, Ontario.
47. Rabinovich, I.G., & Urinov, M.I., 1974. Characteristics of the Development of Collapse in Loess Soils with Time. Soil Mech. & Found. Eng. V. 11, No. 5, pp. 331-223.
48. Reginatto, A. R. and Ferrero, J.C., 1973. Collapse Potential of Soils and Soil Water Chemistry. In 'Problems of Soil Mechanics And Construction on Soft Clays and Structurally Unstable Soils (Collapsible, Expansive and Others)'. Proceedings of the Eighth International Conference on Soil Mechanics and Foundation Engineering., pp. 177-183.

49. Ryder, J.M., 1971. The Stratigraphy and Morphology of Para-glacial Alluvial Fans in South-Central B.C. Canadian Journal of Earth Sciences, V. 8, pp. 279-298.
50. Scheeler, J.B., 1968. Summarization and Comparison of Engineering Properties of Loess in the United States. U.S. Highway Research Record, Conference on Loess; Design & Construction, No. 212, pp. 1-9.
51. Schultze, E. & Odendahl, R., 1967. The Shear Strength of Undisturbed Rhineland Silts. Proceedings of the Geotechnique Conference, Oslo, 1967. pp. 239-242.
52. Schuurman, I.E., 1966. The Compressibility of an Air/Water Mixture and a Theoretical Relation Between the Air and Water Pressures. Geotechnique, V. 16, No. 4, pp. 269-281.
53. Spangler, M.G., 1960. Soil Engineering (2nd ed.). New York, International Textbook Co., 483p.
54. Taylor, D.W., 1948. Fundamentals of Soil Mechanics. New York, John Wiley & Sons, p. 459.
55. Terzaghi, K., 1943. Theoretical Soil Mechanics. New York, John Wiley & Sons, 510p.
56. Terzaghi, K. & Peck, R.B., 1948. Soil Mechanics in Engineering Practice (2nd ed.). New York, John Wiley & Sons, 729p.
57. Townsend, D.L.; Sangrey, D.A. & Walker, L.K., 1969. The Brittle Behaviour of Naturally Cemented Soils. Proc. of the 7th Int. Conf. SMFE, Mexico, p. 411-417.
58. Turnbull, W.J., 1968. Construction Problems Experienced With Loess. U.S. Highway Research Record, Conference on Loess; Design & Construction, No. 212.
59. Zur, A. & Wiseman, G., 1973. A Study of Collapse Phenomenon of an Undisturbed Loess. Proceedings of the Eighth International Conference on Soil Mechanics and Foundation Engineering, pp. 265-269.